Metabolic Lipid Tracing in the Rodent Heart

Dissertation

zur

Erlangung des Doktorgrades (Dr. rer. nat.)

der

Mathematisch-Naturwissenschaftlichen Fakultät

der

Rheinischen Friedrich-Wilhelms-Universität Bonn

vorgelegt von

Aleksandra Shiian

aus

Moskau (Russland)

Bonn, 2025

Angefertigt mit Genehmigung der Mathematisch-Naturwissenschaftlichen Fakultät der
Rheinischen Friedrich-Wilhelms-Universität Bonn

Gutachter/Betreuer:

Herr Prof. Dr. Christoph Thiele

Gutachter:

Herr Prof. Dr. Christoph Wilhelm

Tag der Promotion: 27.05.2026
Erscheinungsjahr: 2026

Declaration of authorship

Hereby I declare that I am the sole author of this dissertation and that all sources I used to support my thesis are clearly indicated. The work presented in it has been generated by me as the result of my own original research. It is clearly stated, where the work is based on research done jointly with others.

Bonn,

_____ Signature

Table of content

Summary

Cardiovascular diseases remain the leading cause of death worldwide and represent enormous medical challenge. Therefore, the search for better treatment strategies and markers for early cardiovascular diseases detection is of a great importance. Changes in lipid metabolism have been observed in many cardiac diseases and are often a target of the drug therapy.

This thesis aims to use alkyne-lipid tracers to deepen the understanding of lipid metabolism in a rodent heart. The goals are (I) to compare the metabolism of different alkyne-fatty acid tracers in various cardiac setups; (II) to study cardiac triglycerides pool; (III) to follow the effect of erucic acid on cardiac lipid accumulation; and (IV) to study influence of hypoxia and oxidative stress on lipid metabolism and remodeling.

(I) Alkyne-fatty acid tracers allowed to follow lipid metabolism in heart lysates, H9c2 cells, viable slices and isolated perfused heart (Langendorff heart). Medium-chain alkyne-fatty acids were catabolized more intensively than long-chain alkyne-fatty acids, whereas long-chain alkyne-fatty acids were the preferred substrate for the cardiac anabolism. The fatty acid length influenced the distribution of the tracer within major lipid classes. Modification of alkyne-palmitic and alkyne-linoleic acid-derived phosphatidylcholines was observed. (II) ATGListatin caused significant accumulation of triglycerides, supporting the existence of cardiac triglycerides pool with a high turnover. ATGListatin slowed down the triglycerides cycling speed and caused lipid droplet accumulation. (III) Erucic acid affected metabolism of common dietary long-chain fatty acids (neutral lipid accumulation, arachidonic acid-containing phosphatidylinositol amount, acyl-carnitines formation), systematically influenced cardiac lipidome (total lipid amount, neutral-to-polar lipids ratio, long-chain species enrichment) and caused lipid droplet accumulation and enlargement. (IV) Hypoxia and oxidative stress resulted into persistent changes in polar-to-neutral lipid ratio, alterations in membrane phospholipid biosynthesis and remodeling.

This study pioneered the application of alkyne-fatty acid tracers in cardiac setup and showed differences in various fatty acid handling by the heart under physiological and pathological conditions. This project confirmed the existence of the cardiac triglycerides pool and showed the effect of erucic acid on cardiac lipid accumulation.

Abbreviations

ATGL	Adipose triglyceride lipase
ATGLi	ATGListatin
ATP	Adenosine triphosphate
Av.	Average
BSA	Bovine serum albumin
C171-73; C175-73/75/77	Different azide-reporters for mass spectrometric detection of alkyne-lipids
C atom	Carbon atom number in the side chain
CAR	Carnitine
CE	Cholesterol ester
CER	Ceramide
Cpt1	Carnitine palmitoyltransferase I
DAPI	4′,6-Diamidin-2-phenylindol
db	Double bonds number
DG	Diacylglycerol
DMEM	Dulbecco's Modified Eagle Medium
DMSO	Dimethyl sulfoxide
DTT	Dithiothreitol
dUTP	2´-Deoxyuridine, 5´-Triphosphate
EGTA	Ethylene glycol-bis(β-aminoethyl ether)-N,N,N′,N′-tetraacetic acid
FA	Fatty acid
FA;Y	Alkyne-fatty acid
FA10:0	Capric acid
FA16:0	Palmitic acid
FA22:1	Erucic acid
FA11:0;Y	Alkyne-capric acid
FA12:0;Y	Alkyne-lauric acid
FA16:0;Y ($^{13}C_6$)	Alkyne-palmitic acid (even-numbered version with 6 isotopes)
FA17:0;Y	Alkyne-palmitic acid (odd-numbered version)
FA18:2;Y	Alkyne-linoleic acid
FA19:1;Y	Alkyne-oleic acid (odd-numbered version)
FBS	Fetal bovine serum
GlcCer	Glucosylceramides
HexCer	Hexosylceramide

ID	Intercalated disc
IOD	Integrated optical density
IS	Internal standard
LD540	Lipophilic dye for lipid droplets staining
LPA	Lysophosphatidyc acid
LPC	Lysophosphatidylcholines
LPE	Lysophosphatidylethanolamines
M-199	Medium-199
MG	Monoacylglycerol
MFQL	Molecular fragment query language
MS	Mass spectrometry
N	Nucleus
NL	Neutral lipids
P/S	Penicillin-streptomycin
PA	Phosphatidic acid
PBS	Phosphate buffered saline
PC	Phosphatidylcholine
PE	Phosphatidylethanolamines
PFA	Paraformaldehyde
PG	Phosphatidylglycerol
PIP2	Phosphatidylinositol 4,5-bisphosphate
PIPs	Phosphatidylinositol polyphosphates
PL	Polar lipids
PS	Phosphatidylserine
SDS	Sodium dodecyl sulfate
SM	Sphingomyelin
St. dev.	Standard deviation
TG	Triacylglycerol
Tdt	Terminal deoxynucleotodyl transferase
TLC	Thin layer chromatography
;Y	Terminal triple bond
;Y1	Single-labelled / one terminal triple bond
;Y2	Double-labelled / two terminal triple bonds
;Y3	Triple-labelled / three terminal triple bonds

1. Introduction

1.1. Cardiovascular diseases and cardiac remodeling

Cardiovascular diseases are the leading cause of mortality worldwide and remain an enormous medical and societal burden. Heart failure can be disabling and can severely reduce patient's life quality. Even though there is significant improvement in treatment of cardiac diseases, the mortality rate still remains very high. The number of patients diagnosed with cardiovascular diseases and financial burden are expected to grow further in the future due to population ageing. Therefore, the search for better treatment strategies and markers for early cardiac diseases identification are one of the major challenges in cardiology field nowadays (Neubauer, 2007; Palm et al., 2022; Sternberg et al., 2023; World Health Organization, 2023).

When the heart is exposed to some physiological (high-level athletes) or pathological stimuli (hypoxia, oxidative stress), this organ can undergo certain adaptations, that allow it to temporally adapt and compensate for loss of contracting elements. The observed persistent changes in myocardium structure, function and metabolic patterns are collectively termed as cardiac remodeling (Huang et al., 2016). Typically, cardiac remodeling is observed in the left ventricle first and includes molecular (changes in genes expression, cytoskeletal proteins, intracellular signaling, altered energy metabolism and substrate preference), cellular (apoptosis, necrosis, cardiomyocytes shape and size changes and impairment of the contractile ability), physiological (changes in ejected volume and decline in pumping capacity) and anatomical changes (altered geometry of the left ventricle). Interestingly, these changes seem to be similar irrespectively of the etiology of the original cause and can persist even if the initial stressor is quickly removed. Cardiac remodeling is typically observed in cardiovascular diseases such as myocardial ischemia reperfusion injury, hypertension, valvular heart diseases, myocarditis and dilated cardiomyopathy. While the heart might benefit from these adaptations on a short run, if proceed over longer period of time, these changes could become harmful and could cause irreversible damage to myocardium, which could eventually lead to the heart failure. Relationship between cardiac remodeling and the heart failure progression is depicted on the figure 1. While current therapies focus primarily on attenuation of the heart failure progression and support the work of the remaining healthy myocardium, modulating or even reversing the cardiac remodeling

might be a potential alternative therapeutic strategy for prevention of the progression of the heart failure. Since the cardiac remodeling is a complex and dynamic process that is not completely described, understanding mechanisms, patterns and drivers of the cardiac remodeling onset and progression is of high medical interest (Takano et al., 2003; Fedak et al., 2005; Udelson and Konstam, 2011; Da Dalt et al., 2023).

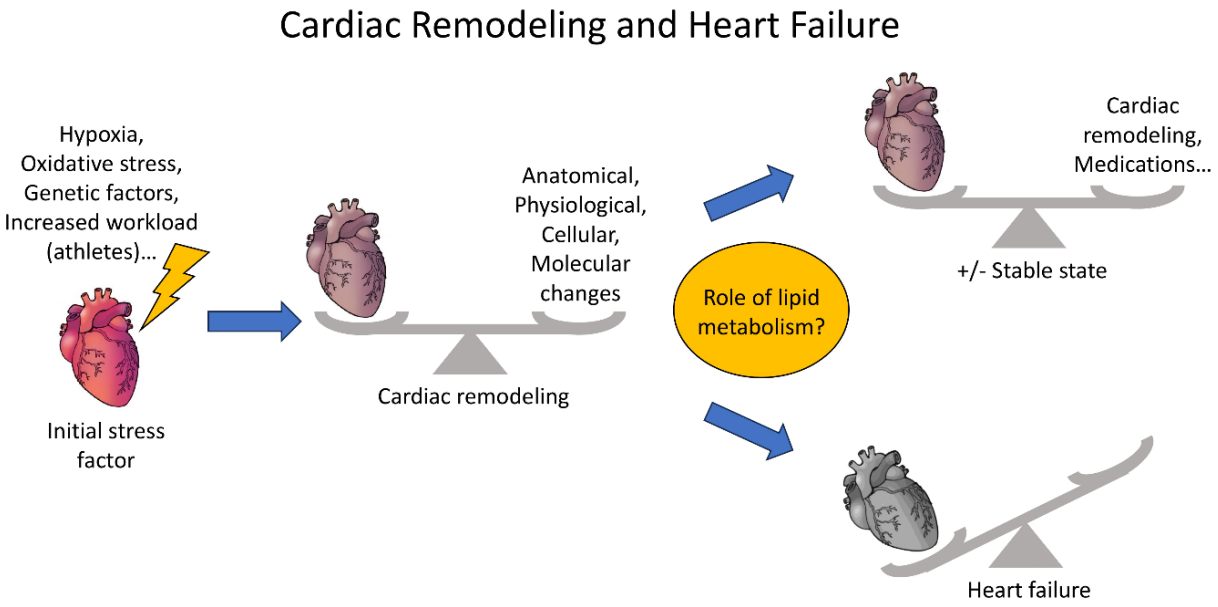

Figure 1: Schematic representation of the relationship between cardiac remodeling and the risk of the heart failure progression. An initial stressor (hypoxia, oxidative stress, etc.) might induce cardiac remodeling to compensate for the loss of myocytes and to maintain stable heart work. Cardiac remodeling might include anatomical, physiological, cellular and molecular changes, and could allow to keep the heart work in a more or less stable state. At some point these adaptations might become maladaptive and cannot meet the heart requirements anymore. This decompensation would eventually lead to imbalance and the heart failure.

1.2. Role of lipids in a healthy and diseased heart

Lipids, a class of chemically diverse group of hydrophobic molecules, are essential for uninterrupted heart functioning. These molecules are formed by combination of fatty acids and various backbone structures and are classified into fatty acids, glycerolipids (mono-, di- and triacylglycerols), glycerophospholipids (e.g. phosphatidylcholines), sphingolipids (sphingomyelins, glucosylceramides, ceramides, lactosylceramides), sterol lipids, prenol lipids, saccharolipids, and polyketides (Fahy et al., 2005). Lipids

serve as major membrane components and cover other functions essential for any cell existence, including signaling, protein modification and energy storage. The last one is of particular importance for the heart, since the heart is the organ with highest energy turnover in the body and has enormous energy requirements to sustain its intense mechanical work (Neubauer, 2007). Although the adult heart can rely on a wide range of substrates for the energy production, the constantly high energy demand is primarily supported by β-oxidation of fatty acids (Lopaschuk et al., 2010). Heart can store enough energy to sustain only three beats, making it extremely sensitive to disturbances in the oxygen and nutrients supply (Palm et al., 2022). Thus, lipids play an important role in the heart homeostasis, metabolic processes and contractile function.

Alterations in metabolism and composition of glycerolipids, glycerophospholipids, sphingolipids and sterol lipids have been long reported in heart diseases and are thought to contribute to irreversible changes in ischemic myocardium (Chien et at., 1983; Schulze et al., 2016). The observed lipid changes in a diseased heart could be categorized into changes in membrane lipid composition, abnormalities in fatty acid oxidation and aberrant bioactive lipid signaling.

1.2.1. Lipids as essential cardiac membrane components

Lipids are an essential structural component of cellular membranes and their normal composition is crucial for proper membranes functioning (Das et al., 1986). This holds especially true for the cardiac cells, due to their continuous contraction and relaxation. The membrane connects tightly to the cytoskeleton in cardiac cells, indicating that the alterations in membrane properties will result in direct biological actions and might affect the health of the whole organ (Samarel, 2014). Uninterrupted signal conduction is also crucial for synchronized myocytes contraction. This makes cardiac health highly dependent on membrane glycerophospholipid composition.

Alterations in glycerophospholipid metabolism and membrane lipid composition might cause the mechanical fragility of cardiomyocytes, loss of membrane integrity and irreversible heart tissue injury (Ježová et al., 2002). Both diet and stress factors (chronic hypoxia, acute ischemic insult and epinephrine administration) can change the fatty acid composition of the glycerolipids in the heart muscle (Benediktsdottir and Gudbjarnason, 1988). Mice, exposed to high-altitude hypoxia simulated in hypobaric chamber,

experienced significant alterations in fatty acid composition of glycerophospholipids in heart ventricles (Ježová et al., 2002). Detectable changes in membrane lipid composition, depletion of membrane phospholipids and defects in cardiac membrane systems were observed in patients with heart failure, myocardial ischemia and other cardiac disorders (Chien et al., 1983; Das et al., 1986).

1.2.2. Lipids as an important energy source

The heart requires enormous energy amounts for its continuous uninterrupted work. Although the heart is considered to be a metabolic omnivore, fatty acids are the major energy source in the healthy adult heart (Lopaschuk et al., 2010, Kienesberger et al., 2013 (A); Heier and Haemmerle, 2016).

Abnormalities in the fatty acid oxidation for the energy production are commonly observed in many pathologies, like ischemia, sepsis and diabetic cardiomyopathies. Under those conditions the oxidation of fatty acids is significantly reduced, and the heart switches to anaerobic glycolysis as a compensatory mechanism (Schulze et al., 2016; Da Dalt et al., 2023). On the long run this metabolic switch leads to the energy deficit and accumulation of toxic lipid species (Neubauer, 2007).

1.2.3. Cardiac triglycerides pool

The heart heavily relies on a constant flow of exogenous fatty acids, since the heart cannot produce fatty acids by itself and typically does not store them in big amounts (Lopaschuk et al., 2010). It has been long discussed, what happens to fatty acids, once they come from circulatory system and enter cardiac cells: do fatty acids get directly completely oxidized for the energy production or does some fraction of them get esterified and temporarily stored as triglycerides?

Several pioneer studies suggested the existence of the cardiac triglycerides pool with an extremely high turnover. It has been reported that a significant proportion, if not the majority, of fatty acids that enter the cardiomyocyte are shuttled through the intracellular triglycerides pool for the temporary storage prior to oxidation (Banke et al., 2010). The cardiac triglycerides pool is believed to be never static and is thought to be continuously undergoing cycles of resynthesis and breakdown (lipolysis). The cardiac triglyceride

pool turnover appears to be the most rapid when compared to any other organ, including liver and adipose tissue (Saddik and Lopaschuk, 1991; Banke et al., 2010; Kienesberger et al., 2013 (A)).

The synthesis and breakdown of cardiac triglycerides plays an important role in bioavailability of fatty acids for the energy production as well as allows to prevent lipotoxicity by sequestering excess of fatty acids within lipid droplets (Heier and Haemmerle, 2016). Due to its high biological importance, the formation and breakdown of triglycerides pool is tightly regulated by plethora of enzymes and is highly influenced by hormones and exogenous substrate availability (Heier and Haemmerle, 2016). Typically, the myocardial intracellular triglycerides pool is very low, but tends to increase in various (patho)physiological situations, such as the heart failure, metabolic syndrome, obesity, starvation, aging and exercise, suggesting that the cardiac steatosis (lipid accumulation in the heart) might be a relatively common event in humans (Sharma et al., 2004; Kienesberger et al., 2013 (A); Heier and Haemmerle, 2016). *Per se*, triglycerides accumulation is not considered toxic by itself but is thought to be rather a sign of ongoing pathological processes and lipotoxicity (D'Souza et al., 2016). The tight connection of triglycerides metabolism to other lipid metabolic networks and signaling pathways highlights the role of a proper balance between triglycerides synthesis and breakdown in maintaining the healthy heart functioning (Sharma et al., 2004; Kienesberger et al., 2013 (A); Schulze et al., 2016; Oenarto, 2020).

Importance of the coordinated synthesis and breakdown of triglycerides could be confirmed by several mice models with knockouts or overexpression of central genes responsible for triglycerides balance. Mice lacking both working alleles of adipose triglyceride lipase (ATGL) – the rate-limiting enzyme for triglycerides hydrolysis – experienced cardiac steatosis and severe triglycerides accumulation in the heart. Absence of ATGL caused a massive triglycerides accumulation in all tissues of the body with the most pronounced triglycerides accumulation observed in cardiac and skeletal muscle, testis, kidney and pancreas. The observed massive lipid accumulation in cardiomyocytes caused cardiac failure and premature death of these mice (Haemmerle et al., 2006; Zimmermann et al., 2009; Kienesberger et al., 2013 (B)). However, it is not entirely clear, whether the impaired cardiomyocyte contraction in ATGL-deficient mice is primarily due to excessive triglycerides accumulation or alterations in signaling pathways (Kienesberger et al., 2013 (A)). On the other hand, the cardiac-specific

overexpression of ATGL could protect against obesity-induced cardiac disfunction and prevent cardiac steatosis (Pulinilkunnil et al., 2014). There are recorded cases of patients with ATGL deficiency, who suffered from heart failure and required cardiac transplantation. In this pathologic condition, termed as triglyceride deposit cardiomyovasculopathy, the marked increase of cardiac triglycerides was also observed (Fischer et al., 2007; Li et al., 2019; Kobayashi et al., 2020).

Although, many studies have provided a significant insight into complexities of myocardial triglycerides metabolism and its importance for cardiac health, much remains to be elucidated in in terms of the triglyceride pool kinetics and its behavior depending on fatty acids side-chain diversity.

1.2.4. Erucic acid-induced cardiac steatosis

Not only stress factors and diseases, but also diets rich in erucic acid have shown to cause excessive neutral lipid deposition in the heart. Erucic acid (docos-13-enoic acid, FA22:1) is a monounsaturated fatty acid, which is widely abundant in seeds of the family Brassicaceae (e.g., in rape seed, mustard seed, seeds from cabbages, turnips and kales). Until 1970s this fatty acid was widely abundant in the rapeseed (canola) oil – one of the most consumed edible vegetable oils used for cooking and in farming as a cost-efficient lipid substitute of more expensive fish oils (Carré and Pouzet, 2014; Knutsen et al., 2016; Wang et al., 2022; Liu et al, 2024).

Erucic acid was shown to be able to impair mitochondrial lipid oxidation and cause myocardial lipid accumulation in chicks, rats and farmed fish, when the animals were fed with diets rich in this fatty acid (Abdellatif, 1972; Stam et al., 1980; Chen et al., 2020; Liu et al, 2024; Ma et al., 2024). These experiments lead European Union, New Zealand and Australia to introduce stricter regulations and to set the maximum allowed limit of erucic acid in foods (Dorni et al., 2018). The rapeseed plants, bred for the food purposes, have been selected to be low in erucic acid to ensure food safety. Plants with elevated erucic acid content are still grown commercially, but are used only in oleochemical industry (Knutsen et al., 2016; Wang et al., 2022). However, rapeseed and mustard oils that are rich in erucic acid are still consumed in some regions of India and China (Laryea et al., 1992; Dorni et al., 2018).

Interestingly, while erucic acid is thought to have a negative impact on the heart, this fatty acid was suggested to be a potential remedy for X-linked adrenoleukodystrophy. X-linked adrenoleukodystrophy is a genetic disorder, characterized by damage to nervous system, adrenal cortex and testis. This disease is a result of accumulation of saturated very-long chain fatty acids that happens due to inefficiency of peroxisomal fatty acid β-oxidation (Moser et al., 2007). Dietary supplementation of erucic acid was found to be able to improve the symptoms of the patients with this disease. In a historically famous case (also later depicted in a movie "Lorenzo's oil" from 1992) Augusto and Michaela Odone, parents of Lorenzo Odone, a patient with X-linked adrenoleukodystrophy, introduced "Lorenzo's oil" – a 4:1 mixture of glyceryl trioleate and glyceryl trierucate – which significantly improved the boy's condition (Odone and Odone, 1989). The mechanism by which Lorenzo's oil exerts its action, might include competitive inhibition of ELOVL 1 (elongation of very long-chain fatty acid 1) – the primary enzyme responsible for the endogenous synthesis of saturated and monounsaturated very-long-chain fatty acids (Bourre et al., 1976; Sassa et al., 2014). While some studies doubt the beneficial effect of erucic acid, the Lorenzo's case, as well as recent studies suggested that Lorenzo's oil could have a preventive effect and might slow the disease progression (Aubourg et al., 1993; Koehler and Sokolowski 2005; Moser et al., 2005; Murphy et al., 2008). In clinical studies of Lorenzo's oil application no adverse cardiac effects have been observed, but moderate reduction in platelet counts was recorded in 30-40 % of patients (Kickler et al., 1996).

Due to still ongoing debates on possible adverse effects of erucic acid on the heart health and its potential benefits for patients with X-linked adrenoleukodystrophy, gaining a deeper understanding of erucic acid mechanism of action on neutral lipid accumulation in different tissues is of high interest.

1.2.5. Aberrant bioactive lipid signaling in the diseased heart

Aberrant bioactive lipid signaling is believed to play a central role in the onset of cardiac diseases. Impairments in fatty acid oxidation could promote accumulation of bioactive lipid species and negatively affect cardiac intracellular signaling pathways. Although there might be many potentially toxic intracellular lipids, diacylglycerols and sphingolipids are the most studied bioactive lipid species so far and are believed to be

the major drivers of cardiac lipotoxicity – a process of toxic lipid species accumulation in the heart, which impairs the functioning of this organ (Schulze et al., 2016; Da Dalt et al., 2023).

Growing number of studies show important role of sphingolipids in progression of cardiovascular diseases, including ischemic heart disease, hypertension, heart failure and stroke. (Schulze et al., 2016; Wittenbecher et al., 2021; Zietzer et al., 2022). In isolated rat hearts subjected to ischemia-reperfusion decreased levels of sphingomyelins with a corresponding increase in ceramides were observed (Cordis et al., 1998). Heart biopsies from patients experiencing ischemia showed elevated levels of glucosylceramide and lactosylceramide, while in healthy hearts levels of these lipid species are typically very low. Knockout mice lacking glucosylceramide synthase in the heart develop heart failure and left ventricular dilatation and die prematurely. In these mice the endolysosomal retrograde trafficking and autophagy were defective, and the responsiveness to beta-adrenergic stimulation was reduced. This indicated that in the absence of glucosylceramide synthase, the internalization and trafficking of β1-adrenergic receptors was suppressed, suggesting that cardiac glycosphingolipids are required to maintain β-adrenergic signaling and contractile capacity in cardiomyocytes and to preserve normal heart function. (Andersson et al., 2021). Altering sphingolipid metabolism may represent a new promising therapeutic approach (Schulze et al., 2016; Mitsnefes et al., 2018; Andersson et al., 2021). Indeed, many available medications target sphingolipid metabolism (Kovilakath and Cowart, 2020). It was suggested that selected sphingolipids could serve as markers for prognosis of cardiovascular diseases in clinics (Wittenbecher et al., 2021).

To sum up, under stress conditions certain systemic changes in the cardiac lipid metabolism are observed. However, it is still not entirely clear, which of the above-mentioned processes – alterations in cardiac membrane lipid composition, abnormal fatty acid oxidation, triglycerides pool imbalances, excessive lipid deposition or aberrant bioactive lipid signaling – contribute the most to the development of heart diseases and eventually lead to the heart failure. Understanding lipid metabolism patterns in healthy and diseased hearts and search for novel reliable lipid markers for cardiomyopathies identification remain the actual challenge in the cardiac research.

1.3. Lipid tracing in the heart

1.3.1. Challenges in lipid tracing

Lipid alterations in cardiovascular diseases are highly complex. In order to study dynamic changes in cardiac lipid metabolism methodology for lipid tracing is required. However, in contrast to other molecules like proteins or nucleic acids, there are very limited tools available for lipid tracing. Lipids do not have genetically-encoded toolkit available and no antibodies could be synthesized against them, making lipid tracing in complex cellular systems a challenge (Pistritu et al., 2023).

1.3.2. Fatty acid side-chain diversity

The structural diversity of fatty acids introduces an additional dimension of complexity into the lipid tracing. Fatty acids' side-chain significantly varies in length and saturation degree, as depicted on the figure 2. Based on their length, fatty acids are classified into (I) long-chain fatty acids – fatty acids that have 14 or more carbon atoms in the acyl chain; (II) medium-chain fatty acids (e.g., decanoic acid) have 8-12 carbons; and (III) short-chain fatty acids with 6 carbons or less. Most natural fatty acids have an even number of carbons in the side chain. Depending on the number of double bonds (saturation degree) fatty acids are divided into (A) saturated fatty acids (e.g., palmitic acid), meaning that they do not have any double bonds; (B) monounsaturated fatty acids (e.g., oleic acid) have one double bond; (C) polyunsaturated fatty acids (e.g., linoleic acid) have more than one double bond (Chow, 2008). The fatty acids' chemical structure influences water solubility and lipophilicity, which in its turn might have a huge impact on the receptor-ligand recognition, transport, uptake and metabolism of these molecules (Papamandjaris et al., 1998). Typically, diets do not solemnly consist of one fatty acid but represent a mixture of them. Various diets (e.g., Western diet patterns, Mediterranean diet, Nordic diet, Medium Chain Triglyceride diet) have a highly variable fatty acids content. While olive oil, common for Mediterranean diet, is high in unsaturated long-chain oleic acid, other foods like coconut butter, palm kernel oil and diary milk, have high saturated medium-chain fatty acid content. Therefore, any lipid tracing technology should be able to cover this structural diversity and resulting differences in biological effect, and, ideally, also allow to follow metabolism of several fatty acids in parallel to mimic natural fatty acid content in diets.

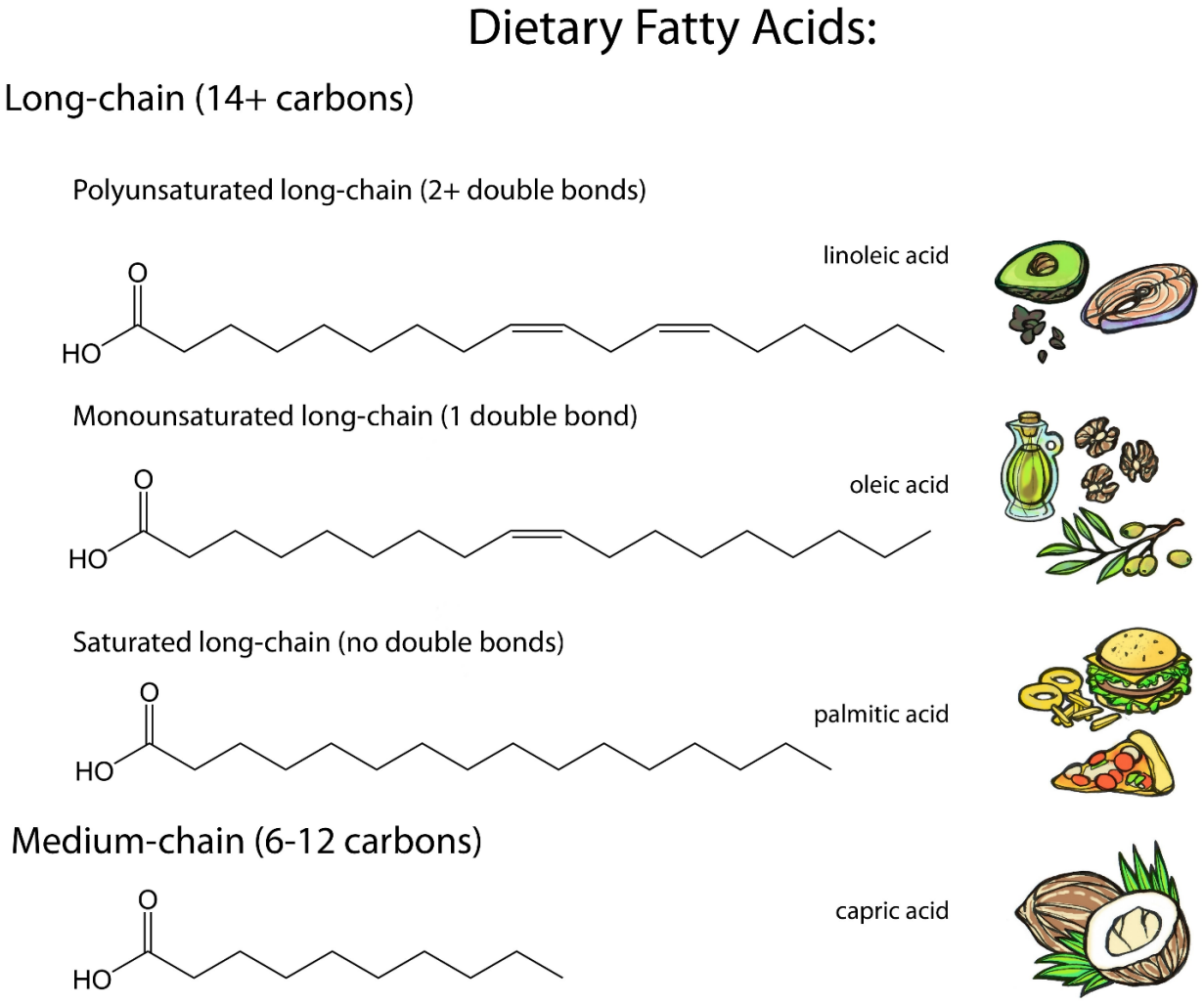

Figure 2: Fatty acid classification by number of carbons in the acyl chain and double bond count (saturation). Most natural fatty acids have an even number of carbons in the side chain. Representative fatty acid with its chemical formula and common name is depicted for each group, and some foods rich in corresponding fatty acid are shown.

1.3.3. Alkyne-fatty acid tracers

Alkyne-fatty acids reflect the chemical diversity of natural fatty acids, and, thus, allow to study the biological action of these molecules depending on their length and saturation degree. Moreover, recent advances in alkyne-lipid technology and mass spectrometry allow to trace several fatty acids simultaneously (Thiele et al., 2019). Alkyne-lipids emerged as a non-radioactive, easy-to-handle, relatively cheap and highly sensitive alternative to the earlier used radio-, isotope-, spin-labelled lipid analogs and fluorescent probes (Thiele et al., 2012; Kuerschner and Thiele, 2014). Briefly, alkyne-fatty acids are analogs of natural fatty acids that have triple bond at the end of the acyl chain. These

tracers could be applied to almost any biological system and are then incorporated into cellular lipids. Upon the click-reaction with a corresponding azide-tracer in the presence of copper (I) as a catalyst, the triazole ring is formed, and the reporter molecule is attached to the alkyne-group, as shown on the figure 3 (Thiele et al., 2012). Thereafter, alkyne-lipids could be detected via mass spectrometry, thin layer chromatography and fluorescent microscopy (Thiele et al., 2012; Gaebler et al., 2016; Hofmann et al., 2017; Thiele et al., 2019; Kuerschner et al., 2022; Wunderling et al., 2023). As agreed within the lipid research community, alkyne-lipids get a suffix ";Y" in their naming to be easily distinguishable from the natural lipids present in the cell (LIPID MAPS, 2025). For example, alkyne-linoleic acid will get a name FA18:2;Y according to this nomenclature.

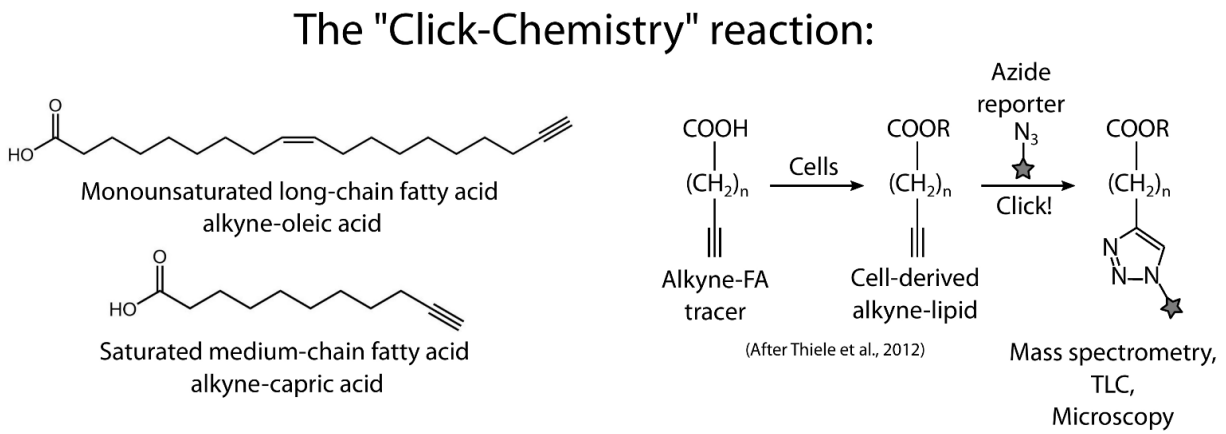

Figure 3: A schematic representation of the click-chemistry reaction. Fatty acid tracers of a varying side-chain length and saturation degree containing terminal alkyne group are fed to cells and are incorporated into cellular lipids. Thereafter the click-reaction with an azide-reporter is performed, and triazole ring is formed allowing to attach the reporter to newly synthesized lipids. The labeled lipids could be identified via mass spectrometry and thin layer chromatography or visualized via fluorescent microscopy. The figure is adapted after Thiele et al., 2012.

1.3.4. Mass spectrometric tracing of alkyne-lipids

Alkyne-fatty acid tracing combined with mass spectrometric analysis of lipids emerged as a powerful tool to investigate various aspects of lipid metabolism with high resolution and sensitivity (Thiele et al., 2019; Kuerschner and Thiele 2022; Wunderling et al., 2023). Lipidomics is a rapidly growing discipline that studies a wide spectrum of lipids and has already provided novel valuable data on pathogenesis of cardiovascular disease and mechanisms of lipid-based diseases, and is a valuable tool for biomarker discovery and monitoring of therapeutic efficacy (Park et al., 2015; Paapstel et al., 2018).

Alkyne-lipid mass spectrometric tracing became possible with the development of C171-73 azide-reporter and its variations: C175-73, C175-75 and C175-77. Upon the click-reaction one of these azide-reporters is attached to alkyne-lipids from the sample, and the resulting product gets a permanent positive charge that enhances it mass spectrometric detection. C171 or C175 stay for the mass shift of the lipid species by 171 Dalton or 175 Dalton, respectively, when lipid species are analyzed in the positive mode in the mass spectrometer. For glycerolipids, sterol esters, ceramides, fatty acids and their simple derivatives upon increasing collision energies this isolated ion is predictably fragmented with a neutral loss of 73, 75 or 77 Dalton. Complex lipids with more labile bonds, especially glycerophospholipids (phosphatidylcholines, phosphatidylethanolamines, phosphatidic acid and phosphatidylinositol) fragment by a combined neutral loss of 73, 75 or 77 Dalton together with the phospho-head group, leading to a characteristically different neutral loss for each phospholipid class. Samples clicked to C175-73, C175-75 or C175-77 azide-reporters could be combined (multiplexed) in one pool, allowing to handle and analyze three samples simultaneously. The labeled molecules that react with C175-73, C175-75 or C175-77 reporters have identical mass shift of 175 Dalton, but different neutral loss peaks (Thiele et al., 2019; Kuerschner and Thiele, 2022; Wunderling et al., 2023). The advances in mass spectrometric lipid tracing are schematically depicted on the figure 4.

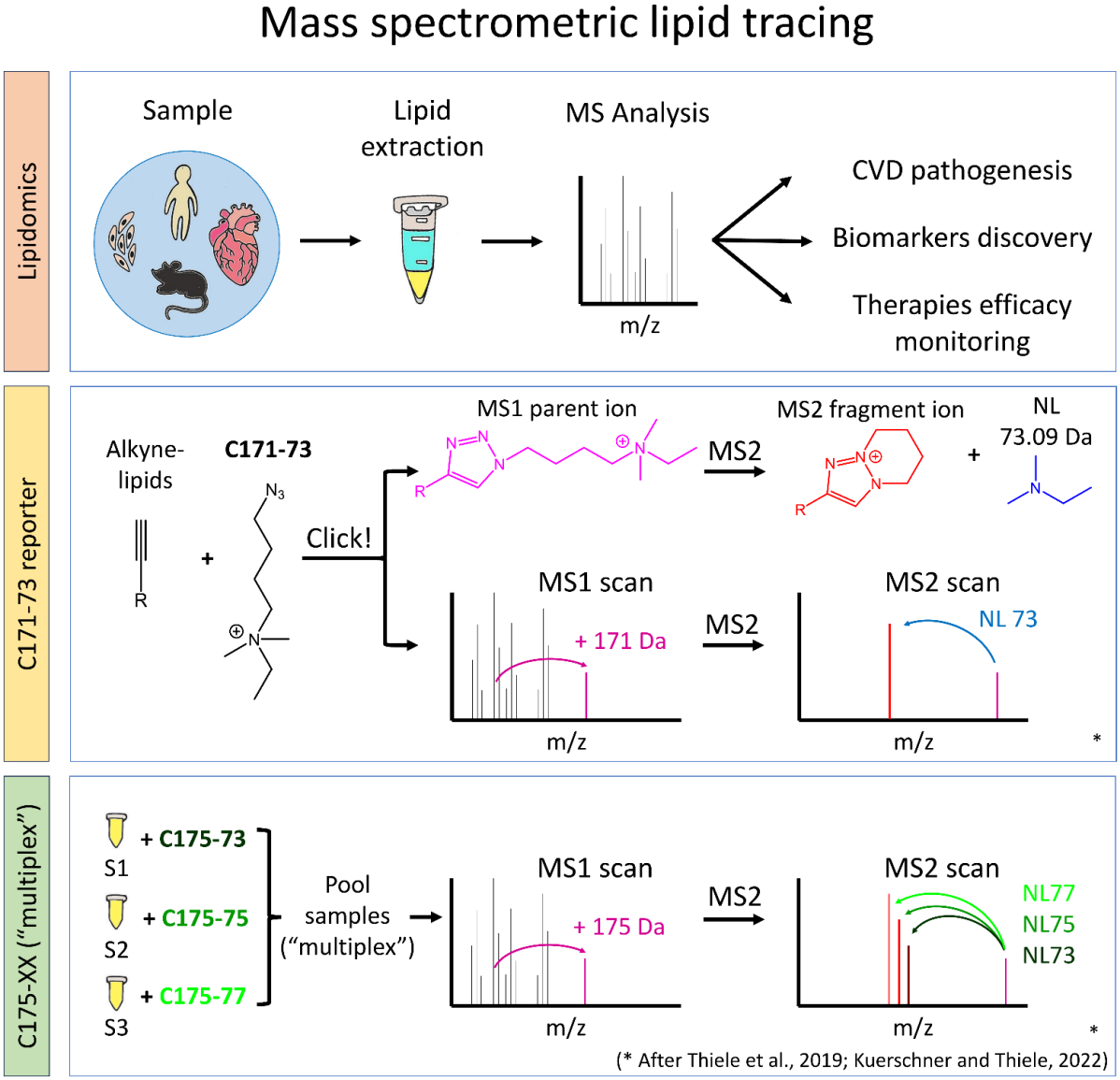

Figure 4: Schematic representation of different mass spectrometric lipid tracing technologies. Lipidomics is a rapidly growing field which aims to describe the complete lipid profile within the biological sample. It had already provided significant insights into pathogenesis of cardiovascular diseases and is a valuable tool for biomarkers discovery and monitoring of therapies efficacy. C171-73 and C175-XX reporters are advancements in mass spectrometric lipid detection, allowing to specifically trace alkyne-lipids in the sample separately from other cellular lipids. C171-73 azide-reporter could be attached to alkyne-lipids via the click-reaction. The resulting product (magenta, see MS1 scan) gets a permanent positive charge and mass shift of 171 Dalton. Upon increasing collision energies the isolated parent ion (magenta) is predictably fragmented with a neutral loss of 73.09 Dalton (blue). The newly-formed positively-charged MS2 fragment ion (red) could be registered on the MS2 spectra. C175-XX is a set of azide-reporters, that allow to combine (multiplex) several samples to speed up their handling and analysis. Here samples 1 to 3 are click-reacted with one of C175-XX azide-reporters (C175-73, C175-75 or C175-77) and are thereafter pooled together. Alkyne-lipids that react with C175-73, C175-75 or C175-77 reporters have an identical mass shift of 175 Dalton observed on MS1 scan, but different neutral loss peaks of 73, 75 or 77 Dalton (greens). On MS2 scan three different fragment ions are registered (reds). Abbreviations: CVD, cardiovascular diseases; Da, Dalton; m/z, mass-to-charge; MS, mass spectrometric; MS1, mass spectra of the whole molecule; MS2, mass spectra of fragments formed from the selected mass window upon certain collision energies; NL, neutral loss; R, rest of the molecule; S, sample. C171-73 and C175-XX figures are adapted after Thiele et al., 2019; Kuerschner and Thiele, 2022).

1.3.5. Compound tracing in the heart

Patients' cohort studies have been extensively used for studying metabolic alterations in cardiovascular diseases. However, human data represents majorly a static snapshot at a certain timepoint and gives only partial information about complex metabolic networks in the heart. Also, patients' data is often quite heterogeneous with many variables unknown or not controlled. Therefore, compound tracing in a laboratory setup with only few changeable parameters could provide a valuable complimentary piece of information in addition to human studies (Milani-Nejad and Janssen, 2014).

Animal models allowed to make a significant progress in understanding the pathology and progression of cardiovascular diseases. Nevertheless, the choice of animal model should be done with caution, since there is no perfect animal model of a human heart available, and each has their strengths and limitations. Hearts of different animals have evolved differently regarding the needs of that species; thus, experimental data should be interpreted with caution when translated to humans. Mice and rats are the most commonly used mammals in the cardiovascular research. These animals are widely used to study cardiac disease development and progression, genetics, pharmacology and long-term effects. Major advantages of using rodents include lower maintenance cost and lower gestation time compared to larger animals. Also, numerous genetic models and toolkits are available for rodents, making them indispensable for the cardiology field. However, major differences (like higher heart rate in rodents) should also be taken into consideration when comparing the experimental outcomes to human data. Obviously, no rodent model will be able to completely recapitulate all the aspects of human cardiac diseases, but will at least partially mimic some of them, allowing to gain a deeper understanding of heart physiology in health and disease (Milani-Nejad and Janssen, 2014; Joukar et al., 2021).

Heart is a very delicate organ, that is extremely sensitive to any environmental changes. This makes compound tracing experiment in the heart quite tricky. The feeding of a tracer to an animal might help to avoid this problem and represents the most physiological setup. However, the downside of feeding a compound to an animal might be the inter-organ cross-talk and possible influence of other metabolically active organs on the results. Currently, no organ-specific lipid tracers for feeding to mammals have been developed. Also, feeding a tracer molecule to an animal might be quite costly and requires many animals for statistically significant results. Heart lysates, cardiac cell lines,

viable heart slices and Langendorff heart allow to study heart metabolism without the influence of other organs. Strengths and weaknesses of these methods are summarized on the figure 5.

Tissue lysates are an easy approach, highly suitable for testing many conditions in parallel and studying catabolism of fatty acids. Alkyne-fatty acid tracers have been successfully tested earlier on the liver lysates to study fatty acid β-oxidation (Kuerschner et al., 2022). The downside of this methodology is that the tissue architecture and intracellular compartments are disrupted during the sample preparation, making this method not suitable for studying anabolic pathways.

Primary heart cells and cardiac cell lines have been extensively used for compound screening and drug testing. Few immortalized cardiac cell lines are available (e.g., H9c2 cells) and represent an animal-free alternative to the other methods. H9c2 cells are an immortalized cell line that was originally derived from the embryonic rat ventricular tissue (Kimes and Brandt, 1976). H9c2 cells are extensively used for studying signaling pathways, cardiac metabolism and cardiac hypertrophy, and have proved to accurately mimic hypertrophic response when compared to primary cardiomyocytes (Watkins et al., 2011). Even though H9c2 cells cannot beat, they show many confirmed similarities to primary cardiomyocytes, including membrane morphology, g-signaling protein expression and electrophysiological properties (Hescheler et al. 1991; Sipido and Marban 1991). While cell cultures allow to test many conditions simultaneously with a high throughput, interpretation of the data should be taken with caution in relation to the whole organ, since the heart consists of many interacting cell types.

Viable heart slices have emerged as a useful method to test several conditions on the same heart with medium throughput, while at least partially maintaining the initial tissue architecture, physiology and cell-cell interactions. Viable heart slices are semi-thin slices of myocardium, usually up to 300 µm thickness, which permits oxygen and nutrients to diffuse to cells maintaining them viable even in the absence of the coronary circulation (Watson et al., 2017).

The Langendorff heart represents the most physiological methodology that allows to study the cardiac metabolism separately from other organs. In this technique the heart is rapidly excised from the animal, mounted on a cannula and attached to the Langendorff apparatus. Once attached, the heart is perfused in a reverse fashion via the aorta with nutrient rich, oxygenated and prewarmed solution. The backwards

pressure causes aortic valve to shut, forcing the solution to flow into the coronary vessels, which normally supply the heart tissue with blood. This feeds nutrients and oxygen to the cardiac muscle, allowing it to continue beating for several hours after the heart's removal from the body. As an advantage, the heart is still intact, and tissue architecture and all cellular interactions are present. However, this technique is laborious and only one condition could be tested on one heart, which requires sacrifice of many animals for the study (Liao et al., 2012; Motayagheni, 2017).

Combination of cardiac techniques and highly sensitive alkyne-lipid tracing could provide a deeper insight on the complex lipid network dynamics in the heart. The information gained could be of high interest for better understanding of cardiac lipid metabolism in health and disease, search for markers for identification of early disease onset and development of novel treatment strategies.

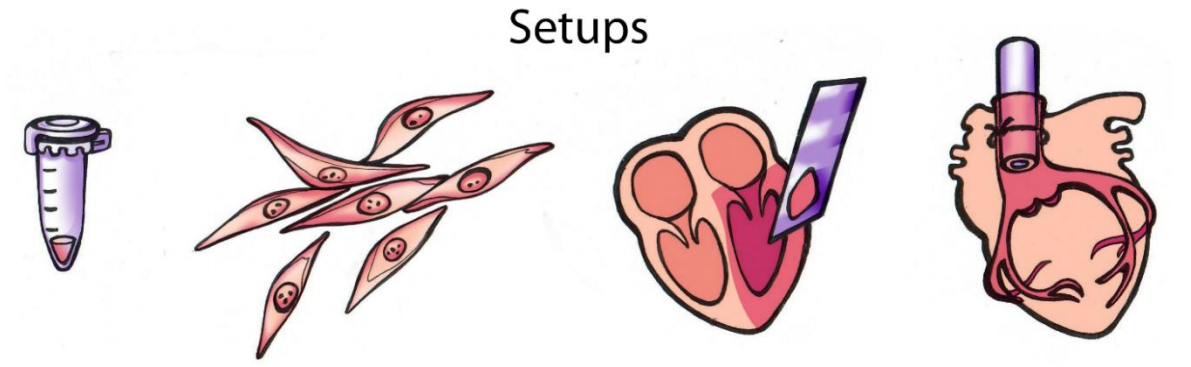

Heart lysates	H9c2 cells	Viable heart slices	Langendorff heart
+ Easy to handle; + Many conditions simultaneously; + Good for catabolism and kinetics studies.	+ Easy to handle; + Many conditions simultaneously; + Animal-free.	+ Tissue architecture is preserved; + Multicellularity, original cell types present; ± Medium difficulty.	+ The most physiological approach; + Tissue architecture is intact, all interactions present.
– No preserved cellular and tissue architecture; – Pathways only partially intact, no intracellular compartments.	– Only a few cardiac cell lines available; – Caution with interpretation since immortalized.	– Low throughput; – Short viability.	– Laborious; – Short viability; – Very low throughput, only one condition can be tested; – Many test animals required.

Figure 5: A schematic representation of some commonly used methodologies for compound tracing in the heart. Methodological toolbox includes, but is not limited to, heart lysates, cell cultures, viable heart slices and the Langendorff heart. Strengths and weaknesses are summarized for each approach. These setups allow to study heart metabolism without the influence of other organs.

2. The aim of the thesis

The existing data on dynamic lipid alterations in the heart is still limited. Alkyne-fatty acid tracers have only been applied once to heart tissues in the earlier work of K. Klizaite in the thin layer-chromatography setup to study major lipid classes formed (Klizaite, 2017). Recent development of azide-reporters allowed a highly sensitive mass spectrometric identification of alkyne-lipids on the lipid species resolution, and more sensitive detection of less abundant lipid classes (Thiele et al., 2019). Additionally, alkyne-fatty acids have not been applied to other cardiac setups so far. Also, alkyne-lipids have not been imaged in the heart via fluorescent microscopy before.

This thesis aims to deepen the understanding of lipid metabolism in a rodent heart under normal and stressed conditions. In this research different alkyne-fatty acid tracers would be used to study lipid metabolism dynamics using advances in mass spectrometric lipid detection and fluorescent microscopy. Several key questions would be addressed:

I. How do alkyne-fatty acid tracers of different length and saturation degree behave in different cardiac setups under non-stressed condition?

II. Does cardiac triglyceride pool exist and what are its kinetics for different fatty acids?

III. Does erucic acid affect cardiac lipid accumulation?

IV. How do cobalt chloride-induced chemical hypoxia and hydrogen peroxide-induced oxidative stress influence metabolism of long-chain fatty acids and phosphatidylcholines remodeling?

3. Materials and methods

3.1. List of materials

3.1.1. Chemicals and reagents

Name	Supplier (Catalog number)	Additional information
Acetic acid	Fisher Scientific (A11350)	MS grade, OPTIMA LC/MS
Acetic acid glacial	VWR International GmbH (20104.298)	TLC grade
Aceton	Fischer Chemical (A/0600/PC17)	-
Acetonitrile	Fischer Chemical (A/0638/17)	LC-MS, 99.9% HPLC
Agarose	Invitrogen (15510-027)	low-melt UltraPure Agarose
Alexa Fluor 488 Picolyl-Azide	Jena Bioscience (CLK-1276-5)	Abs/Em = 494/517 nm
Alexa Fluor 488 Secondary antibody	Invitrogen (A-11001)	Goat anti-mouse IgG antibody; 499/520 nm; 1:500 dilution
Alexa Fluor 555 Secondary antibody	Invitrogen (A-21428)	Goat anti-Rabbit IgG antibody; 555/565 nm; 1:500 dilution
Ammonium acetate	Merck (101116)	$C_2H_7NO_2$ (Mr = 77.08 g/mol)
ATGListatin	TargetMol (TGM-T1875-10mg)	ATGL inhibitor
ATP	Applichem (A1348.0100)	-
3-Azido-7-hydroxycoumarin	(Thiele et al., 2012)	-
2,3-Butanedione-2-monoxime	Cayman Chemical (20828)	$C_4H_7NO_2$ (Mr = 101.1 g/mol)
Boric acid	Merck (1.00160.1000)	H_3BO_3
BSA	Sigma-Aldrich (A7030-100G)	Bovine serum albumin lipid-free, heat shock fractionated
C-171 and C-175-73/75/77 MS azide-reporters	(Thiele et al., 2019)	-
Calcium Chloride	Grüssing (10234)	$CaCl_2$ x2H_2O (Mr = 147.02 g/mol)
Capric acid	Merck Chemicals (C1875-100G)	-
Carbogen	Air Liquide (P3750V12R2A001)	5 % CO_2, 95 % O_2
Carnitine	TCI (C3058)	L-Carnitine hydrochloride
Chloroform, MS grade	Sigma Aldrich, Merck (67-66-3)	MS grade, Stabilized with 0.6 % Ethanol
Chloroform, TLC grade	Fisher Chemical (67-66-3)	TLC grade, >= 99.8 % analytical reagent grade
Cobalt Chloride	Merck Chemicals (202185-25G)	Cobalt(II)-Chloride Hexahydrate
Coenzyme A	Calbiochem (234101-100)	Coenzyme A trulithium salt
Copper (I) tetrafluoroborate	TCI (T2666)	$C_8H_{12}BCuF_4N_4$

Name	Supplier (Catalog number)	Additional information
DAKO	Dako (S3023)	Dako Fluorescence Mounting Medium
DAPI	Applichem (A1001)	4',6-Diamin-2-phenylindol
Dimethyl sulfoxide	Sigma-Aldrich (D8418-50ML)	-
Disodium hydrogen phosphate	ChemSolute (8622.0500)	Na_2HPO_4 x2H_2O
DMEM Media	Thermo Fisher Scientifc Inc. (31966047)	High glucose, GlutaMAX™ supplement, pyruvate
DMSO	Merck (D8418-100ML)	-
DTT	Applichem (3485-12-3)	-
EDTA	Applichem (A5097.1000)	-
EGTA	Carl Roth (3054.3)	-
Erucic acid	TargetMol (TGM-T4867-100mg)	97.85% (Mr = 338.57 g/mol)
Ethanol	Fisher Chemical (64-17-5)	Absolute, 99.8 % analytical reagent grade
Ethyl acetate	JULI.O GmbH (141-78-6)	-
FBS (Fetal bovine serum)	Thermo Fisher Scientific Inc. (10270106)	-
Fluorescamine	Biomol (CDX-F0003-M250)	-
Gelatin	Sigma-Aldrich (G7041-100G)	From cold water fish skin
Glucose monohydrate	Applichem (A3730.1000)	D(+)-Glucose monohydrate Molecular biology grade (Mr = 198.17 g/mol)
Glutamine	Thermo Fisher Scientific Inc. (25030-024)	L-Glutamine, 200 mM
Heparin	Ratiopharm (U02637)	-
HEPES	Applichem (A1069.1000)	Buffer grade (Mr = 238.31 g/mol)
Hexane	Honeywell (15613-2.5L)	Mixture of isomers >=85%
Hünig's base (N,N-diisopropylethylamine)	TCI (7087-68-5)	-
Isopropanol	Fisher Chemical (P/7507/17)	MS grade
LD540	(Spandl et al., 2009)	Lipophilic dye for lipid droplet staining (Mr = 300 g/mol)
Magnesium chloride	Applichem (A3618)	$MgCl_2$ x6H2O (Mr = 203.30 g/mol)
Malate	Applichem (A4984.0025)	L-malic acid disodium salt monohydrate
Methanol	VWR Chemical (83638.320)	-
Mowiol	Calbiochem (475904)	100 g, Mowiol 4-88
M-199 Media	Gibco (31150-022)	-
Palmitic acid	TCI (P0002)	>97.0%
Paraformaldehyde	Sigma-Aldrich (15512)	37 % H_2CO
Penicillin-Streptomycin Solution	Thermo Fisher Scientific Inc. (15140122)	10.000 U/ml (x100)
PIP2 primary antibody	Merck Chemicals (MABS2283-25UG)	Mouse anti-PIP2 antibody, clone KT10

Name	Supplier (Catalog number)	Additional information
Potassium dihydrogen phosphate	Carl Roth (3904.1)	KH_2PO_4 (Mr = 136.09 g/mol)
Potassium chloride	Grüssing (12008)	KCl (Mr = 74.55 g/mol)
Saponin	Applichem (A2542.0500)	from Quillaja Bark pure, pH (20 %; H_2O): 4.5 – 5.5 Sapogenin content: 10 – 14 %
SDS	Carl Roth GmbH (8029.4)	SDS Pellets, 1 kg
Sodium chloride	Fisher Bioreagents (7647-14-5)	NaCl (Mr = 58.44 g/mol)
Sodium hydrogen carbonate	Merck (1063291000)	$NaHCO_3$ (Mr = 84.01 g/mol)
Sodium pyruvate	Sigma (P5280-25G)	-
Sucrose	Fein Zucker Südzucker	-
TOM20 primary antibody	Santa Cruz Biotechnology (sc-11415)	Rabbit polyclonal IgG, 200 µg/ml
Trimetazidine	Biomol (Cay18165-10)	Trimetazidine hydrochloride
Tris HCl	Carl Roth (2449.2)	-
Triton X-100	Sigma-Aldrich (T9284-199ML)	t-Octyl phenoxypolyethoxy ethanol ether
Trypsin-EDTA	Thermo Fisher Scientific (25300054)	Trypsin-EDTA (0.05%), phenol red
TUNEL Apoptosis Kit	Elabscience (E-CK-A320)	One-step TUNEL *In Situ* Apoptosis Kit for 100 assays with Elab Fluor Labeling Solution
Water, MS grade	Fischer Chemical (7732-18-5)	LC-MS grade 2.5L

3.1.2. Nomenclature of alkyne-lipids

In this work alkyne-fatty acids are used. These are fatty acids that have a terminal alkyne-group (triple bond). Alkyne-lipids get a suffix ";Y" in their naming to be easily distinguishable from the natural lipids present in the cell. If alkyne-lipids have two alkyne-groups, they will get a suffix ";Y2". Each lipid species gets a prefix that corresponds to its lipid class, followed by side chain length and number of double bonds. According to this nomenclature alkyne-linoleic acid will get a name FA18:2;Y (fatty acid with 18 carbon atoms in the side chain, two double bonds and one terminal alkyne group). Other alkyne-lipid classes mentioned in this thesis are: CAR, carnitines; CE, cholesterol esters; CER, ceramides; DG, diacylglycerols; GlcCer, Glucosylceramides; MG, monoacylglycerols; PI, phosphatidylinositol; PC, phosphatidylcholines; SM, sphingomyelins; TG, triacylglycerols.

3.1.3. Alkyne-fatty acid tracers

Alkyne-fatty acid	Source
Alkyne-capric acid FA11:0;Y ($C_{11}H_{18}O_2$) 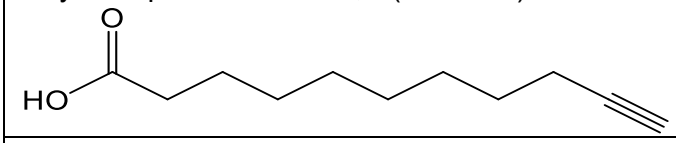	TCI (U0054)
Alkyne-lauric acid FA12:0;Y ($C_{12}H_{20}O_2$) 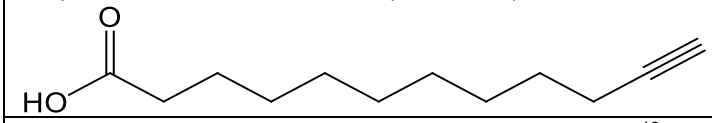	Synth. by C. Thiele
Alkyne-palmitic acid, isotope-version FA16:0;Y ($^{13}C_6$) ($C_{10}{}^{13}C_6H_{28}O_2$; for MS) 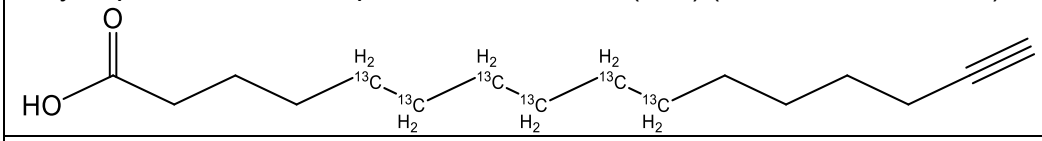	Synth. by C. Thiele
Alkyne-palmitic acid FA17:0;Y ($C_{17}H_{30}O_2$; for TLC and microscopy) 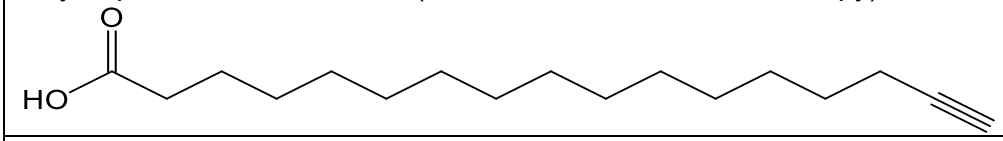	Synth. by C. Thiele
Alkyne-linoleic acid FA18:2;Y ($C_{18}H_{28}O_2$) 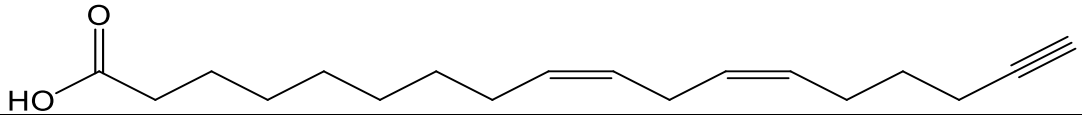	Synth. by C. Thiele
Alkyne-oleic acid FA19:1;Y ($C_{19}H_{32}O_2$) 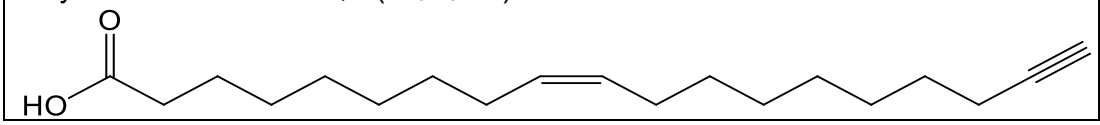	Synth. by C. Thiele

3.1.4. Internal standards for mass spectrometric analysis of alkyne-lipids

Internal standard (IS)	Class	Parent ion	(m/z)	Pmol per sample
CE(17:0;Y)	Cholesterol esters (single-labeled)	C_{52} H_{82} D_{11} O_2 N_4 (+)	816.7972	26.00
CER(15:1;Y)	Ceramides (single-labeled)	C_{41} H_{68} D_{12} O_3 N_5 (+)	702.7000	15.80
DG(32:1;Y)	Diacylglycerols (single-labeled)	C_{43} H_{69} D_{12} O_5 N_4 (+)	745.6942	14.60
DG(38:2;Y2)	Diacylglycerols (double-labeled)	C_{54} Ci_3 H_{98} D_8 O_5 N_8 (+)	496.9429	15.50
GlcCer(15:0;Y)	Glucosylceramides (single-labeled)	C_{45} Ci_2 H_{86} D_4 O_8 N_5 (+)	858.7090	33.00
MG(19:1;Y)	Monoacylglycerols (single-labeled)	C_{27} Ci_3 H_{53} D_4 O_4 N_4 (+)	544.4718	40.68
PA(32:1;Y)	Phosphatidic acid (single-labeled)	C_{43} H_{70} D_{12} O_8 N_4 P_1 (+)	825.6609	12.80

Internal standard (IS)	Class	Parent ion	(m/z)	Pmol per sample
PA(38:2;Y2)	Phosphatidic acid (double-labeled)	C_{54} Ci_3 H_{99} D_8 O_8 N_8 P_1 (+)	536.9274	27.60
PE(32:1;Y)	Phosphatidylethanolamines (single-labeled)	C_{45} H_{75} D_{12} O_8 N_5 P_1 (+)	868.7029	36.00
PE(38:2;Y2)	Phosphatidylethanolamines (double-labeled)	C_{56} Ci_3 H_{104} D_8 O_8 N_9 P_1 (+)	558.4484	26.10
PI(41:1;Y)	Phosphatidylinositol (single-labeled)	C_{49} H_{80} D_{12} O_{13} N_4 P_1 (+)	987.7122	30.70
PC(32:1;Y)	Phosphatidylcholines (single-labeled)	C_{48} H_{82} D_{12} O_8 N_5 P_1 (+)	455.8778	113.40
PC(38:2;Y2)	Phosphatidylcholines (double-labeled)	C_{59} Ci_3 H_{111} D_8 O_8 N_9 P_1 (+)	386.6501	49.40
SM(15:0;Y)	Sphingomyelins (single-labeled)	C_{44} Ci_2 H_{89} D_4 O_6 N_6 P_1 (+)	431.3596	31.00
TG(48:1;Y)	Triacylglycerols (single-labeled)	C_{59} H_{99} D_{12} O_6 N_4 (+)	983.9234	103.00
TG(49:1;Y2)	Triacylglycerols (double-labeled)	C_{68} H_{112} D_{16} O_6 N_8 (+)	584.5466	20.34
TG(57:3;Y3)	Triacylglycerols (triple-labeled)	C_{81} Ci_3 H_{143} D_{12} O_6 N_{12} (+)	481.1012	32.70

3.1.5. Internal standards for mass spectrometric analysis of the whole lipidome

Internal standard (IS)	Class	Parent ion	(m/z)	Pmol per sample
CAR(15:0)	Carnitines	C_{22} H_{44} O_4 N_1 (+)	386.3265	51.70
CE(18:1)	Cholesterol esters	C_{45} H_{76} D_6 O_2 N_1 (+)	674.6715	111.60
CER(d18:1/17:0)	Ceramides	C_{35} H_{70} O_3 N_1 (+)	552.5347	32.20
DG(31:1)	Diacylglycerols	C_{34} H_{68} O_5 N_1 (+)	570.5094	64.30
HexCer (d18:1/12:0)	Hexosylceramide	C_{36} H70 O8 N1 (+)	644.5101	55.20
LPA(17:0)	Lysophosphatidyc acid	C_{20} H_{45} O_7 N_1 P_1 (+)	442.2928	39.80
LPC(17:1)	Lysophosphatidylcholines	C_{25} H_{51} O_7 N_1 P_1 (+)	508.3382	35.00
LPE(17:1)	Lysophosphatidyl ethanolamines	C_{22} H_{45} O_7 N_1 P_1 (+)	466.2932	38.20
MG(17:1)	Monoacylglycerols	C_{20} H_{42} O_4 N_1 (+)	360.3115	104.00
PA(31:1)	Phosphatidic acid	C_{34} H_{69} O_8 N_1 P_1 (+)	650.4758	56.20
PC(31:1)	Phosphatidylcholines	C_{39} H_{77} O_8 N_1 P_1 (+)	718.5381	396.20
PE(33:1-d7)	Phosphatidylethanolamines	C_{38} H_{68} D_7 O_8 N_1 P_1 (+)	711.5671	250.10
PG(28:0)	Phosphatidylglycerol	C_{34} H_{71} O_{10} N_1 P_1 (+)	684.4812	51.60
PS(31:1)	Phosphatidylserine	C_{37} H_{71} O_{10} N_1 P_1 (+)	720.4814	98.80
SM(17:0)	Sphingomyelin	C_{40} H_{82} O_6 N_2 P_1 (+)	717.5905	99.20
TG(47:1)	Triacylglycerols	C_{50} H_{98} O_6 N_1 (+)	808.7398	359.50

3.1.6. Consumables

Consumable	Company
Capillaries, glass, for TLC applications	Marienfeld
Caps for autosampler	Carl Roth
Cell culture dish 6 cm diameter	VWR
Glass vials for autosampler	Carl Roth
Falcon tubes 15 ml, 50 ml	Corning Inc.
Filter tips 10 µl, 200 µl, 1000 µl for cell culture applications	Sarstedt
Filtertop Filtropur BT50, 500 ml, for filter-sterilization of big volumes, pore size 0.22 µm	Sarstedt
Eppendorf tubes 1.5 ml, 2 ml, safe-lock for MS applications	Eppendorf
Microscope cover glasses	VWR
Microscope slides Super Frost® Green	Menzel GmbH
Needles 21 G	Braun Melsungen
PARAFILM®	Sigma-Aldrich
Pasteur pipets, glass, long tip	VWR
Paster pipets, plastic	VWR
Pipette tips 10 µl, 200 µl, 1000 µl for MS applications	Starlab
Serological pipettes 5 ml, 10 ml, 25 ml	Sarstedt
Syringe for filter-sterilization of small volumes, 10 ml	B Braun
Syringe, 1ml	BD Medical
Syringe filter unit for small volumes sterilization, pore size 0.2 µm	GE Healthcare
T-75 flask, type red	Sarstedt
TLC plates, glass, silica gel 60	Merck
TC inserts / Transwells for 6-well plates	Sarstedt
Well plates with 6 and 24 wells, type red	Sarstedt

3.1.7. Equipment

Equipment	Company
Autosampler	Thermo Fisher Scientific
Centrifuges 5424, 5417R, 5430R, 5810	Eppendorf
CO_2 incubator CB210	Binder
Dounce homogenizer for heart lysates	B Braun
Eppendorf Research® plus pipettes, 2.5 µl, 10 µl, 20 µl, 100 µl, 200 µl, 1000 µl	Eppendorf
Fluorescent microscope Zeiss Axio Observer.Z1 with Apotome	Carl Zeiss
Gastight Syringe, 500 µl, borosilicate glass	Hamilton
Homogenizer T10 basic ULTRA-TURRAX® equipped with dispersion tool S10N-5G	IKA
Langendorff apparatus	Home-built, see figure 6
Magnetic stirrer C-MAG M57	IKA® Werke GmbH & Co. KG
Mass spectrometer Thermo Q Exactive Plus, equipped with standard HESI II ion source	Thermo Fisher Scientific

Equipment	Company
Peristaltic pump	Carl Roth
Pipette controller	Fisherbrand
pH-Meter CMG MS7	IKA® Werke GmbH & CO. KG
Polychrome V 150 W xenon lamp (Fluorescence microscope)	Till Photonics
Rolera MGI plus EMCCD camera (Fluorescence microscope)	Decon
Scales	Mettler-Toledo LLC
Sonicating water bath	Bandelin Sonorex Digitec
Spectrofluorometer FluoroMax-4	Horiba
Thermoblock	Eppendorf
TLC developing chamber for 20 x 20 cm plate	VWR
Vacuum centrifuge concentrator	Eppendorf
Vacuum pump Vacusafe comfort	Integra
Vibrating Blade Microtome VT1200S	Leica
Vortex Genie 2	Scientific Industries Inc.
Water bath	Memmert

3.1.8. Computer programs

Program	Company / Developer	Application
Chemdraw	PerkinElmer	Chemical structures drawing and analysis
Chromeleon	Thermo Fisher Scientific	MS data acquisition
FluorEssence	Horiba	Fluorometric assays
GelPro analyzer 6.0	Media Cybernetics	Analysis of TLC plates
Inkscape	Inkscape (http://www.inkscape.org), a free vector graphics software	Vector graphic editor
Krita	Krita (https://krita.org/en/), Krita Foundation, a free and open-source painting program	Image processing
LipidXplorer	(Herzog et al., 2011; Herzog et al., 2012)	MS data analysis
Microsoft Office	Microsoft Corporation	Text, image processing, data analysis
Proteowizard MSConvertGUI	(Adusumilli and Mallick, 2017)	File converter
Tune	Thermo Fisher Scientific	MS data acquisition
ZEN	Carl Zeiss	Fluorescence microscopy

3.2. Methods

3.2.1. Mice handling

For preparation of the heart lysates, viable heart slices and isolated Langendorff heart the C57Bl/6NCrl mice strain from Jackson Laboratories was used. Mice were kept in ventilated cages in a pathogen-free environment at a regular light-dark cycle (12 hours), 21 °C temperature and 55 % humidity. Animals were fed *ad libitum* on a regular chow diet (LASQCdiet® Rod16 from LASvendi; main caloric intake: fat 4.3 %, protein 16.9 %). For experiments 8-10 weeks old male mice were used. Animals were sacrificed by cervical dislocation. Heart was rapidly excised by thoracotomy and placed in corresponding ice-cold buffer until further use. All animal experiments were performed according to the European Directive 2010/63/EU in compliance with national laws (deutsches Tierschutzgesetz vom 01.01.2019, TierschutzVersuchstierordnung vom 13.08.2013).

3.2.2. Alkyne-fatty acid tracing in murine heart lysates

For the lipid tracing in the heart lysates the modified version of the protocol by Kuerschner and colleagues was used (Kuerschner et al., 2022). Briefly, fresh mice hearts were homogenized in 1 ml of the ice-cold homogenization buffer with the help of the Dounce homogenizer. The tissue homogenate was gently centrifuged at 4 °C 200 rpm for 7 minutes.

For studying utilization of different alkyne-fatty acids, to each Eppendorf tube 80 µl of the assay buffer and 10 µl of the supernatant were added. For the assay to start, 10 µl of 2 mM alkyne-fatty acid tracer coupled to 7.7 % BSA was added to each tube. The following alkyne-fatty acid tracers were separately tested: alkyne-capric acid FA11:0;Y, alkyne-palmitic acid FA17:0;Y, alkyne-linoleic acid FA18:2;Y and alkyne-oleic acid FA19:1;Y. Samples were mixed and incubated at 33 °C in a waterbath. Incubation was performed up to 1 hour. The experiment was stopped by addition of 400 µl of the stop mix. Solutions and buffers preparations for this experiment are described in the table 1. Each experiment condition was repeated on hearts from 3 different animals.

When the effect of erucic acid on carnitines formation was studied, tissue homogenate was preincubated with erucic acid first, before adding alkyne-fatty acid-BSA complex. For that to each Eppendorf tube 80 µl of the assay buffer and 10 µl of the centrifuged heart tissue homogenate supernatant were added. Thereafter, to each tube 10 µl of 2 mM erucic acid coupled to 7.7 % BSA were added, and the samples were incubated at 33 °C in a waterbath for 30 minutes. After the incubation, 10 µl of 2 mM alkyne-fatty acid tracer (either FA11:0;Y or FA17:0;Y) coupled to 7.7 % BSA were added to each tube to start the assay. Samples were mixed and incubated at 33 °C in a waterbath. Incubation with alkyne-fatty acids was performed up to 1 hour. The experiment was stopped by addition of 400 µl of the stop mix.

Table 1: Solutions and buffers for the heart lysates alkyne-lipid tracing.

Solution / Buffer	Preparation
Homogenization buffer	For 1 l: • Sucrose 250 mM (Mr = 342.3 g/mol; m = 85.6 g) • Tris HCl 10 mM (Mr = 121.14 g/mol; m = 1.21 g) • EDTA 1 mM (Mr = 292.25 g/mol; m = 0.292 g) Adjust pH 7.4, filter-sterilize, aliquot and keep at - 20 °C
Alkyne-fatty acid tracers-BSA complex	For 210 µl: • H_2O (V = 200 µl) • BSA 7.7% delipidated (m = 15.4 mg) • Alkyne-fatty acid 2 mM (V = 20 µl of 20 mM stock in ethanol)
Assay buffer	For 1 l: • Tris HCl 10 mM (Mr = 121.14 g/mol; m = 1.21 g) • Sucrose 94 mM (Mr = 343.3 g/mol; m = 32 g) • EDTA 0.125 mM (Mr = 292.25 g/mol; m = 36.5 mg) • KH_2PO_4 6.25 mM (Mr = 136.09 g/mol; m = 850 mg) • KCl 100 mM (Mr = 74.55 g/mol; m = 7.46 g) • $MgCl_2$ hexahydrate 1.25 mM (Mr = 203.3 g/mol; m = 250 mg) • L-Carnitine hydrochloride 2.5 mM (Mr = 197.66 g/mol; m = 490 mg) • L-malic acid disodium salt monohydrate 0.125 mM (Mr = 196.06 g/mol; m = 24.5 mg) Adjust pH 8.0, filter-sterilize, aliquot and keep at - 20 °C For 50 ml prewarmed aliquots shortly before the assay start: • Coenzyme A trulithium salt 0.065 mM (Mr = 785.33 g/mol; m = 2.55 mg, add fresh) • ATP 2.5 mM (Mr = 551.15 g/mol; m = 69 mg, add fresh) • DTT 1.25 mM (Mr = 154.25 g/mol; m = 9.64 mg, add fresh)
Stop mix	Methanol/chloroform mix at 2 to 1 ratio, for 30 ml: • Methanol (V = 20 ml) • Chloroform (V = 10 ml)

3.2.3. Click-reaction for detection of alkyne-lipids by thin-layer chromatography

Samples from 3.2.2. were centrifuged at 20000 g for 2 minutes. Thereafter, alkyne-lipids were coupled to the azide-fluorescent reporter via the click-reaction and analyzed by the thin-layer chromatography. For the click-reaction 40 µl of the click-mix with 3-azido-7-hydroxycoumarin were added beforehand to the 1.5 Eppendorf reaction tube. Thereafter, 10 µl of the sample (from 3.2.2. experiment) were added. As a standard the mixture of alkyne-fatty acids (FA11:0;Y, FA17:0;Y, FA18:2;Y, or FA19:1;Y) or alkyne-fatty acids carnitines (CAR5:0;Y, CAR7:0;Y, CAR9:0;Y, CAR11:0;Y, CAR13:0;Y, and CAR17:0;Y) were used. The click-reaction was performed overnight at 42 ^{o}C in a thermoblock. Solutions preparations for this experiment are described in the table 2.

Table 2: Solutions for the click-reaction with 3-azido-7-hydroxycoumarin for subsequent fluorescent detection by thin-layer chromatography.

Solution	Preparation
Click-mix with 3-azido-7-hydroxycoumarin for fluorescent detection by thin-layer chromatography	For 1110 µl: • Ethanol 100 % (V = 850 µl) • Copper (I) tetrafluoroborate (V = 250 µl of 10 mM stock in acetonitrile) • 3-azido-7-hydroxycoumarin (V = 10 µl of 2 mg/ml stock in acetonitrile)
Copper (I) tetrafluoroborate 10 mM in acetonitrile	For 10 ml: • Copper (I) tetrafluoroborate (Mr = 314.56 g/mol; m = 31.5 mg) • Acetonitrile (V = 10 ml)

3.2.4. Fluorescent detection of the clicked alkyne-lipids by thin-layer chromatography

After the click-reaction with the fluorescent 3-azido-7-hydroxycoumarin reporter (see 3.2.3.) the reaction tubes were vortexed for 10 minutes. During that time the thin layer chromatography plates were prepared the following way: a line was drawn 2 centimeters from the bottom of the plate and spaces for loading the lipids were marked. After vortexing samples were shortly centrifuged and loaded on the plate using glass capillaries. The plate was placed in the first developing chamber saturated with a solvent mixture I and let to run almost completely, until the front of the solvent reached around 2 centimeters from the top of the plate. Thereafter the plate was taken out, left to dry

and transferred to the second developing chamber saturated with a solvent mixture II. The plate was left in the chamber until the solvent line reached the near top of the plate, around 2 centimeters from the end. Then the plate was taken out, left to dry again and was soaked in 4 % Hünig's base solution. Thereafter the plate was taken out and left to dry. Labelled lipids were imaged with 420 nm LED lamp with a glass emission filter. Images were acquired with an EMCCD camera system equipped with a 494/20 nm (coumarin fluorescence signal) and 528/28 nm (noise signal) bandpass emission filter set. In each channel eight images were acquired with exposure times between 20 milliseconds and 5 seconds. For the imaging and analysis GelPro analyzer software was used. Fluorescence signals were saved as integrated optical density (IOD) values for further analysis. Solutions preparations for this experiment are described in the table 3.

Table 3: Solutions for the thin-layer chromatography.

Solution	Preparation
Solvent mixture I	Chloroform/methanol/water/acetic acid mix at 60/40/5/1 ratio, for 106 ml: • Chloroform (V = 60 ml) • Methanol (V = 40 ml) • Water (V = 5 ml) • Acetic acid glacial (V = 1 ml)
Solvent mixture II	Isohexane/ethyl acetate mix at 1 to 1 ratio, for 100 ml: • Isohexane (V = 50 ml) • Ethyl acetate (V = 50 ml)
Hünig's base solution 4%	4 % N,N-Diisopropylethylamine in isohexane, for 100 ml: • N,N-Diisopropylethylamine (m = 4 g) • Isohexane (V = 100 ml)

3.2.5. Alkyne-fatty acid tracing in murine viable heart slices

Murine viable heart slices were prepared as described in Watson and colleagues' protocol (Watson et al., 2017). Briefly, male mice were sacrificed by cervical dislocation. The heart with lungs and surrounding tissues was rapidly excised and immediately transferred to the Petri dish with heparinized slicing solution prewarmed to 37 ^{o}C. The heart was gently compressed between two fingers for 10 seconds to eject the remaining blood from the chambers. Thereafter, the heart with lungs was transferred to the new

Petri dish with the ice-cold heparinized slicing solution and again gently compressed with fingers for 10 seconds to wash out the remaining blood. For dissection, complete heart with lungs was transferred to the new Petri dish with ice-cold slicing solution. The left ventricular tissue block was prepared as following: using a razor blade, the lungs and other surrounding tissues were removed to expose the intact heart. Atria and right ventricle were removed. The left ventricle was cut along the ventricular-septal junction towards apex and flattened. Thereafter, the left ventricular muscle tissue was embedded into pre-cooled 4 % agarose in slicing solution. After the agarose block has solidified, it was mounted on the Vibrating Blade Microtome (Leica VT1200S). The heart tissue was cut into 300 µm thick slices in the ice-cold degassed slicing solution which was constantly cooled with ice. Cutting was performed with the amplitude of 0.85 mm at the speed of 0.4 mm per second. Slices were collected into 24-well plates filled with ice-cold degassed slicing solution and kept on ice until further steps. For the incubation viable slices were transferred to 6-well plates with transwells, containing 2 ml of the pulse media with alkyne-fatty acid mix in the lower compartment and 1 ml of the pulse media in the upper compartment to improve the oxygenation of the slices. Slices were left in pulse media for 1 hour. The pulse media contained either alkyne-fatty acid mix 1 (alkyne-palmitic acid FA16:0;Y($^{13}C_6$), alkyne-linoleic acid FA18:2;Y and alkyne-oleic acid FA19:1;Y), or mix 2 (alkyne-capric acid FA11:0;Y and alkyne-linoleic acid FA18:2;Y) or mix 3 (alkyne-lauric acid FA12:0;Y and alkyne-oleic acid FA19:1;Y). Each fatty acid was at 50 µM final concentration. Thereafter the pulse media was exchanged with the chase media without alkyne-fatty acids. Slices were kept in the chase media for 0, 3, 6 or 24 hours. After incubation each slice was transferred to a new Eppendorf tube and washed once with ice-cold phosphate buffered saline with 1 % bovine serum albumin. Thereafter, the liquid was removed and slices were washed with ice-cold 155 mM ammonium acetate. Liquid was completely removed, slices were weighted and then stored at - 80 ^{o}C until the lipid extraction for the further mass spectrometric analysis. Each condition was done in triplicates. Solutions and buffers preparations for this experiment are described in the table 4.

Table 4: Solutions and buffers for viable heart slices culturing and lipid tracing.

Solution / Buffer	Preparation
Slicing solution (Tyrode's solution with addition of 30 mM 2,3-Butanedione-2-monoxime)	For 1 l: • 2,3-Butanedione-2-monoxime 30 mM (Mr = 101.1 g/mol; m = 3 g) • Glucose monohydrate 10 mM (Mr = 198.17 g/mol; m = 1.98 g) • HEPES 10 mM (Mr = 238.31 g/mol; m = 2.38 g) • KCl 6 mM (Mr = 74.55 g/mol; m = 0.45 g) • NaCl 140 mM (Mr = 58.44 g/mol; m = 8.18 g) • $MgCl_2$ 1 mM (V = 1 ml of 1 M stock solution) • $CaCl_2$ 1.8 mM (V = 1.8 ml of 1 M stock solution) Adjust to pH 7.4 with NaOH; add H_2O until 1 liter; filter through 0.2-micron-pore filter; store at 4 °C; degas with carbogen on ice directly before use
Heparinized slicing solution	For ~25 ml: • Slicing solution (degassed, V = 25 ml) • Heparin (V = 50 µl) Prepare twice; prewarm one at 37 °C and cool the other on ice before use
Agarose 4 % in slicing solution for left ventricular tissue block embedding	For 100 ml: • Agarose (m = 4 g) • Slicing solution (V = 100 ml) Heat in the microwave; keep at 50 °C; cool until 37 °C directly before embedding the heart tissue
M-199 media with 5 % FBS and 1 % P/S = chase media for viable heart slices	• M-199 media • FBS 5 % • Penicillin-Streptomycin solution 1 %
Pulse media with alkyne-fatty acids for viable heart slices	For 10 ml: • M-199 media (V = 10 ml) • BSA 1 % (m = 0.1 g) • Alkyne fatty acid tracers 50 µM each (10 µl of 50 mM stock solution in 100 % ethanol; add slowly to solution while swirling to allow fatty acid to effectively to bind to BSA) Alkyne-fatty acid **mix 1:** FA16:0;Y($^{13}C_6$), FA18:2;Y, FA19:1;Y Alkyne-fatty acid **mix 2:** FA11:0;Y, FA18:2;Y Alkyne-fatty acid **mix 3:** FA12:0;Y, FA19:1;Y
Phosphate buffered saline (PBS) buffer x1 Na/K-Phosphate 2.3 mM; NaCl 155 mM	For x10 concentrated PBS stock solution: • NaCl (m = 80 g) • KCl (m = 2 g) • Na_2HPO_4 (m = 14.4 g) • KH_2PO_4 (m = 2.4 g) Adjust to pH 7.4; add H_2O until 1 liter; for use dilute from x10 PBS to get x1 PBS buffer
Ammonium acetate 155 mM for washing	For 1 l: Ammonium acetate 155 mM (Mr = 77.08 g/mol; m = 11.95 g); Cool before use
PBS with 1 % BSA for washing	For 100 ml, cool before use: • BSA (m = 1 g) • PBS (V = 100 ml)

3.2.6. Alkyne-fatty acid tracing in the Langendorff heart

Adult male mice were sacrificed by cervical dislocation. The hearts with surrounding tissues were rapidly excised and submerged into the ice-cold degassed Krebs-Henseleit solution prepared after Tse and coworkers' protocol (Tse et al., 2016). The surrounding lungs and tissues were removed and the aorta was cannulated using 21-gauge syringe needle attached to the fixed syringe prefilled with Krebs-Henseleit buffer. The position of the heart was secured with 2 silk ligatures, and the successfully cannulated hearts were attached to the home-built Langendorff perfusion apparatus (for the scheme see figure 6). The time between mice killing and mounting of the heart on the Langendorff apparatus was less than 10 minutes. Hearts were perfused with Krebs-Henseleit buffer, which was oxygenated with carbogen and prewarmed to 37 ^{o}C with the help of surrounding water jacket. Hearts that regained their pink color and began to spontaneously contract were further perfused with 10 ml of the Krebs-Henseleit buffer containing mix of alkyne-fatty acids (alkyne-lauric acid FA12:0;Y and alkyne-oleic acid FA19:1;Y, or 18:2;Y alone, each alkyne-fatty acid was at 100 µM concentration) prebound to the 0.5 % bovine serum albumin. The eluate dripping from the heart was collected and recycled. After 30 minutes of perfusion hearts were detached from the Langendorff apparatus and transferred to a new Petri dish with fresh Krebs-Heinseleit buffer. For the mass spectrometric analysis of alkyne-lipids atria and ventricles were collected separately and snap-frozen at - 80 ^{o}C. For visualization of alkyne-lipid distribution via fluorescent microscopy the whole perfused heart was fixed with 4 % paraformaldehyde in phosphate buffered saline for at least 1 night and kept at 4 ^{o}C until cutting and staining. Solutions and buffers preparations for this experiment are described in the table 5 (part 1 and 2).

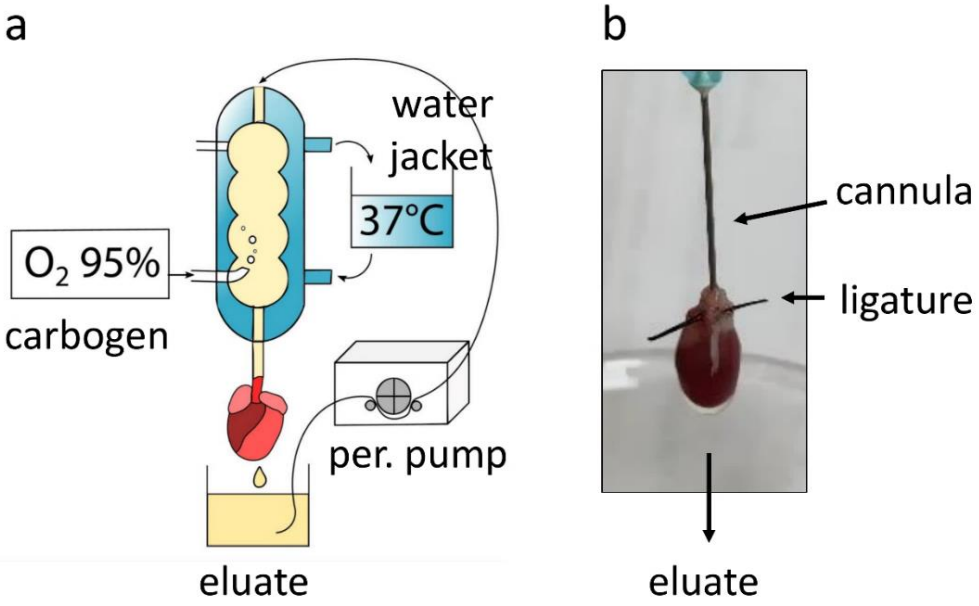

Figure 6: Schematic representation of the home-built Langendorff apparatus. (a) Aorta of the mouse heart was cannulated, and the heart was attached to the Langendorff apparatus. Through the cannula the buffer with tracer molecules was supplied. The eluate dripping from the heart was then collected and returned to the system with the help of the peristaltic pump. The buffer was constantly oxygenated with carbogen (95 % O_2) and prewarmed to 37 °C with the help of the water jacket. **(b)** Closer view of the heart attached to the Langendorff apparatus. Cannulation via the aorta allowed to retrogradely perfuse the heart with the buffer, ligatures helped to secure the heart position.

Table 5: Solutions and buffers for the Langendorff heart preparation and alkyne-lipid tracing (part 1).

Solution / Buffer	Preparation
Krebs-Henseleit buffer	For 1 l: • NaCl 119 mM (Mr = 58 g/mol; m = 6.9 g) • $NaHCO_3$ 25 mM (Mr = 84 g/mol; m = 2.1 g) • KCl 4 mM (Mr = 75 g/mol; m = 0.3 g) • KH_2PO_4 1.2 mM (Mr = 136 g/mol; m = 0.163 g) • $MgCl_2$ hexahydrate 1mM (Mr = 203 g/mol; m = 0.203 g) • $CaCl_2$ x$2H_2O$ 1.8 mM (Mr = 147 g/mol; m = 0.265 g) • Glucose monohydrate 10 mM (Mr = 198 g/mol; m = 1.98 g) • Sodium pyruvate 2 mM (Mr = 110 g/mol; m = 0.22 g) Adjust to pH 7.4 with HCl; filter through 0.2-micron-pore filter; store at 4 °C
Krebs-Henseleit buffer with alkyne-fatty acids	For 10 ml: • Krebs-Henseleit buffer (V = 10 ml) • BSA 0.5 % (m = 50 mg) • Alkyne-fatty acid tracer 100 µM each (V = 10 µl of 100 mM stock solution in ethanol; add slowly while swirling to allow the fatty acid to efficiently bind to BSA) Alkyne-fatty acid **mix 1:** 12:0;Y, 19:1;Y Alkyne-fatty acid **mix 2:** 18:2;Y

Table 5: Solutions and buffers for the Langendorff heart preparation and alkyne-lipid tracing (part 2).

Solution / Buffer	Preparation
Phosphate buffered saline (PBS) buffer x1 Na/K-Phosphate 2.3 mM; NaCl 155 mM	For x10 concentrated PBS stock solution, 1l: • NaCl (m = 80 g) • KCl (m = 2 g) • Na_2HPO_4 (m = 14.4 g) • KH_2PO_4 (m = 2.4 g) Adjust to pH 7.4; add H_2O until 1 liter; for use dilute from x10 PBS to get x1 PBS buffer
4 % paraformaldehyde (PFA) in PBS	For 200 ml: • PFA 4 % (V = 20 ml of 40 % PFA stock) • PBS (V = 180 ml)

3.2.7. Alkyne-fatty acid tracing in H9c2 cell line

H9c2 cells were cultured in Dulbecco Modified Eagle's Medium (DMEM) with 1 % penicillin-streptomycin, 10 % fetal bovine serum and 4 mM glutamine in T75 flasks in humidified cell culture incubator at 37 ^{o}C in the presence of gas mixture with 5 % CO2 and 95 % air. The media was exchanged every 3 days. Cells were allowed to grow up to 70 % confluence. Splitting and passaging of the cells in a new flask or well plate was performed by washing the cells with 10 ml of the phosphate buffered saline, which was followed by addition of 2 ml of Trypsin-EDTA. The cells were left in the incubator at 37 ^{o}C for 5 minutes, and thereafter 8-10 ml of the fresh DMEM media was added. Then 2 ml of the cell suspension was transferred to a new flask with 10 ml of DMEM media added earlier.

For the cell cryopreservation, the remaining cell suspension after the passaging was transferred to a new Falcon tube. Cells were centrifuged at 200 rpm for 7 minutes. Thereafter, the supernatant was removed, and cells were resuspended in 3-5 ml of the freezing solution. Into each cryotube 500 µl of the resuspended cells were transferred, and the cells were left in a cryopreservation container at - 80 ^{o}C for slow cooling. After 2-3 days, the cells were transferred into liquid nitrogen for storage. Solutions and buffers preparations for H9c2 culturing, freezing and alkyne-lipid tracing experiments are described in the table 6.

For the pulse-chase experiments for mass spectrometric analysis 200 µl of the cell suspension was added into 24-well plates with 300 µl of the fresh DMEM media. Cells

were left to attach for 24 hours. If required, preincubation step with various reagents in 500 µl of the fresh DMEM media was included before the pulse-chase experiment. For more details for each experiment condition refer to the table 7 (“preincubation” column). For the pulse-chase experiment, the media was aspirated and cells were first fed (pulsed) with 500 µl of fresh DMEM with alkyne-fatty acid mix, each at 50 µM final concentration, for 1 hour. Alkyne-fatty acid mix 1 contained alkyne-capric acid FA11:0;Y, alkyne-palmitic acid FA16:0;Y($^{13}C^{6}$) and alkyne-linoleic acid FA18:2;Y. Alkyne-fatty acid mix 2 contained alkyne-palmitic acid FA16:0;Y($^{13}C_{6}$), alkyne-linoleic acid FA18:2;Y and alkyne-oleic acid FA19:1;Y. In some experiments the pulse media also contained some compounds (Table 7 (“pulse” column)) in addition to the alkyne-fatty acid mix. Thereafter the pulse media was aspirated and 500 µl of the plain DMEM media (or with some additives, as shown on table 7 (“chase” column)) were added and cells were left in this media (chased) up to 24 hours. Thereafter, the chase media was aspirated and cells were washed with 500 µl of the ice-cold phosphate buffered saline containing 0.5 % bovine serum albumin. Solution was again aspirated and cells were washed with 500 µl of ice-cold 155 mM ammonium acetate. Solution was completely aspirated from wells and the well-plates were stored at - 80 ^{o}C until the lipid extraction for mass spectrometric analysis.

For fluorescent microcopy imaging H9c2 cells were grown on cover glass put into wells (24-well plate format) at low density (typically, 50 µl of the cell suspension after passaging were added to 450 µl of the DMEM media). Cells were left to attach for 24 hours and thereafter were fed for 1 hour with DMEM media containing 50 µM of one of alkyne-fatty acids (alkyne-capric acid FA11:0;Y, alkyne-palmitic acid FA17:0;Y, alkyne-linoleic acid FA18:2;Y or alkyne-oleic acid FA19:1;Y). Thereafter the cells were washed with plain DMEM media and fixed with 500 µl of 4 % paraformaldehyde in phosphate buffered saline.

Table 6: Solutions and buffers for pulse-chase experiments with H9c2 cell line.

Solution / Buffer	Preparation
Culture media for H9c2 cells	• Dulbecco Modified Eagle's Medium (DMEM), high glucose • 1 % penicillin-streptomycin • 10 % fetal bovine serum • 4 mM L-glutamine
Freezing media for H9c2 cells cryopreservation	For 20 ml, ice-cold: • Culture media with 1 % penicillin-streptomycin, 10 % fetal bovine serum and 4 mM L-glutamine (V = 18 ml) • Dimethyl sulfoxide (V = 2 ml)
Phosphate buffered saline (PBS) buffer x1 Na/K-Phosphate 2.3 mM; NaCl 155 mM	For x10 concentrated PBS stock solution, 1 l: • NaCl (m = 80 g) • KCl (m = 2 g) • Na_2HPO_4 (m = 14.4 g) • KH_2PO_4 (m = 2.4 g) Adjust to pH 7.4; add H_2O until 1 liter; for use dilute from x10 PBS to get x1 PBS buffer
Ammonium acetate 155 mM for washing	For 1 l: Ammonium acetate 155 mM (Mr = 77.08 g/mol; m = 11.95 g); cool before use
4 % paraformaldehyde (PFA) in PBS	For 200 ml: • PFA 4 % (V = 20 ml of 40 % PFA stock) • PBS (V = 180 ml)

Table 7: Incubation conditions for the alkyne-lipid tracing in H9c2 cells (part 1).

Figure	Description	Preincubation	Pulse	Chase
7 (b,c), 8 (upper row), 17	Alkyne-fatty acid preference, distribution within major lipid classes and phosphatidylcholines remodeling in H9c2 cells	No	**mix 1:** 50 µM FA11:0;Y, 50 µM FA16:0;Y($^{13}C_6$), 50 µM FA18:2;Y in DMEM media for 1 hour or **mix 2:** 50 µM FA16:0;Y($^{13}C_6$), 50 µM FA18:2;Y, 50 µM FA19:1;Y in DMEM media for 1 hour	Plain DMEM media for 0 / 3 / 6 / 24 hours
9, 12-15	Fluorescent imaging of alkyne-fatty acid incorporation in H9c2 cells	No	50 µM FA11:0;Y or 50 µM FA17:0;Y or 50 µM FA18:2;Y or 50 µM FA19:1;Y in DMEM media for 1 hour	Washed and fixed directly

Table 7: Incubation conditions for the alkyne-lipid tracing in H9c2 cells (part 2).

Figure	Description	Preincubation	Pulse	Chase
18	Effect of ATGListatin on H9c2 cells (ATGListatin at all stages present, MS data)	50 µM ATGListatin in DMEM media for 30 minutes; DMSO as carrier control	50 µM FA11:0;Y, 50 µM FA16:0;Y($^{13}C_6$), 50 µM FA18:2;Y in the presence of 50 µM ATGListatin in DMEM media for 1 hour; DMSO as carrier control	DMEM media with 50 µM ATGListatin up to 24 hours; DMSO as carrier control
19	Effect of ATGListatin on H9c2 cells (ATGListatin at all stages present, MS data)	50 µM ATGListatin in DMEM media for 30 minutes; DMSO as carrier control	50 µM FA11:0;Y, 50 µM FA16:0;Y($^{13}C_6$), 50 µM FA18:2;Y in the presence of 50 µM ATGListatin in DMEM media for 1 hour; DMSO as carrier control	DMEM media with 50 µM ATGListatin up to 24 hours; DMSO as carrier control
20	Reversibility of ATGListatin effect on H9c2 cells (ATGListatin removed from chase media)	50 µM ATGListatin in DMEM media in all samples for 30 minutes	50 µM FA11:0;Y, 50 µM FA16:0;Y($^{13}C_6$), 50 µM FA18:2;Y in the presence of 50 µM ATGListatin in DMEM media for 1 hour	DMEM media with 50 µM ATGListatin or DMSO as carrier control, up to 24 hours
22-24	Effect of erucic acid on H9c2 cells	0, 25, 50 or 100 µM FA22:1 in DMEM media for 24 hours	50 µM FA11:0;Y, 50 µM FA16:0;Y($^{13}C_6$), 50 µM FA18:2;Y in DMEM media for 1 hour	Plain DMEM media for 0, 3, 6 or 24 hours
25	Effect of erucic and palmitic acid on H9c2 cells	Combination of palmitic and erucic acid at different concentrations to reach total fatty acid concentration of 100 µM	50 µM FA11:0;Y, 50 µM FA16:0;Y($^{13}C_6$), 50 µM FA18:2;Y in DMEM media for 1 hour	Plain DMEM media for 0, 3, 6 or 24 hours
34 (a,c,e), 35 (a,c,e), 36 (a), 37 (a)	Effect of cobalt chloride induced chemical hypoxia on H9c2 cells	0, 100, 200 or 400 µM cobalt chloride in DMEM media for 24 hours	50 µM FA16:0;Y($^{13}C_6$), 50 µM FA18:2;Y, 50 µM FA19:1;Y in DMEM media for 1 hour	Plain DMEM media for 0, 3, 6 or 24 hours
34 (b,d,f), 35 (b,d,f), 36 (b), 37 (b)	Effect of hydrogen peroxide induced oxidative stress on H9c2 cells	0, 100, 200 or 400 µM hydrogen peroxide in DMEM media for 3 hours	50 µM FA16:0;Y($^{13}C_6$), 50 µM FA18:2;Y, 50 µM FA19:1;Y in DMEM media for 1 hour	Plain DMEM media for 0, 3, 6 or 24 hours

Table 7: Incubation conditions for the alkyne-lipid tracing in H9c2 cells (part 3).

Figure	Description	Preincubation	Pulse	Chase
38	Effect of trimetazidine on sphingomyelin biosynthesis in hydrogen peroxide-treated H9c2 cells	200 µM hydrogen peroxide in DMEM media for 3 hours	50 µM FA16:0;Y($^{13}C_6$), 50 µM FA18:2;Y, 50 µM FA19:1;Y in DMEM media for 1 hour	DMEM media with 0, 1, 10 or 50 50 µM trimetazidine for 0, 3, 6 or 24 hours
39 (a-c), 40 (d-f)	Fluorescent imaging of cobalt chloride-treated H9c2 cells (chemical hypoxia)	200 µM cobalt chloride in DMEM media for 24 hours	50 µM FA 18:2;Y in DMEM media for 1 hour	Washed and fixed directly
39 (d-f), 40 (a-c)	Fluorescent imaging of hydrogen peroxide-treated H9c2 cells (oxidative stress)	200 µM hydrogen peroxide in DMEM media for 3 hours	50 µM FA 18:2;Y in DMEM media for 1 hour	Washed and fixed directly
Supl. 2	Effect of ATGListatin on H9c2 cells (ATGListatin only in chase media)	No	**mix 1:** 50 µM FA11:0;Y, 50 µM FA16:0;Y($^{13}C_6$), 50 µM FA18:2;Y in DMEM media for 1 hour or **mix 2:** 50 µM FA16:0;Y($^{13}C_6$), 50 µM FA18:2;Y, 50 µM FA19:1;Y in DMEM media for 1 hour	DMEM media with 50 µM ATGListatin up to 24 hours; DMSO as carrier control

3.2.8. Alkyne-lipid extraction for mass spectrometric analysis

10 to 50 mg of the heart tissue samples (from 3.2.5. and 3.2.6.) were homogenized in 100 µl of MS-grade water on ice using T10 basic ULTRA-TURRAX® (IKA) homogenizer equipped with dispersion tool S10N-5G (IKA). Depending on the starting wet tissue weight 10 to 30 µl of the homogenate were transferred to a new Eppendorf tube containing 500 µl of the extraction mix (see table 8 for solutions preparation).

For the lipid extraction from cells (see 3.2.7), 500 µl of the extraction mix was added directly to each well using gas-tight Hamilton syringe. The whole well-plate was sonicated for 1 minute in a bath sonicator. Thereafter cell samples were transferred from wells to new 1.5 ml Eppendorf tubes.

The tissue or cell samples were centrifuged for 5 minutes at 20000 g to precipitate proteins. The pellet from cell samples was stored at - 20 °C for later protein amount

determination by fluram assay (see 3.2.12.). The supernatant was transferred to a new 2 ml Eppendorf reaction tube. To each tube 300 µl of chloroform and 700 µl of 1 % acetic acid in water were added. The samples were shaken for 30 seconds and centrifuged for 5 minutes at 20000 g. From the resulting biphasic solution the upper aqueous phase was removed and the lower organic phase was transferred to a new 1.5 ml Eppendorf reaction tube. The organic phase was evaporated in a vacuum centrifuge at 45 °C for 20 minutes. The lipid film was redissolved in 10 µl of chloroform. If the samples were not combined later, this extract was reacted with 40 µl of the click-reaction mixture containing C171-73 azide-reporter molecule. If 3 samples were combined with each other later (multiplexed), each sample from the triplicate was first reacted with 40 µl of the click-reaction mixture, containing one of the azide-reporters: C175-73 or C175-75 or C175-77. All the samples were sonicated in bath sonicator for 5 minutes and incubated at 42 °C for 16-20 hours in a heat block.

After the overnight incubation 200 µl of chloroform were added to the samples clicked to C171-73 reporter, which was followed by addition of 400 µl of the MS-grade water. Samples were shaken for 30 seconds and centrifuged at 20000 g for 2 minutes. Thereafter the upper aqueous phase was removed, and the lower organic phase was evaporated for 15 minutes at 45 °C in a vacuum centrifuge.

To the samples, clicked to one of C175-XX reporters (C175-73 or C175-75 or C175-77), 100 µl of chloroform were added. The experimental triplicates were pooled together. Thereafter, 600 µl of the MS-grade water were added to each pool, the mixture was shaken for 30 seconds and centrifuged at 20000 g for 2 minutes. The upper aqueous phase was removed, and the lower organic phase was evaporated for 20 minutes at 45 °C in a vacuum centrifuge.

All samples after evaporation were redissolved in 1 ml of the spray buffer, sonicated for 5 minutes in a bath sonicator and stored at - 20 °C. At the day of mass spectrometric analysis the samples were again sonicated for 5 minutes in a bath sonicator and centrifuged for 20 minutes at 20000 g. Thereafter, 500 µl from each sample were transferred to a glass bottle and 500 µl of the spray buffer were added to each sample. Glass bottles were sealed and put in the autosampler for the mass spectrometric analysis.

Table 8: Solutions for alkyne-lipids extraction, click-reaction and mass spectrometric analysis.

Solution/Buffer	Preparation
Extraction mix for alkyne-lipids mass spectrometric analysis (for internal standard mix content see 3.1.4.)	For 10 samples: • Methanol MS-grade (V = 4083 µl) • Chloroform MS-grade (V = 817 µl) • Internal standard mix (prepared by adding 500 µl of chloroform and 500 µl of methanol to the dried mix, and sonicating the vial for 2 minutes in a bath sonicator before use, V = 100 µl)
1 % acetic acid in MS-grade water	For 100 ml: • Acetic acid MS-grade (V = 1 ml) • Water MS-grade (V = 100 ml)
Copper (I) tetrafluoroborate 5 mM in acetonitrile	For 10 ml: • Copper (I) tetrafluoroborate (Mr = 314.56 g/mol; m = 15.75 mg) • Acetonitrile MS-grade (V = 10 ml)
Click-reaction mix with C171-73 azide-reporter	For 1020 µl: • C171-73 azide-reporter (V = 20 µl) • Ethanol MS-grade (V = 800 µl) • Copper (I) tetrafluoroborate (V = 200 µl of 5 mM stock in acetonitrile)
Click-reaction mix with C175-73/75/77 azide-reporters	For 1010 µl: • C175-73, C175-75 or C175-77 azide-reporter (V = 10 µl) • Ethanol MS-grade (V = 800 µl) • Copper (I) tetrafluoroborate (V = 200 µl of 5 mM stock in acetonitrile)
Spray buffer	For 500 ml: • Isopropanol MS-grade (V = 285.5 ml) • Methanol MS-grade (V = 178.5 ml) • Water MS-grade (V = 36 ml) • Ammonium acetate (Mr = 77.08 g/mol; m = 385 mg) • Acetic acid MS-grade (V = 0.5 ml)

3.2.9. Whole cellular lipidome extraction for mass spectrometric analysis

For the analysis of the whole cellular lipidome, to the samples 500 µl of the extraction mix was added using gas-tight Hamilton syringe. The whole well-plate was sonicated for 1 minute in a bath sonicator. Thereafter cell samples were transferred from wells to new 1.5 ml Eppendorf tubes. The samples were centrifuged for 5 minutes at 20000 g to precipitate proteins. The supernatant was transferred to a new 2 ml Eppendorf reaction tube. To each tube 300 µl of chloroform and 700 µl of 1 % acetic acid in water were added. The samples were shaken for 30 seconds and centrifuged for 5 minutes at 20000 g. From the resulting biphasic solution the upper aqueous phase was removed and the lower organic phase was transferred to a new 1.5 ml Eppendorf reaction tube. The

organic phase was evaporated in a vacuum centrifuge at 45 °C for 20 minutes. All samples after evaporation were redissolved in 1 ml of the spray buffer, sonicated for 5 minutes in a bath sonicator and stored at - 20 °C. At the day of mass spectrometric analysis the samples were again sonicated for 5 minutes in a bath sonicator and centrifuged for 20 minutes at 20000 g. Thereafter, 500 µl from each sample were transferred to a glass bottle and 500 µl of the spray buffer were added to each sample. Then, glass bottles were sealed and put in the autosampler for the mass spectrometric analysis. For solutions preparations see table 9.

Table 9: Solutions for whole cellular lipidome extraction and mass spectrometric analysis.

Solution/Buffer	Preparation
Extraction mix for mass spectrometric analysis of the whole lipidome (for internal standard mix content see 3.1.5.)	For 10 samples: • Methanol MS-grade (V = 4083 µl) • Chloroform MS-grade (V = 817 µl) • Internal omics standard mix (prepared by adding 250 µl of chloroform and 250 µl of methanol to the dried mix, and sonicating the vial for 2 minutes in a bath sonicator before use, V = 100 µl)
1 % acetic acid in MS-grade water	For 100 ml: • Acetic acid MS-grade (V = 1 ml) • Water MS-grade (V = 100 ml)
Spray buffer	For 500 ml: • Isopropanol MS-grade (V = 285.5 ml) • Methanol MS-grade (V = 178.5 ml) • Water MS-grade (V = 36 ml) • Ammonium acetate (Mr = 77.08 g/mol; m = 385 mg) • Acetic acid MS-grade (V = 0.5 ml)

3.2.10. Instrument setup for mass spectrometric analysis

The samples from 3.2.8. and 3.2.9. were analyzed on a Thermo Scientific Q Exactive Plus Hybrid quadrupole orbitrap mass spectrometer, equipped with an atmospheric pressure ion source operating in the high-voltage electrospray ionization modus. The samples were injected with the help of autosampler (Thermo Scientific) under the control of Tune and Chromeleon software. The following parameters were used for data acquisition (Tune data): Positive mode; Spray voltage: 4100; Capillary temperature: 280; Sheath gas 6; Aux gas 2; Spare gas: 0; Max spray current: 100; Probe heater temp: 0; S-Lens RF level: 55; Ion source: HESI. The following parameters were used for the

autosampler: Pump. Flow: 0.01 ml/min; Pump. Pressure upper limit: 1500 psi; Pump. Pressure lower limit: 50 psi; Sampler temperature: 15 ^{o}C.

For 3.2.8. alkyne-lipids, clicked to C171 or C175-73/75/77 reporters, were analyzed in the positive mode at 280000 resolution. First, the MS1 spectra were recorded within the mass-to-charge (m/z) ratio from 300 to 1200 in 100 m/z windows for 1 minute at 280000 resolution. Thereafter, MS2 scans were done by data independent acquisition (DIA) for 20 minutes, using inclusion list from m/z 309 (C171) or 340 (C175) to 1200 with 1.0006 m/z intervals at 280000 resolution.

For the analysis of the whole lipidome, samples from 3.2.9. were analyzed in a positive mode. First, the MS1 spectra were recorded within the m/z ratio from 400 to 1200 in 100 m/z windows for 1 minute at 280000 resolution. Thereafter, MS2 scans were done by data independent acquisition (DIA) for 8 minutes, using inclusion list from m/z 240 to 1200 with 1.0006 m/z intervals at 70000 resolution.

3.2.11. Analysis and normalization of mass spectrometric data

The acquired raw data from 3.2.10 was first converted to .mzml format using the Proteowizard MSConvertGUI program. Thereafter, the .mzml files were uploaded to the LipidXplorer program. The alkyne-lipids were identified and quantified using molecular fragment query language (MFQL) files. A typical .mfql file contains information about the peaks that correspond to the expected masses of the labeled lipid species classes and their characteristic neutral losses. As an output a .csv file is generated, which could be further analyzed in Excel software. For the absolute quantification, peak intensities were normalized to corresponding internal standards, which gave lipid species amounts in picomoles. For cellular samples, where significant cell death was expected (figures 34-37), the samples were additionally normalized by dividing picomoles by milligrams of protein present in the sample (measured by Fluram assay, see 3.2.12).

3.2.12. Protein quantification via the Fluram assay

The protein pellet, obtained during the lipid extraction (3.2.8.) after the first centrifugation step, was used to determine protein amounts in cellular samples, where significant cell

death was expected. The protein pellet was dissolved in 500 µl of 0.1 M borate buffer pH 8.9 with 2 % SDS added. From that solution 50 µl were dissolved in 750 µl of 0.1 M borate buffer pH 8.9. To that mix 200 µl of fluorescamine in acetone were added. The samples were mixed and left to incubate for 20 minutes in the dark. Directly before measurements the samples were mixed again. The samples were measured in the Spectrofluorometer FluoroMax-4 with the help of FluorEssence software. The excitation filter wavelength was 391 nm, the emission filter wavelength was 475 nm. As a standard bovine serum albumin dissolved in 0.1 M borate buffer pH 8.9 was used, with concentrations starting from 0.98 µg/ml up to 500 µg/ml. Of that dilution series 50 µl were added to 750 µl of 0.1 M borate buffer pH 8.9, and 200 µl of fluorescamine were added to each tube to start the reaction. As a blank 800 µl of plain borate buffer were used, to which 200 µl of fluorescamine were added. Buffers and solutions' preparations for this experiment are shown in the table 10.

Table 10: Solutions and buffers for the protein quantification via the Fluram assay.

Solution/Buffer	Preparation
Borate buffer 0.1 M pH 8.9	For 1 l: Boric acid 0.1 M (Mr = 61.83 g/mol, m = 6.183 g) Dissolve in water, adjust pH to 8.9 and fill water up to 1 l
Borate buffer + 2 % SDS	For 100 ml: • SDS (m = 2 g) • Borate buffer (V = 100 ml)
Fluorescamine working solution	For 50 assays: • Fluorescamine (m = 2.5 mg) • Acetone (V = 10 ml)
Bovine serum albumin standard curve	1 to 2 dilution series of bovine serum albumin in borate buffer, starting from 500 µg/ml down to 0.98 µg/ml

3.2.13. Heart tissue microscopy

Murine isolated Langendorff hearts (see 3.2.6. for experimental procedure) were perfused for 30 minutes with alkyne-linoleic acid FA18:2;Y, dissolved in Krebs-Henseleit solution. After perfusion completion hearts were washed with plain Krebs-Henseleit solution and fixed with 4 % paraformaldehyde in PBS for at least 2 days. Thereafter, fixed tissues were washed overnight in PBS at 4 °C. Before cutting PBS was additionally exchanged 4-5 times. Hearts were separated into chambers, and each chamber was mounted into 4 % agarose in PBS. Agarose blocks were cut on the Vibrating Blade

Microtome (Leica VT1200S) in PBS at the room temperature with thickness of 200 µm, the amplitude of 0.85 mm and at the speed of 0.4 mm per second. Thereafter the slices were stored at 6-7 °C in 4 % paraformaldehyde in PBS until staining.

For the mitochondria visualization the slices were incubated with primary antibodies against TOM20. For that the slices were washed with 2 ml of 155 mM ammonium acetate for 5 minutes to remove the fixative, and, thereafter, 3 times with 2 ml of PBS for 15 minutes each time. Thereafter, the samples were preincubated with 1 ml of the blocking buffer with 0.1 % Triton X-100 and 1 % cold fish gelatin in PBS for 30 minutes. Then the slices were incubated with primary antibodies in the blocking buffer containing 0.1 % saponin and 1 % cold fish gelatin in PBS at 4 °C overnight covered with aluminum folium and slightly shaking at 2 rpm. The next day the sections were rinsed twice with 2 ml of PBS for 8 minutes and incubated with secondary Alexa Fluor-conjugated antibodies in the blocking buffer with 0.1 % saponin and 1 % cold fish gelatin for 4 hours at the room temperature, slightly shaking at 2 rpm and protected from light. After the incubation was completed, the slices were washed 2 times with 2 ml of PBS for 15 minutes.

After antibodies staining completion the click-reaction was performed to visualize alkyne-lipids distribution. Sections were washed with 2 ml of 155 mM ammonium acetate for 5 minutes and later twice with 2 ml of 50 mM HEPES/KOH for 5 minutes. Thereafter, slices were incubated with 2 ml of 0.1 % saponin in 50 mM HEPES/KOH for 30 minutes, protected from light, at room temperature, slightly shaking at 2 rpm. During this time the fluorescent azide-reporter was diluted in prewarmed to 43 ^{o}C HEPES/KOH buffer to reach the final concentration of 25 µM. Slices were incubated in 1 ml of the fluorescent dye for 1 hour at 43 ^{o}C in the waterbath protected from light. For the reaction catalyzation 10 µl of 100 mM Cu(I)TFB were added to each well and after 30 minutes additional 10 µl of 100 mM Cu(I)TFB were added to the slices. After the reaction was completed, the slices were washed twice with 2 ml of HEPES/KOH for 8 minutes and then twice with 2 ml of PBS for 8 minutes. After additional PBS exchange the slices were washed in PBS overnight at 4 ^{o}C protected from light.

For the nuclei imaging the samples were stained with DAPI. For that the next day the slices were washed twice with 2 ml of PBS for 15 minutes. Thereafter, nuclei were stained with 1 ml of DAPI in PBS for 30 minutes, protected from light. After 3 consecutive washes with 2 ml of PBS for 7 minutes the slices were washed twice with 1 ml of

bidistilled water for 5 minutes. Directly thereafter the slices were transferred to microscope glass slides and were left to dry on air. Then the samples were covered with DAKO fluorescence mounting medium and cover glass, their position was fixed with nail polish, and the samples were left for 1 hour before visualization. The slices were stored at 4 °C between imaging sessions. Solutions and buffers for this experiment are shown in the table 11 (part 1 and 2).

Table 11: Solutions and buffers for tissue samples preparation for fluorescent microscopy (part 1).

Solution / Buffer	Preparation
Ammonium acetate 155 mM for washing	For 1 l: • Ammonium acetate 155 mM (Mr = 77.08 g/mol; m = 11.95 g)
Phosphate buffered saline (PBS) buffer x1 Na/K-Phosphate 2.3 mM; NaCl 155 mM	For x10 concentrated PBS stock solution, 1 l: • NaCl (m = 80 g) • KCl (m = 2 g) • Na_2HPO_4 (m = 14.4 g) • KH_2PO_4 (m = 2.4 g) Adjust to pH 7.4; add H_2O until 1 l; for use dilute from x10 PBS to get x1 PBS
4 % paraformaldehyde (PFA) in PBS	For 200 ml: • PFA 4 % (V = 20 ml of 40 % PFA stock) • PBS (V = 180 ml)
4 % agarose in PBS	For 100 ml; heat in the microwave; keep at 50 °C; cool until 37 °C before use: • Agarose (m = 4 g) • PBS (V = 100 ml)
Blocking solution for 30 minutes preincubation before primary antibodies (0.1 % Triton X-100; 1 % cold-fish gelatin in PBS x1 pH 7.4)	For 0.8 % Triton X-100 stock solution (prepare fresh): • Triton X-100 (V = 800 µl) • PBS (V = 100 ml) For 2 % fish gelatin stock solution (prepare fresh): • Cold-fish gelatin (m = 2 g) • PBS (V = 100 ml) For 20 ml of blocking solution (prepare fresh): • 0.8 % Triton X-100 stock solution (V = 2.5 ml) • PBS (V = 7.5 ml) • 2 % cold-fish gelatin stock solution (V = 10 ml)
Blocking solution for incubation with primary or secondary antibodies (0.1 % Saponin from Quillaja Bark, 1 % cold-fish gelatin in PBS x1 pH 7.4)	For 0.2 % saponin stock solution (prepare fresh): • Saponin (m = 0.2 g) • PBS (V = 100 ml) For 2 % fish gelatin stock solution (prepare fresh): • Cold-fish gelatin (m = 2 g) • PBS (V = 100 ml) For 20 ml of blocking solution (prepare fresh): • 0.2 % saponin stock solution (V = 10 ml) • 2 % cold-fish gelatin (V = 10 ml)

Table 11: Solutions and buffers for tissue samples preparation for fluorescent microscopy (part 2).

Solution / Buffer	Preparation
Primary antibodies mix in the blocking buffer	For 1 ml: • TOM20 primary antibody (rabbit, V = 2 µl) • 0.1 % saponin, 1 % cold-fish gelatine blocking solution (V = 1 ml)
Secondary antibodies mix in the blocking buffer	For ~400 µl: • Goat anti-Rabbit secondary AF555 antibody (V = 0.4 µl) • 0.1 % saponin, 1 % cold-fish gelatine blocking solution (V = 400 µl)
DAPI in PBS pH 7.4	For 20 ml, 1:1000 dilution: • DAPI 5 µg/ml (V = 20 µl of 5 mg/ml stock solution) • PBS (V = 20 ml)
HEPES/KOH buffer 50 mM; pH 7.4	For 1 l; adjust pH to 7.4 with 1 M KOH: • HEPES 50 mM (Mr = 238.3 g/mol; m = 11.92 g)
0.1 % Saponin from Quillaja Bark in 50 mM HEPES/KOH pH 7.4	For 30 ml: • Saponin (m = 0.03 g) • HEPES/KOH (V = 30 ml)
Copper (I) tetrafluoroborate (Cu(I)TFB) 100 mM in acetonitrile	For 12 ml: • Cu(I)TFB (Mr = 314.56 g/mol, m = 0.377 g) • Acetonitrile (V = 12 ml)
Click-dye / azide-reporter for alkyne-lipid distribution visualization	For 12 samples: • HEPES/KOH buffer 50 mM pH 7.4 (prewarmed to 43 °C, V = 12 ml) • AF488-Picolyl-Azide reporter 25 µM (V = 30 µl of 10 mM stock solution in DMSO)

3.2.14. TOM20 antibodies, alkyne-lipid and nuclear fluorescent triple-staining in H9c2 cells

Cells on cover slides after alkyne-fatty acids feeding (3.2.7) were fixed with 4 % paraformaldehyde in PBS. To remove the fixative the samples were washed with 155 mM ammonium acetate for 5 minutes, followed by 3 washes with PBS for 15 minutes each. PBS was exchanged for the blocking solution (1 ml per well) and samples were incubated for 10 minutes. During that time the sterile piece of parafilm was placed into container and a layout for the samples was drawn. On the sterile side of the parafilm 30 µl of primary antibodies mix in blocking buffer was pipetted. The coverslids with cells were placed on respective antibodies drop with cells facing down. Wet paper towels soaked in PBS were placed inside, and the container was sealed and covered with aluminum folium to protect samples from dryness and light. The incubation with antibodies was performed at the room temperature overnight. The next day 1 ml of PBS

was added to each well of a new 24 well plate. The coverslids were transferred into the fresh PBS (cells facing up) and left for 10 minutes. 30 µl of secondary antibodies mix in the blocking buffer were put on a new piece of parafilm in the wet chamber. Coverslids were transferred on the respective antibodies drop facing cells down. Samples were left for 1 hour protected from light in humid chamber. Thereafter the coverslids were transferred to the 24 well-plate with new PBS (cells facing up). The samples were washed with PBS for 15 minutes twice.

For alkyne-lipid staining the cells were thereafter washed with 155 mM ammonium acetate for 5 minutes, followed by 2 washes with HEPES/KOH for 5 minutes each. Thereafter the cells were incubated with 1 ml of 0.1 % saponin in HEPES for 10 minutes without shaking at room temperature. During this time the click-dye was dissolved in the prewarmed HEPES buffer. The saponin solution was exchanged for the click-dye solution and samples were left at 43 ^{o}C in a waterbath protected from light for 1 hour. For the click-reaction catalyzation 10 µl of the 100 mM Cu(I)TFB was added to each well. After 30 minutes of the incubation at 43 ^{o}C in a waterbath additional 10 µl of Cu(I)TFB was added to each well and samples were left for the incubation for another 30 minutes. After click-reaction completion samples were washed twice with HEPES/KOH for 8 minutes. Thereafter, the cells were washed twice with PBS for 8 minutes. PBS was exchanged, and the samples were left at 4 ^{o}C overnight to wash out the remaining click-dye.

The next day the samples were washed twice with PBS for 15 minutes and incubated with DAPI in PBS for 30 minutes. Cells were washed 3 times with PBS for 7 minutes and once with double-distilled water shortly. Thereafter coverslids were directly mounted in Mowiol, their position was fixed with nail polish, and the samples were left for 1 hour before imaging. The slides were stored at 4 ^{o}C between imaging sessions. For solutions and buffers preparations for this experiment see table 12.

Table 12: Solutions and buffers for the antibodies, alkyne-lipids and nuclear fluorescent staining in cells.

Solution / Buffer	Preparation
Ammonium acetate 155 mM for washing	For 1 l: Ammonium acetate 155 mM (Mr = 77.08 g/mol; m = 11.95 g)
Phosphate buffered saline (PBS) buffer x1 Na/K-Phosphate 2.3 mM; NaCl 155 mM	For x10 concentrated PBS stock solution, 1 l: • NaCl (m = 80 g) • KCl (m = 2 g) • Na_2HPO_4 (m = 14.4 g) • KH_2PO_4 (m = 2.4 g) Adjust to pH 7.4; add H_2O until 1 liter; for use dilute from x10 PBS to get x1 PBS buffer
4 % paraformaldehyde (PFA) in PBS	For 200 ml: • PFA 4 % (V = 20 ml of 40 % PFA stock) • PBS (V = 180 ml)
Blocking solution (0.01 % saponin, 1 % cold fish gelatine in PBS)	For 100 ml (prepare fresh): • Saponin (m = 0.01 g) • Cold-fish gelatin (m = 1g) • PBS (V = 100 ml)
Primary antibodies mix in the blocking buffer	For 1 ml: • TOM20 primary antibody (rabbit, V = 2 µl) • 0.01 % saponin, 1 % cold-fish gelatine blocking solution (V = 1 ml)
Secondary antibodies mix in the blocking buffer	For ~400 µl: • Goat anti-Rabbit secondary AF555 antibody (V = 0.4 µl) • 0.01 % saponin, 1 % cold-fish gelatine blocking solution (V = 400 µl)
DAPI in PBS pH 7.4	For 20 ml, 1:1000 dilution: • DAPI 5 µg/ml (V = 20 µl of 5 mg/ml stock solution) • PBS (V = 20 ml)
HEPES/KOH buffer 50 mM; pH 7.4	For 1 l: HEPES 50 mM (Mr = 238.3 g/mol; m = 11.92 g); Add water; adjust pH to 7,4 with 1 M KOH; add water until 1 liter
0.1 % Saponin from Quillaja Bark in 50 mM HEPES/KOH pH 7.4	For 30 ml: • Saponin (m = 0.03 g) • HEPES/KOH (V = 30 ml)
Copper (I) tetrafluoroborate (Cu(I)TFB) 100 mM in acetonitrile	For 12 ml: • Cu(I)TFB (Mr = 314.56 g/mol, m = 0.377 g) • Acetonitrile (V = 12 ml)
Click dye / azide-reporter for alkyne-lipid distribution visualization	For 12 samples: • HEPES/KOH buffer 50 mM pH 7.4 (prewarmed to 43 °C, V = 12 ml) • AF488-Picolyl-Azide reporter 25 µM (V = 30 µl of 10 mM stock solution in DMSO)

3.2.15. PIP2 antibodies and nuclear fluorescent staining of H9c2 cells

The protocol for PIP2 antibodies was similar to 3.4.14. with minor modifications. H9c2 cells on cover slides after exposure to 100 µM erucic acid for 24 hours were washed with DMEM medium and fixed with 4 % paraformaldehyde in PBS. To remove the fixative the samples were washed with 155 mM ammonium acetate for 5 minutes, followed by 3 washes with PBS for 15 minutes each. PBS was exchanged for the blocking solution (1 ml per well) and samples were incubated for 10 minutes. During that time the sterile piece of parafilm was placed into container and a layout for the samples was drawn. On the sterile side of the parafilm 30 µl of primary antibodies mix in blocking buffer was pipetted for each sample. The coverslids with cells were placed on respective antibodies drop with cells facing down. Wet paper towels soaked in PBS were placed inside, and the container was sealed and covered with aluminum folium to protect samples from dryness and light. The incubation with antibodies was performed at the room temperature overnight. The next day 1 ml of PBS was added to each well of a new 24 well plate. The coverslids were transferred into the fresh PBS (cells facing up) and left for 10 minutes. 30 µl of secondary antibodies mix in the blocking buffer were put for each sample on a new piece of parafilm in the wet chamber. Coverslids were transferred on the respective antibodies drop facing cells down. Samples were left for 1 hour protected from light in humid chamber. Thereafter the coverslids were transferred to the 24 well-plate with new PBS (cells facing up). Thereafter the samples were washed 3 times with PBS for 15 minutes and incubated with DAPI in PBS for 1 hour. Cells were washed 3 times with PBS for 7 minutes and once with double-distilled water shortly. Thereafter coverslids were directly mounted in Mowiol, their position was fixed with nail polish, and the samples were left for 1 hour to solidify until imaging. The slides were stored at 4 ^{o}C between imaging sessions. For solutions and buffers preparations for this experiment see table 13.

Table 13: Solutions and buffers for the antibodies, alkyne-lipids and nuclear fluorescent staining in cells.

Solution / Buffer	Preparation
Ammonium acetate 155 mM for washing	For 1 l: Ammonium acetate 155 mM (Mr = 77.08 g/mol; m = 11.95 g)
Phosphate buffered saline (PBS) buffer x1 Na/K-Phosphate 2.3 mM; NaCl 155 mM	For x10 concentrated PBS stock solution, 1 l: • NaCl (m = 80 g) • KCl (m = 2 g) • Na_2HPO_4 (m = 14.4 g) • KH_2PO_4 (m = 2.4 g) Adjust to pH 7.4; add H_2O until 1 liter; for use dilute from x10 PBS to get x1 PBS buffer
4 % paraformaldehyde (PFA) in PBS	For 200 ml: • PFA 4 % (V = 20 ml of 40 % PFA stock) • PBS (V = 180 ml)
Blocking solution (1 % cold fish gelatine in PBS)	For 100 ml (prepare fresh): • Cold-fish gelatin (m = 1g) • PBS (V = 100 ml)
Primary antibodies mix in the blocking buffer	For 250 µl: • PIP2 primary antibody (mouse, V = 2.5 µl, 1:100 dilution) • 1 % cold-fish gelatine blocking solution (V = 250 µl)
Secondary antibodies mix in the blocking buffer	For ~400 µl: • Goat anti-mouse secondary AF488 antibody (V = 0.4 µl) • 1 % cold-fish gelatine blocking solution (V = 400 µl)
DAPI in PBS pH 7.4	For 20 ml, 1:1000 dilution: • DAPI 5 µg/ml (V = 20 µl of 5 mg/ml stock solution) • PBS (V = 20 ml)

3.2.16. Lipid droplet and nuclear fluorescent double-staining in H9c2 cells

H9c2 cells were grown on cover slides and were exposed to different fatty acids or chemicals (ATGListatin) for 24 hours. After washing with PBS, cells were fixed with 500 µl of 4 % paraformaldehyde in PBS and stored at 4 °C. At the day of staining cells were washed once with 500 µl of 155 mM ammonium acetate for 5 minutes and 3 times with 500 µl of PBS for 15 minutes. Thereafter, cells were incubated with 500 µl of LD540 (1:5000 dilution) together with DAPI (1:1000 dilution) dissolved in PBS for an hour in the dark. LD540 is a lipophilic dye used for lipid droplets imaging in the cell (Spandl et al., 2009). After the staining step, the cells were washed 3 times for 10 minutes with 500 µl of plain PBS and mounted in 9 µl of Mowiol. After 30 minutes of waiting, the slides position was fixed with nail polish. Samples were left for an additional hour to solidify before imaging. The slides were stored at 4 °C between imaging sessions. Solutions and buffers for this experiment are shown in the table 14.

Table 14: Solutions and buffers for the lipid droplets and nuclei staining in cells.

Solution / Buffer	Preparation
Ammonium acetate 155 mM for washing	For 1 l: Ammonium acetate 155 mM (Mr = 77.08 g/mol; m = 11.95 g)
Phosphate buffered saline (PBS) buffer x1 Na/K-Phosphate 2.3 mM; NaCl 155 mM	For x10 concentrated PBS stock solution, 1 l: • NaCl (m = 80 g) • KCl (m = 2 g) • Na_2HPO_4 (m = 14.4 g) • KH_2PO_4 (m = 2.4 g) Adjust to pH 7.4; add H_2O until 1 liter; for use dilute from x10 PBS to get x1 PBS buffer
4 % paraformaldehyde (PFA) in PBS	For 200 ml: • PFA 4 % (V = 20 ml of 40 % PFA stock) • PBS (V = 180 ml)
DAPI and LD540 in PBS pH 7.4	For 20 ml: • DAPI 5 µg/ml (V = 20 µl of 5 mg/ml stock solution; 1:1000 dilution) • LD540 0.02 µg/ml (V = 4 µl of 0.1 mg/ml stock; 1:5000 dilution) • PBS (V = 20 ml)

3.2.17. Apoptosis assay

The Elabscience One-step TUNEL *In Situ* Apoptosis Kit with Elab Fluor555 fluorophore was used to detect apoptosis in H9c2 cells. The assay is based on the following principle: during apoptosis specific DNA endonucleases are activated, which cut the genomic DNA between the nucleosomes; thereafter, the Terminal Deoxynucleotodyl Transferase (TdT) can attach fluorescently-labeled dUTP to the exposed 3'-OH ends of the broken DNA, and the label can be detected by fluorescence microscope. For the apoptotic assay H9c2 cells were grown on cover glass. Cells were left for 24 hours to attach. Thereafter, the media was exchanged with 500 µl of DMEM media with 200 µM $CoCl_2$ or 200 µM H_2O_2, and the cells were incubated with these additives for 24 or 3 hours, respectively. After the exposure to chemical hypoxia or oxidative stress the media was aspirated, and the cells were fixed with 500 µl of 4 % paraformaldehyde in PBS for 2 hours. Thereafter, the cells were washed 3 times with 500 µl of PBS for 5 minutes. For the positive control just before permeabilization step with Triton X-100 cells were incubated with 100 µl of DNase(I) buffer for 5 minutes at room temperature; the liquid was blotted, 100 µl of DNase(I) working solution was added, the samples were incubated for 30 minutes at 37 ^{o}C and washed thereafter 3 times with 500 µl of PBS for

5 minutes. For the negative control 100 µl of DNase(I) buffer was added; the samples were incubated for 5 minutes at the room temperature and, thereafter, incubated at 37 °C for 30 minutes, followed by 3 washes with 500 µl of PBS for 5 minutes. All samples (including positive, negative controls and experiment samples) were permeabilized with 500 µl of 0.2 % Triton X-100 dissolved in PBS for 10 minutes at 37 °C. Thereafter, the cells were washed 3 times with 500 µl of PBS for 5 minutes and left in 100 µl of the equilibrium buffer at 37 °C for 30 minutes. The liquid was blotted, and 50 µl of the labeling solution with the enzyme (or without the enzyme, for the negative control) was added. The cells were left in the dark at 37 °C for 60 minutes and washed thereafter 3 times with 500 µl of PBS for 5 minutes. Nuclear staining was performed by adding 200 µl of DAPI working solution from the kit for 5 minutes. Cells were washed 4 times with 500 µl of PBS for 5 minutes, mounted in 9 µl of Mowiol, fixed with nail polish and left for 1 hour to solidify until imaging. The slides were stored at 4 °C between imaging sessions. For the buffers and solutions preparations for this experiment see the table 15 (part 1 and 2).

Table 15: Solutions and buffers for the TUNEL assay staining (part 1).

Solution / Buffer	Preparation
Phosphate buffered saline (PBS) buffer x1 Na/K-Phosphate 2.3 mM; NaCl 155 mM	For x10 concentrated PBS stock solution, 1 l: • NaCl (m = 80 g) • KCl (m = 2 g) • Na_2HPO_4 (m = 14.4 g) • KH_2PO_4 (m = 2.4 g) Adjust to pH 7.4; add H_2O until 1 liter; for use dilute from x10 PBS to get x1 PBS buffer
4 % paraformaldehyde (PFA) in PBS	For 200 ml: • PFA 4 % (V = 20 ml of 40 % PFA stock) • PBS (V = 180 ml)
Permeabilization buffer with 0.2 % Triton X-100	For 100 ml: • Triton X-100 (V = 200 µl) • PBS (V = 100 ml)
x1 DNase I buffer	For 100 µl: • DNase I buffer 10x (V = 10 µl) • Double-distilled H_2O (V = 90 µl)
DNase I working solution	For 100 µl (200 U/ml): • DNase I (20 U/µl; V = 1 µl) • DNase I buffer x1 (V = 99 µl)

Table 15: Solutions and buffers for the TUNEL assay staining (part 2).

Solution / Buffer	Preparation
Labeling working solution for the positive control and experimental group	For 50 µl: • TdT Equilibration Buffer (V = 35 µl) • Labeling solution (V = 10 µl) • TdT Enzyme (V = 5 µl)
Labeling working solution for the negative control	For 50 µl: • TdT Equilibration Buffer (V = 40 µl) • Labeling solution (V = 10 µl)
DAPI working solution	For 100 µl: • DAPI (x25, 25 µg/ml; V = 4 µl) • PBS (V = 96 µl)

3.2.18. Slices and cells fluorescent microscopic imaging

The cells (from 3.2.14, 3.2.15, 3.2.16 and 3.2.17) and sections (from 3.2.13) were analyzed using Zeiss Axio Observer.Z1 fluorescent microscope (Carl Zeiss) equipped with Hamamatsu Orca-Flosh 4.0 digital camera and motorized stage. Optical sectioning was performed at x40 or x63 magnification with Apotome (Carl Zeiss) with 0.1-0.3 µm interval. Microphotographs represent maximal intensity projections derived from 5-80 triple-ApoTome images. Polychrome V 150 W xenon lamp (Till Photonics) served as a light source. For DAPI imaging (nuclei staining) the wavelength used was 355 nm, exposure time 80 ms. For AF488-Picolyl-Azide click-reporter (alkyne-lipids) or secondary AF488 antibodies (PIP2) – 483 nm, exposure time 100 ms. For secondary AF555 antibodies (mitochondrial TOM20 marker), LD540 (lipid droplets) or TUNEL assay (dUTP, cells undergoing apoptosis) – 534 nm, exposure time 100 ms. Microscopy data was processed in the ZEN software (Carl Zeiss).

4. Results

4.1. Common dietary fatty acids metabolism in the cardiac setup

Alkyne-fatty acid tracers allowed to follow cardiac lipid metabolism in the heart lysates, H9c2 cell line, viable heart slices and isolated Langendorff heart. Alkyne analogs of four common dietary fatty acids with different carbon chain length and saturation degree have been tested: medium chain saturated capric acid, long-chain saturated palmitic acid, long-chain monounsaturated oleic acid and long-chain polyunsaturated linoleic acid. Mass spectrometric lipid tracing allowed parallel identification of lipids, derived from 3 alkyne-fatty acids analogs of these natural fatty acids, allowing to feed different fatty acids simultaneously and, thus, mimic complex fatty acid content in the diet.

Medium-chain fatty acids are catabolized more intensively by the heart lysates than long-chain alkyne-fatty acids. In the heart lysates the catabolic pathways are prevailing, since the anabolic pathways are disrupted during sample preparation. When studying the disappearance of alkyne-fatty acids in this setup, the medium-chain alkyne-capric acid analog (FA11:0;Y) was the most preferred substrate, which decreased 5 times after 60 minutes incubation compared to its initial amounts at the start of the assay (see figure 7 (a) and supplementary figure 1). Among the long-chain alkyne-fatty acids tested, alkyne-linoleic acid (FA18:2;Y) was preferred over alkyne-palmitic (FA17:0;Y) and alkyne-oleic (FA19:1;Y) acid (~3.3, 2.5 and 2 times decrease compared to these fatty acids' initial amounts, respectively).

Long-chain fatty acids are the preferred substrate for the cardiac anabolism compared to medium-chain fatty acids. Length of alkyne-fatty acid tracers had an impact on their incorporation rate into cardiac lipids. Irrespectively from the setup tested (H9c2 cells, viable heart slices or the Langendorff heart) all long-chain alkyne-fatty acids (alkyne-palmitic acid FA16:0;Y($^{13}C_6$), alkyne-linoleic acid FA18:2;Y and alkyne-oleic acid FA19:1;Y) were incorporated in higher amounts than medium-chain alkyne-fatty acids (alkyne-capric acid FA11:0;Y and alkyne-lauric acid FA12:0;Y). This indicates, that the rodent heart prefers long-chain fatty acids for its anabolism (see figure 7 (b-g)). When comparing different long-chain fatty acids between each other, slight preference for linoleic acid analog (FA18:2;Y) was observed. Also, no differences between atria and

ventricles' preferences in the Langendorff heart preparations were seen (see figure 7 (g)).

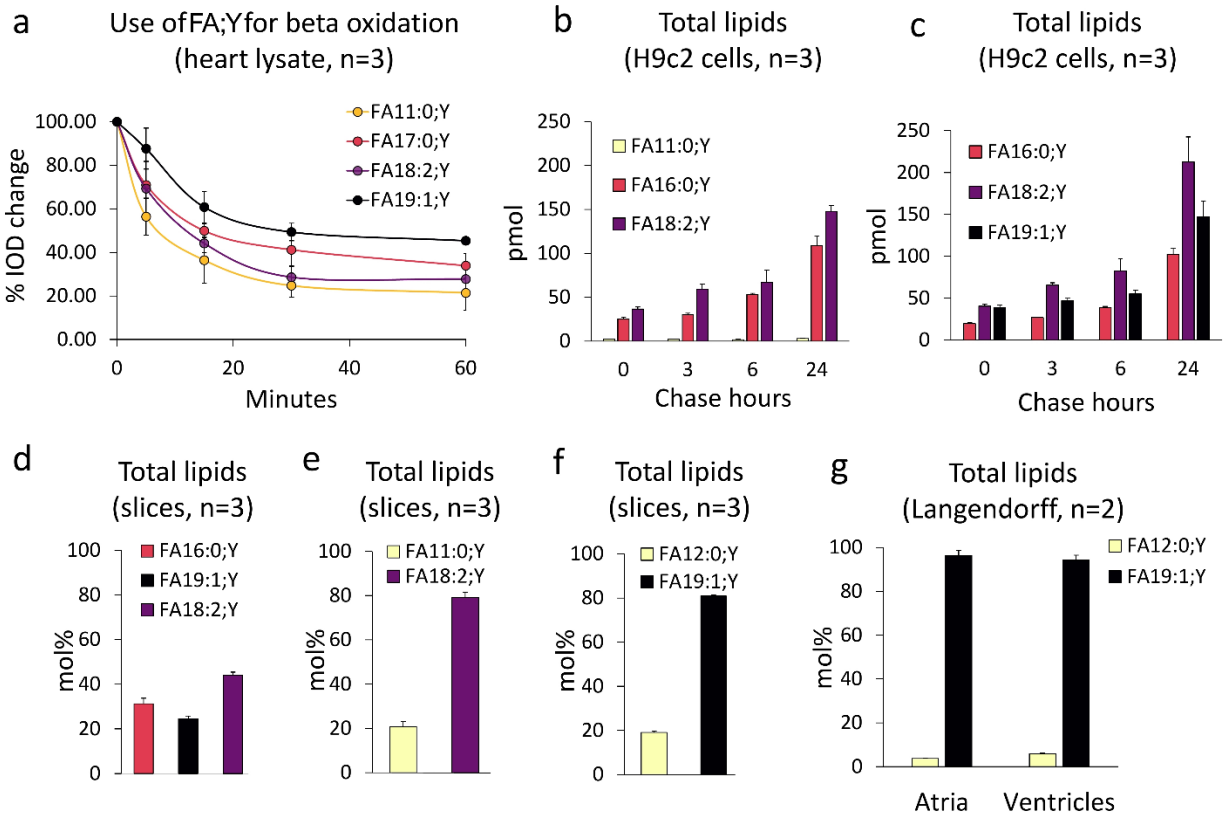

Figure 7: Preference of medium- and long-chain alkyne-fatty acid tracers in various cardiac setups. **(a)** Alkyne-fatty acid tracers' utilization by the heart lysates. Alkyne-fatty acid tracers (alkyne-capric acid FA11:0;Y, alkyne-palmitic acid FA17:0;Y, alkyne-linoleic acid FA18:2;Y or alkyne-oleic acid FA19:1;Y) were incubated with heart lysates up to 60 minutes. Amounts of remaining alkyne-fatty acids in the assay mixture was detected using thin layer chromatography, and integrated optical density (IOD) for each alkyne-fatty acid was calculated. Here IOD change to the corresponding alkyne-fatty acid IOD at the start of the assay (100 % at 0 minutes) over time is shown. Data as average ± standard deviation, n=3 (hearts from 3 different mice). For original thin layer chromatography images used for calculations of average values refer to supplementary figure 1. **(b,c)** H9c2 cells were fed with alkyne-fatty acid mix 1 (alkyne-capric acid FA11:0;Y, alkyne-palmitic acid FA16:0;Y($^{13}C_6$) and alkyne-linoleic acid FA18:2;Y) or mix 2 (alkyne-palmitic acid FA16:0;Y($^{13}C_6$), alkyne-linoleic acid FA18:2;Y and alkyne-oleic acid FA19:1;Y) for 1 hour. Thereafter, cells were chased for 0, 3, 6 or 24 hours. The extracted lipids were analyzed by mass spectrometry. Data shows total picomoles (pmol) of alkyne-lipids identified per well for each alkyne-fatty acid (average ± standard deviation, n=3). **(d-f)** The viable heart slices were fed for 1 hour with alkyne-fatty acid mix 1 (alkyne-palmitic acid FA16:0;Y($^{13}C_6$), alkyne-linoleic acid FA18:2;Y and alkyne-oleic acid FA19:1;Y) or mix 2 (alkyne-capric acid FA11:0;Y and alkyne-linoleic acid FA18:2;Y) or mix 3 (alkyne-lauric acid FA12:0;Y and alkyne-oleic acid FA19:1;Y). The extracted lipids were analyzed by mass spectrometry. Alkyne-lipids, derived from a certain alkyne-fatty acid, are shown as percentage of all labeled lipid species identified in the sample (mol%, average ± standard deviation, n=3). **(g)** The isolated working heart (Langendorff heart) was perfused with a mix of alkyne-fatty acids (alkyne-lauric acid FA12:0;Y and alkyne-oleic acid FA19:1;Y) for 30 minutes. Atria and ventricles were extracted separately and analyzed by mass spectrometry. Alkyne-lipids, derived from a certain alkyne-fatty acid, are shown as percentage of all labeled lipid species identified in the sample (mol%, average ± standard deviation, n=3).

Medium- and long-chain fatty acids have different distribution within major cardiac lipid classes. Lipid classes, formed from different alkyne-fatty acid tracers, were analyzed via mass spectrometry. The length and saturation degree of alkyne-fatty acids influenced their anabolism and incorporation into major cardiac lipid classes (see figure 8). The medium-chain alkyne-capric acid (FA11:0;Y) was primarily used for intracardiac triglycerides synthesis, confirming the ability of cardiac cells to synthesize triacylglycerols from medium-chain fatty acids. The capacity to synthesize medium-chain triglycerides was observed in both cardiac H9c2 cell line and viable heart slices. Differences in long-chain fatty acids distribution within major lipid classes were observed in different setups tested. In the cellular setup, alkyne-palmitic (FA16:0;Y($^{13}C_6$), alkyne-oleic (FA19:1;Y) and alkyne-linoleic (FA18:2;Y) acids were primarily incorporated into phosphatidylcholines and other phospholipids. On the contrary, in the slices setup the tendency of higher triglycerides synthesis was seen, while less phospholipids were produced. However, independently from the setup tested, still a significant portion of long-chain fatty acids, in contrast to medium-chain fatty acids, goes to cardiac phospholipids production. Interestingly, the alkyne-palmitic acid was also significantly incorporated into cholesterol esters and ceramides in comparison to other long-chain fatty acids tested.

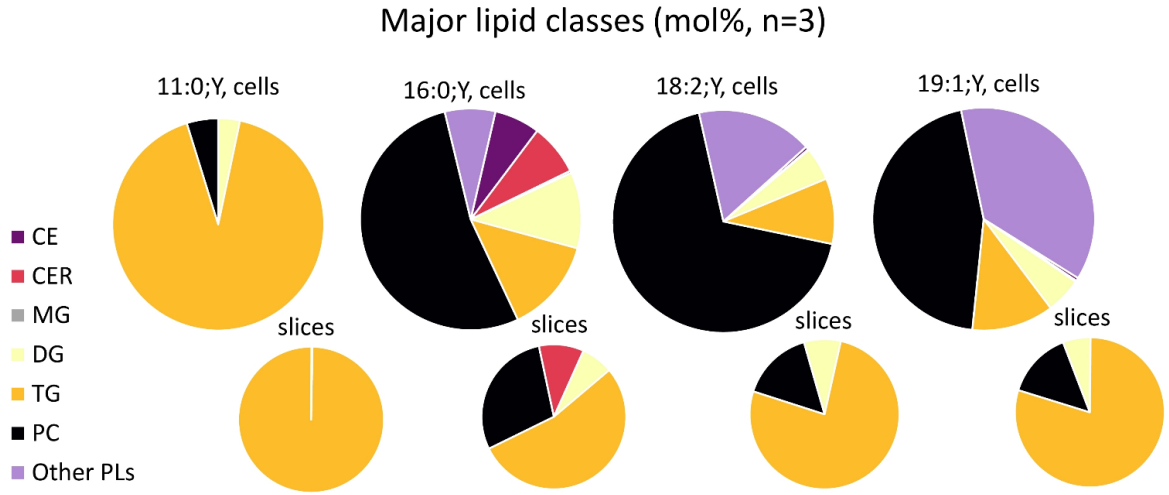

Figure 8: Major cardiac lipid classes synthesized from medium- and long-chain alkyne-fatty acids. The upper row represents cellular data (H9c2 cell line). The lower row shows major lipid classes produces by viable heart slices. Cells or viable heart slices were fed for 1 hour with alkyne-capric acid FA11:0;Y, alkyne-palmitic acid FA16:0;Y($^{13}C_6$), alkyne-linoleic acid FA18:2;Y or alkyne-oleic acid FA19:1;Y. The samples were extracted, and the distribution of the alkyne-label within major lipid classes after 1 hour pulse was analyzed via mass spectrometry. Data shown as mol percent (mol%) of sum of alkyne-lipid class derived from corresponding alkyne-fatty acid to the total alkyne-lipids identified in the sample (average ± standard deviation, n=3). CE, cholesterol esters; CER, ceramides; MG, monoacylglycerols; DG, diacylglycerols; TG, triacylglycerols; PC, phosphatidylcholines; Other PLs, sum of other phospholipids identified in the sample.

Alkyne-lipid visualization via fluorescence microscopy confirms more intense incorporation of long-chain fatty acids into cellular lipids in contrast to medium-chain fatty acids. Incorporation and distribution of the alkyne-label could be followed by fluorescence microscopy in H9c2 cells and the Langendorff heart. In agreement to the mass spectrometric data, the fluorescence microscopy data confirmed that cardiomyocytes prefer long-chain alkyne-fatty acids over medium-chain fatty acids for their anabolism. Cells, fed with polyunsaturated alkyne-linoleic (FA18:2;Y), monounsaturated alkyne-oleic (FA19:1;Y) or saturated long-chain alkyne-palmitic acid (FA17:0;Y), were more intensively stained for the alkyne-lipids after the click-reaction with the azide-fluorescent reporter in contrast to medium-chain alkyne-capric acid (FA11:0;Y), as it could be seen on the figure 9. The alkyne-lipid staining was especially prominent in the area around the nuclei for the long-chain fatty acids, which was independent from the saturation degree of alkyne-fatty acids tested (see figures 9 and 10).

Interestingly, characteristic striation was observed in the Langendorff heart when stained for the lipids derived from the long-chain alkyne-linoleic acid (FA18:2;Y), as it could be seen on the figure 10. When stained for the mitochondrial TOM20 marker, there was significant overlap between mitochondrial and alkyne-lipid staining in the perfused hearts, confirming localization of some of the alkyne-linoleic acid-derived lipids to the cardiac mitochondria and explaining the observed striation (see figure 11). In H9c2 cells also significant overlap between TOM20 and alkyne-lipid signal was seen for all tracers tested, confirming that at least some portion of the newly-synthesized alkyne-lipids were localized to mitochondria (see figures 12-15).

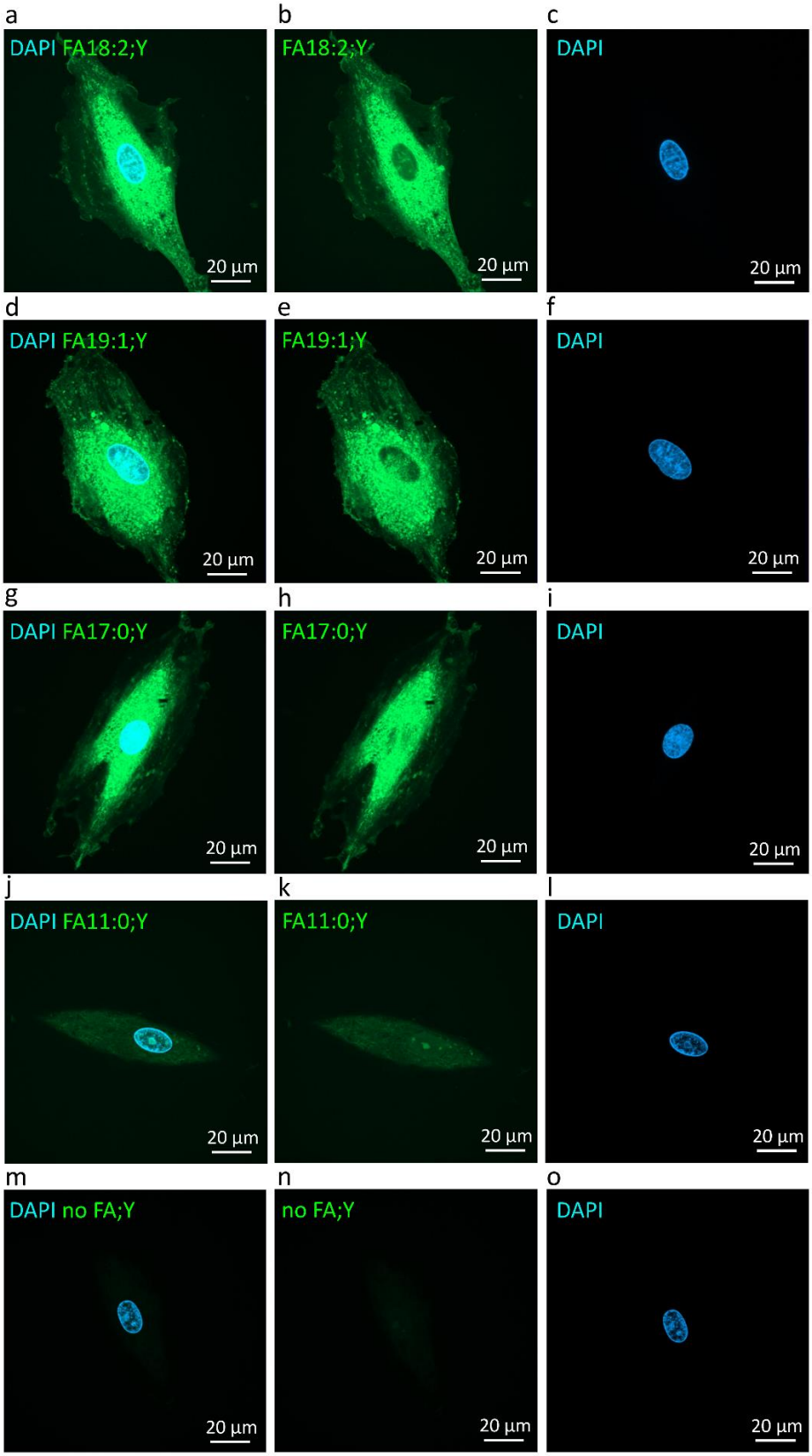

Figure 9: Fluorescent imaging of different alkyne-fatty acids incorporation in H9c2 cells. H9c2 cells were fed with one of the alkyne-fatty acids (alkyne-linoleic FA18:2;Y **(a-c)**, alkyne-oleic FA19:1;Y **(d-f)**, alkyne-palmitic FA17:0;Y **(g-i)** or alkyne-capric acid FA11:0;Y **(j-l)**, or incubated in a plain media **(m-o)** for 1 hour, washed and fixed with 4 % paraformaldehyde. After the click-reaction with the AF488-picolyl-azide reporter (green) and nuclear staining with DAPI (blue), the uptake and distribution of alkyne-lipids was visualized by fluorescence microscopy at x63 magnification. Optical sectioning was performed with Apotome. The scalebar is 20 µm.

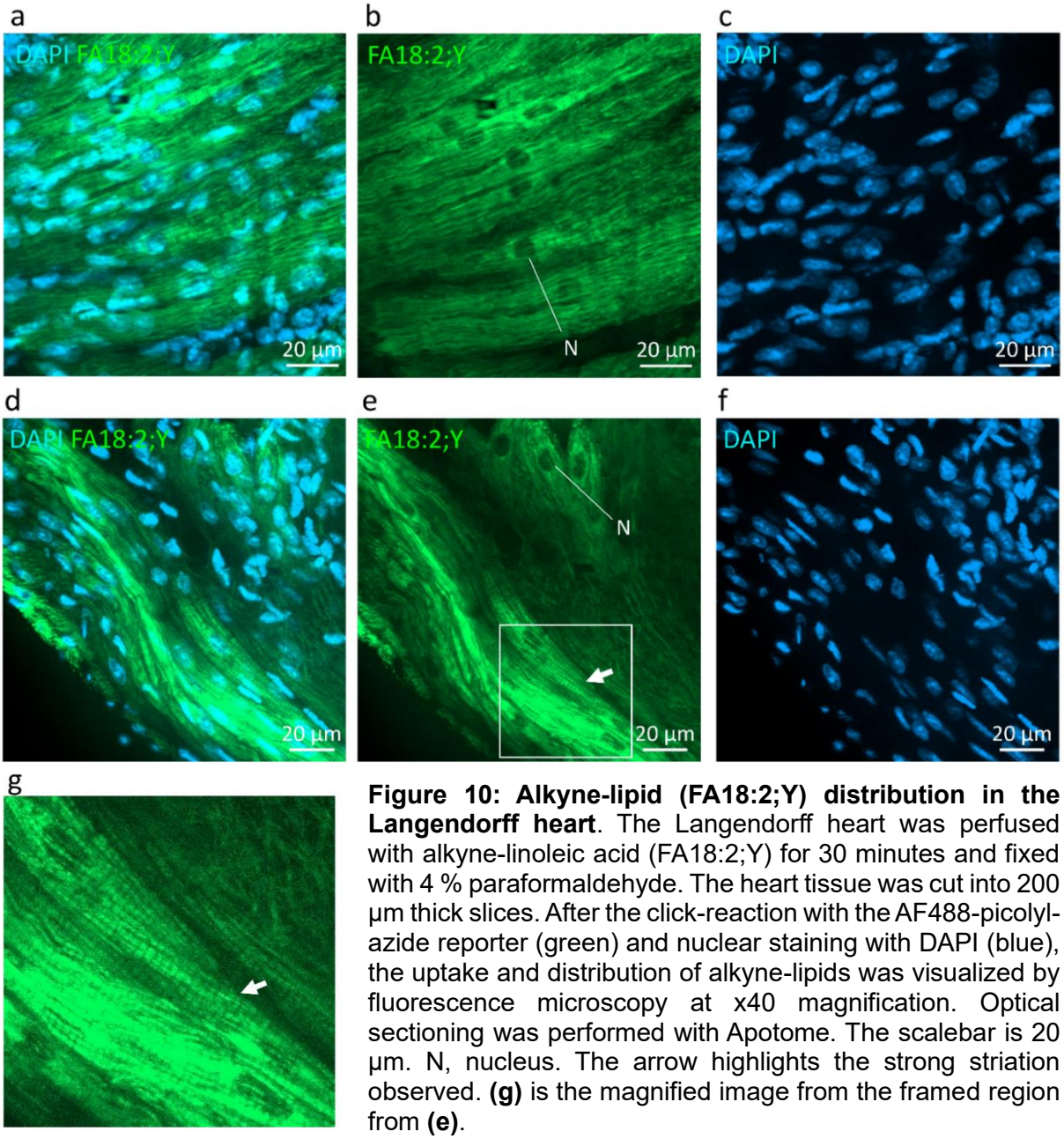

Figure 10: Alkyne-lipid (FA18:2;Y) distribution in the Langendorff heart. The Langendorff heart was perfused with alkyne-linoleic acid (FA18:2;Y) for 30 minutes and fixed with 4 % paraformaldehyde. The heart tissue was cut into 200 µm thick slices. After the click-reaction with the AF488-picolyl-azide reporter (green) and nuclear staining with DAPI (blue), the uptake and distribution of alkyne-lipids was visualized by fluorescence microscopy at x40 magnification. Optical sectioning was performed with Apotome. The scalebar is 20 µm. N, nucleus. The arrow highlights the strong striation observed. **(g)** is the magnified image from the framed region from **(e)**.

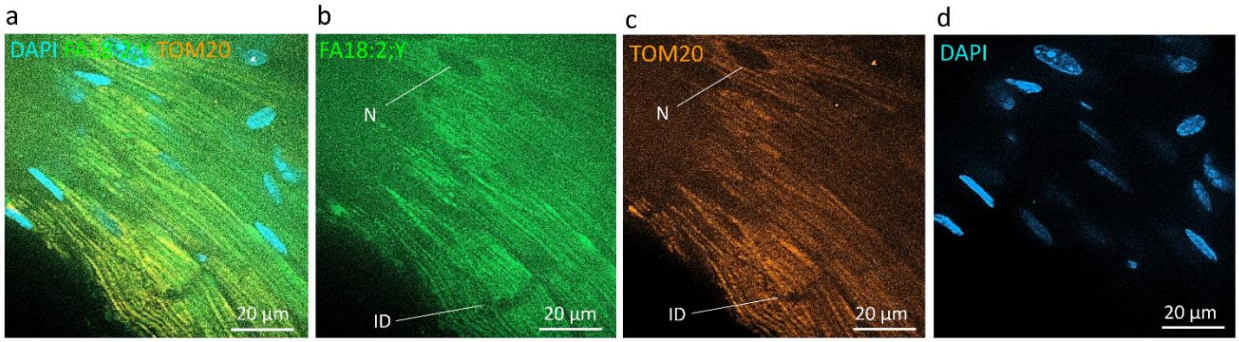

Figure 11: The Langendorff heart triple-staining for alkyne-lipids (FA18:2;Y), mitochondria and nuclei. The Langendorff heart was perfused with alkyne-linoleic acid (FA18:2;Y) for 30 minutes and fixed with 4 % paraformaldehyde. The heart tissue was cut into 200 µm thick slices and stained for mitochondrial marker TOM20 (orange). After the click-reaction with the AF488-picolyl-azide reporter (green) and nuclear staining with DAPI (blue), the uptake and distribution of alkyne-lipids was visualized by fluorescence microscopy at x40 magnification. Optical sectioning was performed with Apotome. The scalebar is 20 µm. ID, intercalated disc; N, nucleus.

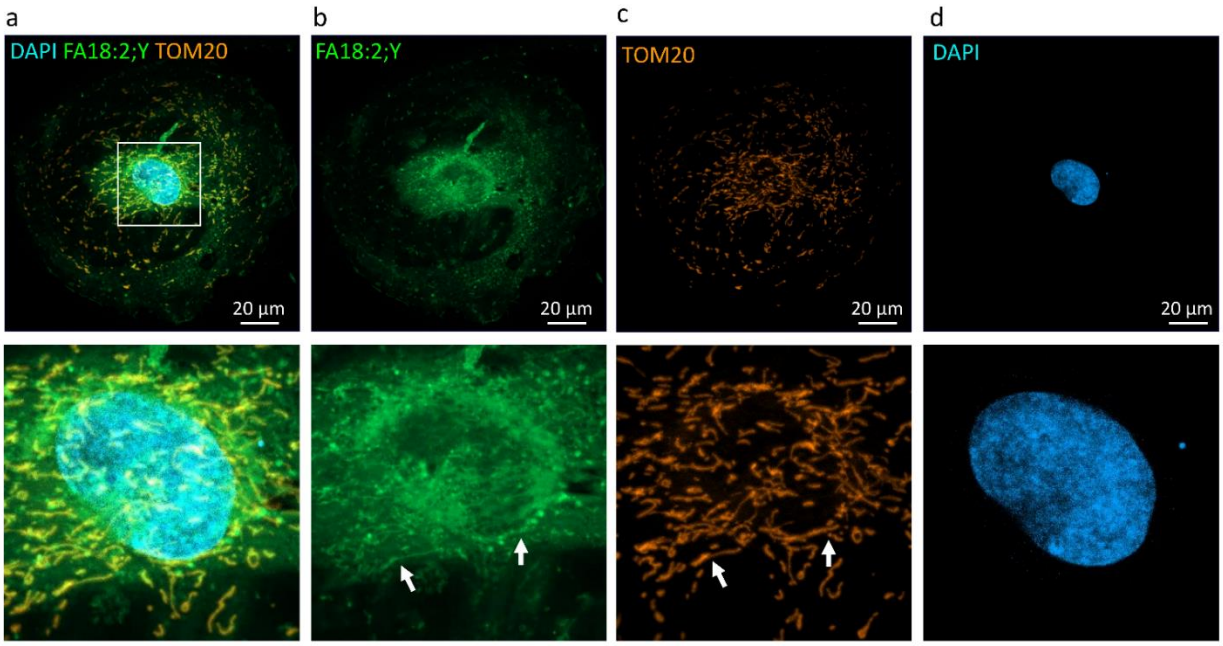

Figure 12: H9c2 triple staining for alkyne-lipids (FA18:2;Y), mitochondria and nuclei. The H9c2 cells were fed with alkyne-linoleic acid (FA18:2;Y) for 1 hour and fixed with 4 % paraformaldehyde. The samples were stained for the mitochondrial marker TOM20 (orange). After the click-reaction with the AF488-picolyl-azide reporter (green) and nuclear staining with DAPI (blue), the uptake and distribution of alkyne-lipids was visualized by fluorescence microscopy at x63 magnification. Optical sectioning was performed with Apotome. The scalebar is 20 µm. The arrow indicates the lipid-mitochondrial signal overlap. The lower row represents the magnified image from the boxed region from **(a)**.

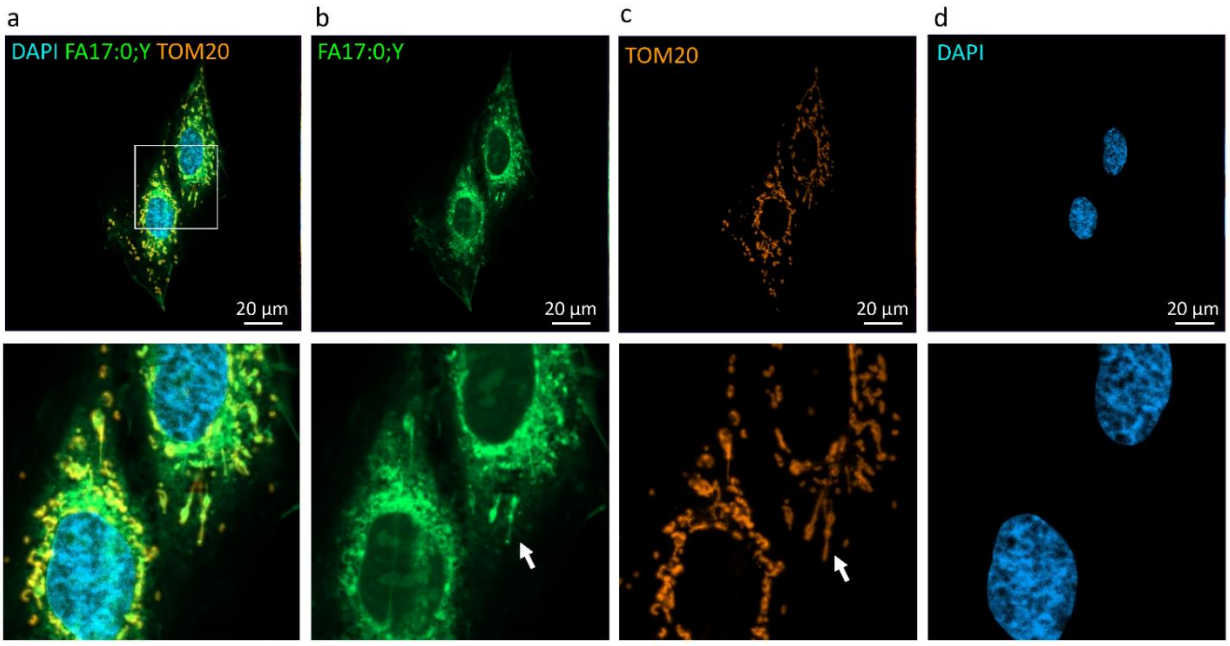

Figure 13: H9c2 triple staining for alkyne-lipids (FA17:0;Y), mitochondria and nuclei. The H9c2 cells were fed with alkyne-palmitic acid (FA17:0;Y) for 1 hour and fixed with 4 % paraformaldehyde. The samples were stained for the mitochondrial marker TOM20 (orange). After the click-reaction with the AF488-picolyl-azide reporter (green) and nuclear staining with DAPI (blue), the uptake and distribution of alkyne-lipids was visualized by fluorescence microscopy at x63 magnification. Optical sectioning was performed with Apotome. The scalebar is 20 µm. The arrow indicates the lipid-mitochondrial signal overlap. The lower row represents the magnified image from the boxed region from **(a)**.

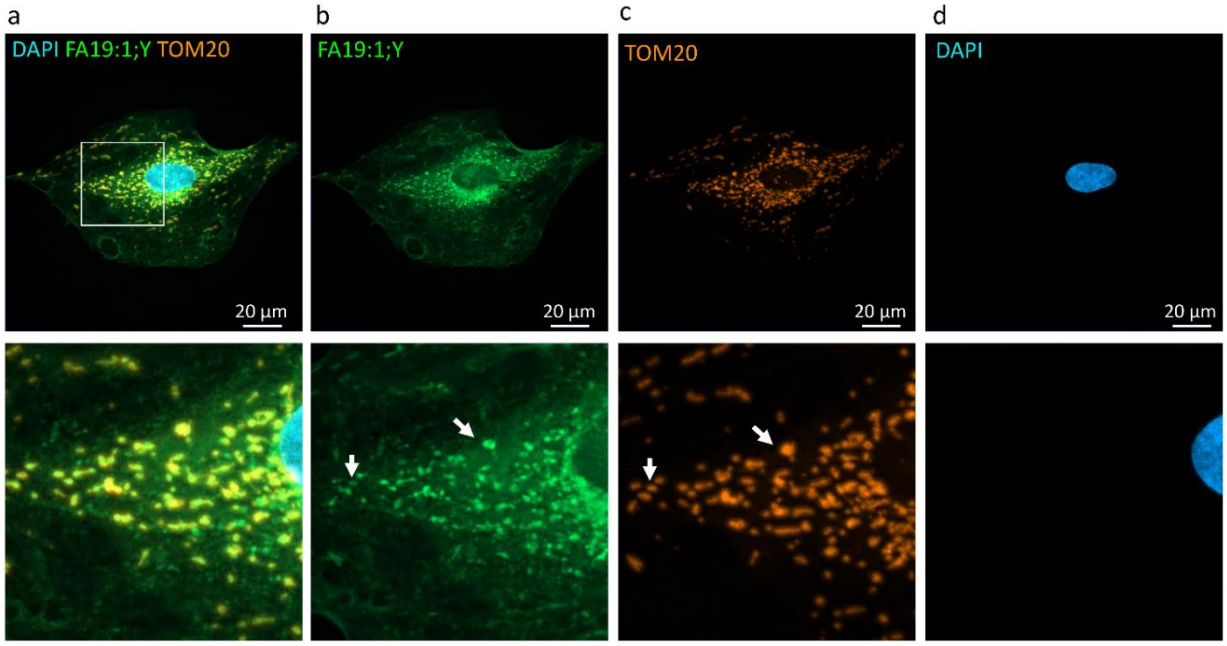

Figure 14: H9c2 triple staining for alkyne-lipids (FA19:1;Y), mitochondria and nuclei. The H9c2 cells were fed with alkyne-oleic acid (FA19:1;Y) for 1 hour and fixed with 4 % paraformaldehyde. The samples were stained for the mitochondrial marker TOM20 (orange). After the click-reaction with the AF488-picolyl-azide reporter (green) and nuclear staining with DAPI (blue), the uptake and distribution of alkyne-lipids was visualized by fluorescence microscopy at x63 magnification. Optical sectioning was performed with Apotome. The scalebar is 20 µm. The arrow indicates the lipid-mitochondrial signal overlap. The lower row represents the magnified image from the boxed region from **(a)**.

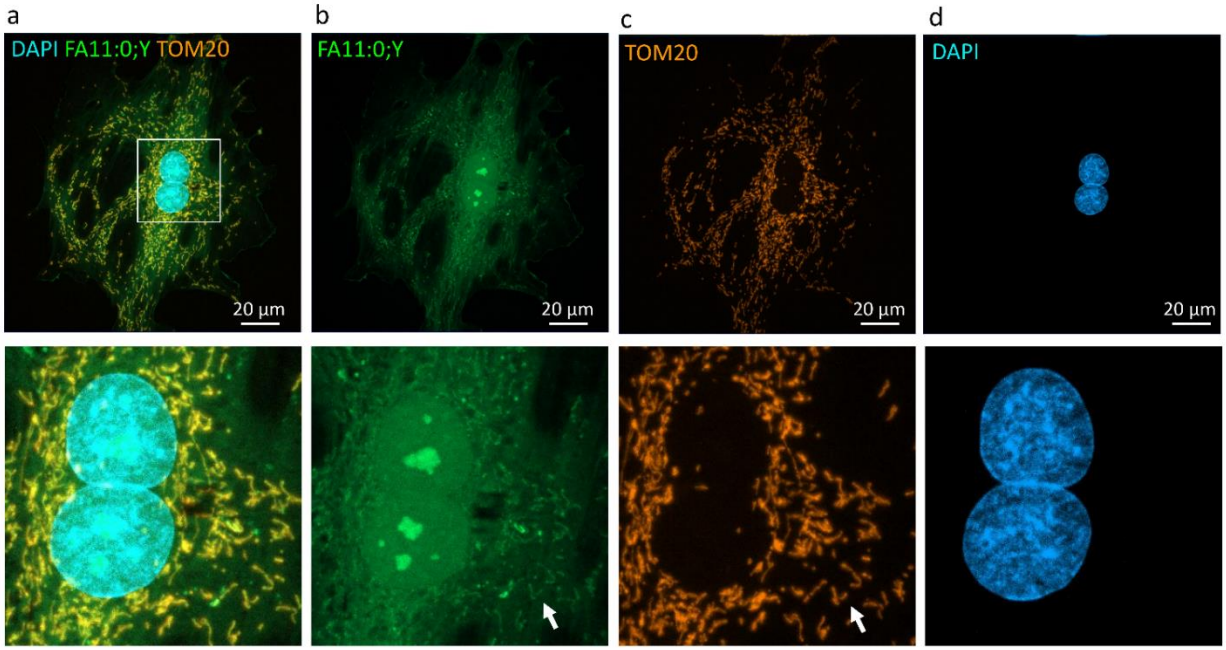

Figure 15: H9c2 cells triple staining for alkyne-lipids (FA11:0;Y), mitochondria and nuclei. The H9c2 cells were fed with alkyne-capric acid (FA11:0;Y) for 1 hour and fixed with 4 % paraformaldehyde. The samples were stained for the mitochondrial marker TOM20 (orange). After the click-reaction with the AF488-picolyl-azide reporter (green) and nuclear staining with DAPI (blue), the uptake and distribution of alkyne-lipids was visualized by fluorescence microscopy at x63 magnification. Optical sectioning was performed with Apotome. The scalebar is 20 µm. The arrow indicates the lipid-mitochondrial signal overlap. The lower row represents the magnified image from the framed region from **(a)**.

Alkyne-fatty acids allowed to observe cardiac phosphatidylcholine side chain remodeling over time. The phosphatidylcholines were one of the most abundant lipid classes synthesized by cardiomyocytes from the long-chain alkyne-fatty acids. The cardiac phosphatidylcholines' remodeling was analyzed on species resolution using mass spectrometer. The significant changes in phosphatidylcholines (PC) species derived from the alkyne-linoleic acid tracer (FA18:2;Y) were observed over time. As it could be seen on slices (figure 16 (b)) and cellular data (figure 17 (b)), the decrease of PC34;Y, derived from alkyne-linoleic acid, is accompanied by increase of PC36;Y and PC38;Y over time. Whether this increase in the phosphatidylcholines carbon chain length is due to ongoing elongation of linoleic acid or due to more frequent association of linoleic-acid containing phosphatidylcholines with the second fatty acid of the increased length is not entirely clear.

No univocal picture could be concluded for alkyne-palmitic (FA16:0;Y($^{13}C_6$)) acid-derived phosphatidylcholines due to differences in data from cellular and slices setups.

In the viable heart slices PC32;Y decreased at the beginning, and this decrease was accompanied with the increase of PC38;Y over time. Also, significant desaturation of alkyne-palmitic acid-derived phosphatidylcholines and accumulation of phosphatidylcholine species with multiple double bonds was observed in the viable heart slices over time. This indicated, that phosphatidylcholines, which incorporated saturated palmitate, underwent a steady change towards pairing with longer and more unsaturated fatty acids over time in the viable heart slices. However, in cells no significant changes in carbon chain length and saturation degree of palmitate-containing phosphatidylcholines were observed.

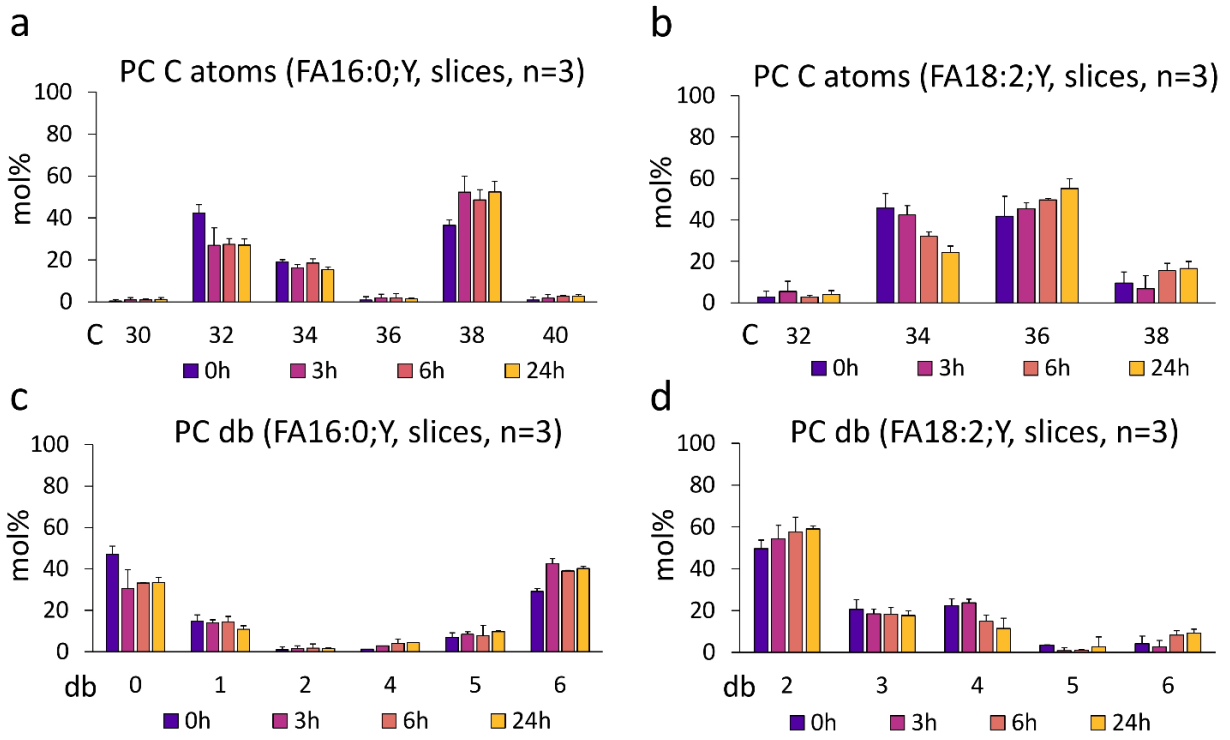

Figure 16: Phosphatidylcholines remodeling in the viable heart slices. Viable heart slices were fed with alkyne-palmitic acid (FA16:0;Y ($^{13}C_6$)) or alkyne-linoleic acid (FA18:2;Y) for 1 hour and, thereafter, chased for 0, 3, 6 or 24 hours (h) in the plain media. Lipids were extracted and analyzed via mass spectrometry. Different phosphatidylcholine (PC) species abundancies were determined. The picomoles of species of the same length (C atoms, **(a, b)**) or saturation degree (db, double bond count, **(c, d)**) were summed together and calculated as mol percent (mol%) to the sum of all phosphatidylcholine species identified for this alkyne-tracer. Data as average ± standard deviation, n=3.

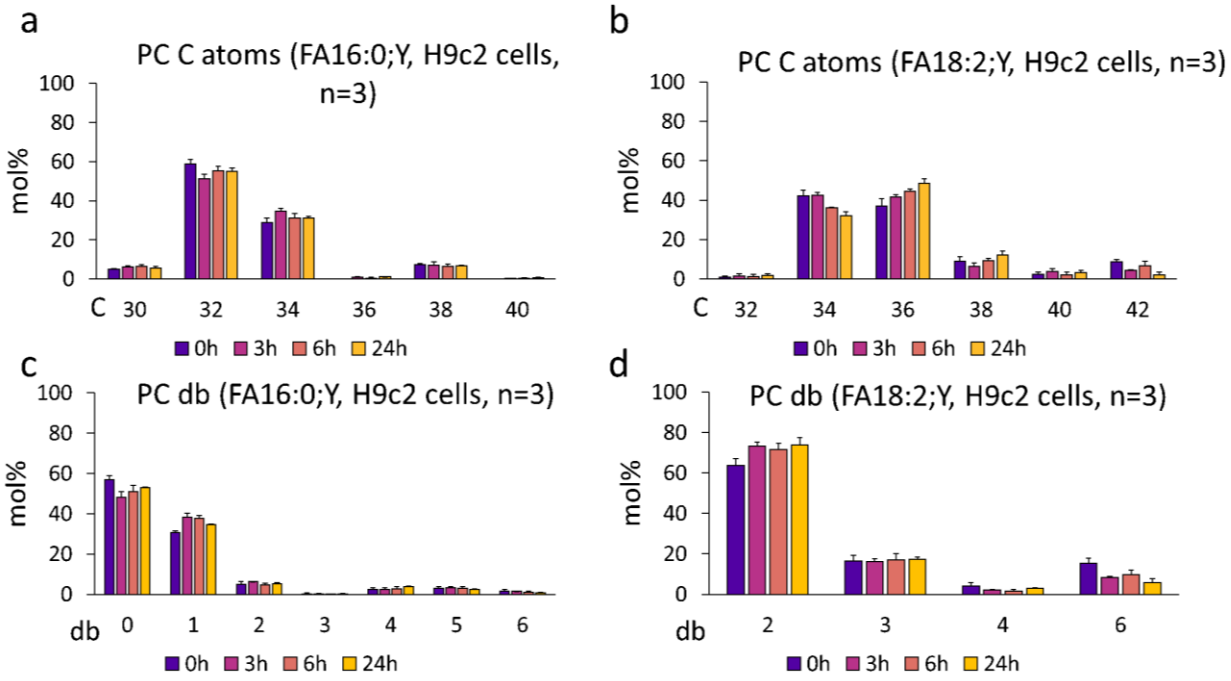

Figure 17: Phosphatidylcholines remodeling in the H9c2 cells. Cells were fed with alkyne-palmitic acid (FA16:0;Y ($^{13}C_6$)) or alkyne-linoleic acid (FA18:2;Y) for 1 hour and, thereafter, chased for 0, 3, 6 or 24 hours (h) in the plain media. Lipids were extracted and analyzed via mass spectrometry. Different phosphatidylcholine (PC) species abundancies were determined. The picomoles of species of the same length (C atoms, **(a, b)**) or saturation degree (db, double bond count, **(c, d)**) were summed together and calculated as mol percent (mol%) to the sum of all phosphatidylcholine species identified for this alkyne-tracer. Data as average ± standard deviation, n=3.

4.2. Cardiac triacylglycerides pool

ATGListatin caused significant accumulation of intracellular triacylglycerides, supporting existence of cardiac triacylglycerides pool with high turnover. To study the fate of exogenous fatty acids and prove the presence of the cardiac triglyceride pool, H9c2 cells were preincubated with ATGListatin – the adipose triacylglyceride lipase inhibitor. Thereafter, the pulse-chase experiments with different medium- and long-chain alkyne fatty acids in the presence or absence of ATGListatin were performed, and the extracted alkyne-lipids were analyzed by mass spectrometry (see figure 18 and supplementary figure 2). Inhibition of adipose triacylglyceride lipase by ATGListatin caused strong accumulation of intracellular long-chain single-labeled triacylglycerides (TG;Y1) and slight accumulation of double-labeled long-chain triacylglycerides (TG;Y2). Triple-labelled triacylglycerides were barely recorded in any conditions. Since ATGListatin does not cause triglycerides synthesis but specifically blocks lipolysis (triacylglycerides breakdown), the effect of ATGListatin on cardiac triacylglycerides accumulation suggests the presence of the triacylglycerides pool in the cardiomyocytes with a very high turnover. ATGListatin had no effect on medium-chain triacylglycerides accumulation, suggesting that the flux of medium-chain fatty acids through the pool is even faster, compared to long-chain fatty acids. The data supports that the majority of the exogenous long-chain fatty acids is running through cardiac triacylglycerides pool at a very high rate. This data also indicates that long-chain fatty acids in the cardiomyocytes are stored and mobilized at the equal speed.

ATGListatin treatment suggested a very high flow rate of fatty acids through cardiac triglycerides pool. The amounts of all labelled triacylglycerides derived from alkyne-palmitic or alkyne-linoleic acid were compared between treated and non-treated cells and are depicted on the figure 18 (f). Significant difference between treated and non-treated conditions indicated that before long-chain fatty acids get oxidized for energy needs or are used for other lipids biosynthesis, their significant portion runs through the triglycerides pool first, and this process happens at a very high rate. After 3 hours of chasing, triacylglycerides accumulation starts to slow down, indicating the saturation of cardiac triacylglycerides pool at longer chasing times. However, the triglycerides production is still far from reaching the plateau, which suggests a high capacity of cardiac cells to store fatty acids within this pool. The saturation degree of the applied long-chain alkyne-fatty acids seems not to influence their incorporation

efficiency intro cellular triacylglycerides. Experiments including longer chasing times to see if triacylglycerides accumulation will reach the plateau after 24 hours were not performed.

Palmitic acid in triacylglycerides was significantly elongated to stearic acid. When H9c2 cells were incubated with ATGListatin, the cells significantly modified alkyne-palmitic acid-derived triacylglycerides. As seen on the figure 18 (g), alkyne-palmitic acid (FA16:0;Y) was majorly elongated to saturated alkyne-stearic acid (FA18:0;Y). Much less shortening of alkyne-palmitic acid to FA14:0;Y or desaturation to FA16:1;Y or FA18:1;Y was observed. Presence of ATGListatin was necessary to observe changes in triglycerides, since triglycerides amounts formed from the alkyne-tracer in the absence of ATGListatin were too low to follow their modifications over time.

ATGListatin slowed down triglycerides cycling. ATGListatin application resulted into reduction of the triglycerides cycling speed at early timepoints, as it could be seen on the figure 19. The presence of the triglycerides cycling could be confirmed by simultaneous decrease of double-labeled triacylglycerides and increase of single-labeled triacylglycerides over time, indicating the diffusion of the alkyne-label from double- to single-labeled triglycerides and the equal distribution of the label within single-labeled triacylglycerides. As it could be seen on the figure 19 (b), this process was slowed down at the early chase timepoints (before 6 hours) in ATGListatin-treated cells. The reason, why after 6 hours of chase the cycling in DMSO-treated cells was not as efficient as in ATGListatin-treated cells could be explained by degradation of the majority of released fatty acids by β-oxidation in DMSO-treated control cells, which would prevent the alkyne-label to be entirely distributed within single-labelled triglycerides (as it was seen for ATGListatin-treated cells). If the initially released fatty acid was degraded by β-oxidation, less single-labelled TG;Y1 species will be produced from unlabelled diacylglycerides, and consequently the apparent efficiency and rate of cycling will be decreased.

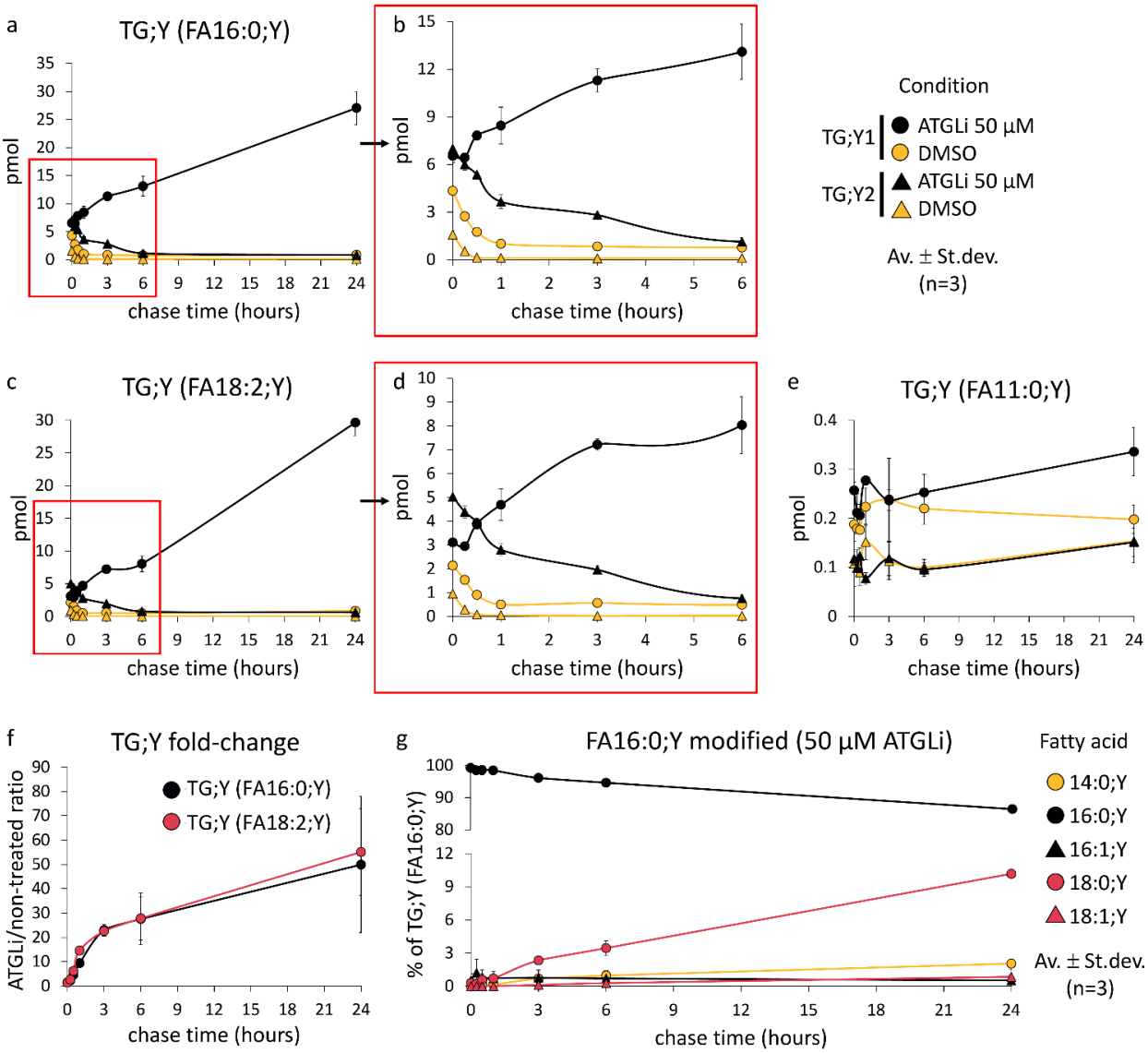

Figure 18: Effect of ATGListatin on triglycerides accumulation in H9c2 cardiomyocytes (ATGLi present at all stages). H9c2 cells were preincubated with 50 µM ATGListatin (ATGLi) for 30 minutes prior the experiment. Thereafter, the cells were fed with alkyne-fatty acid mix containing alkyne-capric acid (FA11:0;Y), alkyne-palmitic acid (FA16:0;Y($^{13}C_6$)) and alkyne-linoleic acid (FA18:2;Y), each at 50 µM concentration, in the presence of 50 µM ATGListatin for 1 hour. Then the cells were washed and chased for 0, 3, 6 or 24 hours in the media with 50 µM ATGListatin. DMSO was used as carrier control. The extracted lipids were analyzed by mass spectrometry. **(a)** Single- (TG;Y1, round marker) and double-labelled (TG;Y2, triangle marker) triglycerides containing alkyne-palmitic acid. Data is presented in picomoles (pmol), average ± standard deviation, n=3. **(b)** Higher magnification (from 0 to 6 hours chase) of palmitic-acid containing triglycerides data. **(c)** Single- (TG;Y1, round marker) and double-labelled (TG;Y2, triangle marker) triglycerides containing alkyne-linoleic acid. Data is presented in picomoles (pmol), average ± standard deviation, n=3. **(d)** Higher magnification (from 0 to 6 hours chase) of linoleic-acid containing triglycerides data. **(e)** Single- (TG;Y1, round marker) and double-labelled (TG;Y2, triangle marker) triglycerides containing alkyne-capric acid. Data is presented in picomoles (pmol), average ± standard deviation, n=3. **(f)** Fold-change of triglycerides amounts upon treatment, calculated as ratio of total alkyne-triglycerides in ATGLi-treated cells divided by amounts of alkyne-triglycerides in DMSO-treated cells. Data as fold-change for alkyne-palmitic and alkyne-linoleic acid, average ± standard deviation, n=3. **(g)** Modification of alkyne-palmitic acid in triglycerides over time. Abundance of each fatty acid is presented as percentage to total amounts of alkyne-palmitic acid-derived triglycerides, data as average ± standard deviation, n=3.

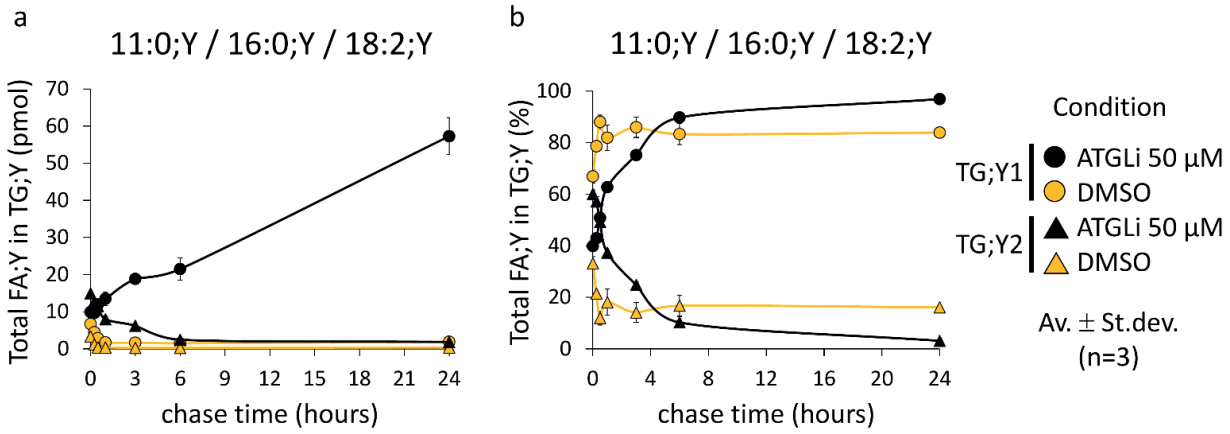

Figure 19: Effect of ATGListatin on triglycerides cycling in H9c2 cardiomyocytes. (ATGLi present at all stages). H9c2 cells were preincubated with 50 µM ATGListatin (ATGLi) for 30 minutes prior the experiment. Thereafter, the cells were fed with alkyne-fatty acid mix containing alkyne-capric acid (FA11:0;Y), alkyne-palmitic acid (FA16:0;Y($^{13}C_6$)) and alkyne-linoleic acid (FA18:2;Y), each at 50 µM concentration, in the presence of 50 µM ATGListatin for 1 hour. Then the cells were washed and chased for 0, 3, 6 or 24 hours in the media with 50 µM ATGListatin. DMSO was used as carrier control. The extracted lipids were analyzed by mass spectrometry. **(a)** Picomoles (pmol) of alkyne-fatty acids (11:0;Y, 16:0;Y and 18:2;Y together) in single- (TG;Y1, round marker) and double-labeled (TG;Y2, triangle marker) triglycerides in the presence of ATGListatin (black) or DMSO as a carrier control (yellow). Note, that double-labelled triglycerides amounts were multiplied twice. **(b)** Same data as **(a)** but presented as percent to total labelled triglycerides. The cycling progression could be seen as reduction of double-labelled species accompanied with increase of single-labeled triglycerides. All data as average ± standard deviation, n=3.

The effect of ATGListatin could be reversed upon its removal. To investigate if the ATGListatin effect on cardiac triglycerides accumulation is reversible, H9c2 cells were preincubated and pulsed with alkyne-fatty acids in the presence of ATGListatin. Thereafter, cells were chased in the media with or without ATGListatin. As seen on the figure 20, upon ATGListatin removal, triglycerides were almost completely used up by heart cells already after 3 hours of chasing, whereas cells with ATGListatin in the chase media further continued to accumulate triglycerides. This data indicates the reversible nature of ATGListatin effect on cardiac triglycerides pool. Remarkable difference between ATGListatin-treated cells and cells where ATGListatin was removed during chase additionally indicated a rapid turnover of cardiac triglycerides pool with its half-life time less than 1 hour.

Fluorescence microscopy analysis revealed lipid droplet accumulation in ATGListatin-treated H9c2 cardiomyocytes. H9c2 cells were treated with ATGListatin and stained with LD540 lipophilic dye for lipid droplets. Without ATGListatin cells usually

had a low number of small lipid droplets, which were relatively equally distributed within the cytoplasm. In the presence of ATGListatin cells formed more lipid droplets of the bigger size, and the lipid droplets were arranged into pronounced clusters (see figure 21). This observation of ATGListatin effect on lipid accumulation in cardiomyocytes was in alignment with the pulse-chase experiments and mass spectrometric data.

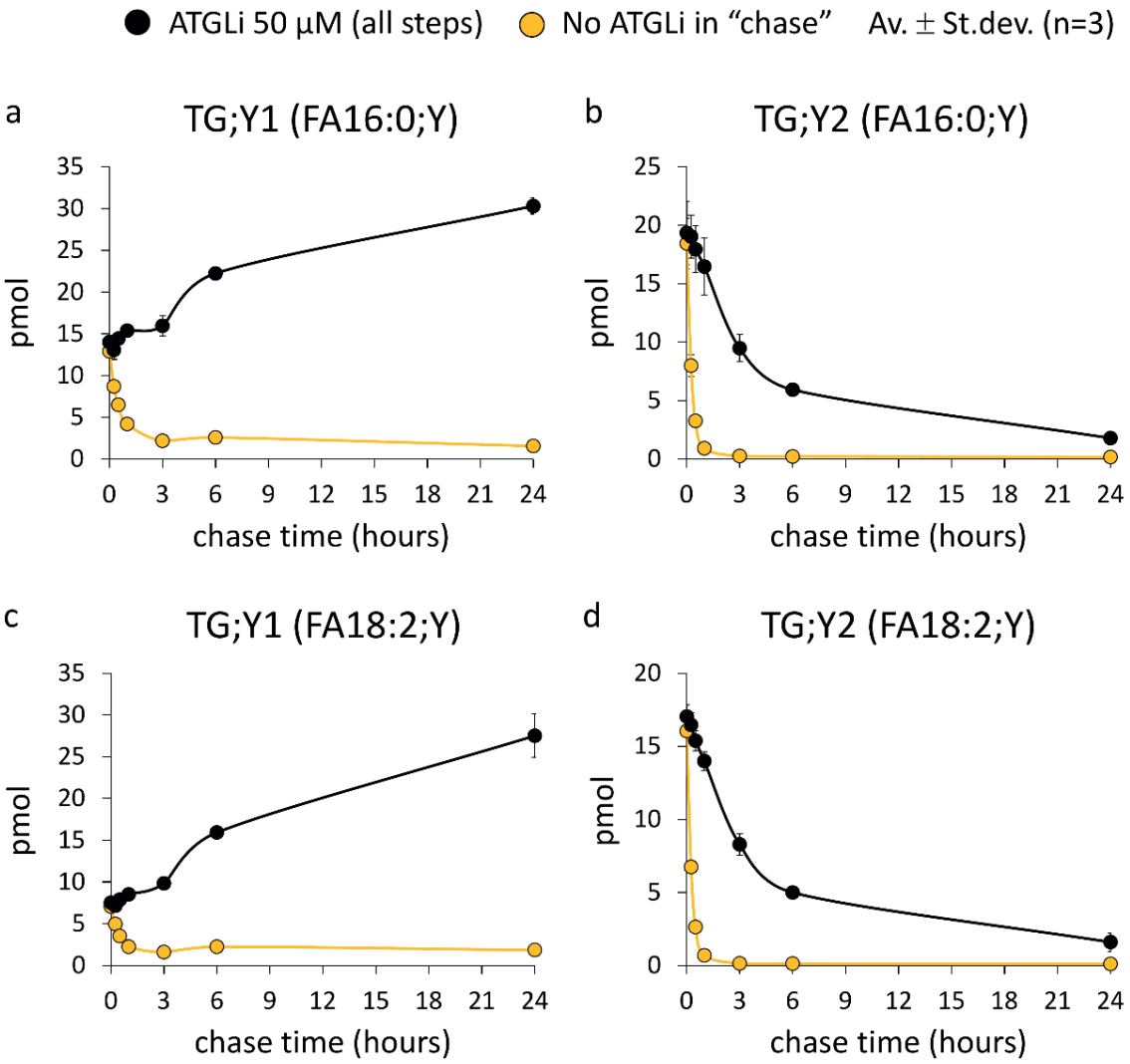

Figure 20: Removal of ATGListatin during chase allowed to reverse its effect on cardiac triglycerides accumulation. H9c2 cells were preincubated with 50 µM ATGListatin (ATGLi) for 30 minutes. Thereafter, the cells were pulsed for 1 hour with alkyne-palmitic (FA16:0;Y($^{13}C_6$) and alkyne-oleic (FA18:2;Y) acids, each at 50 µM concentration, all in the presence of 50 µM ATGListatin. After washing step, the cells were chased up to 24 hours in DMEM media with DMSO as a carrier control (ATGListatin removed; in yellow) or in the media with 50 µM ATGListatin (here shown in black). The extracted lipids were analyzed by mass spectrometry. **(a)** Single-labelled (TG;Y1) triglycerides, containing alkyne-palmitic acid. **(b)** Double-labeled (TG;Y2) triglycerides, containing alkyne-palmitic acid. **(c)** Single-labelled (TG;Y1) triglycerides, containing alkyne-linoleic acid. **(d)** Double-labeled (TG;Y2) triglycerides, containing alkyne-linoleic acid. All data is presented in picomoles (pmol), average ± standard deviation, n=3.

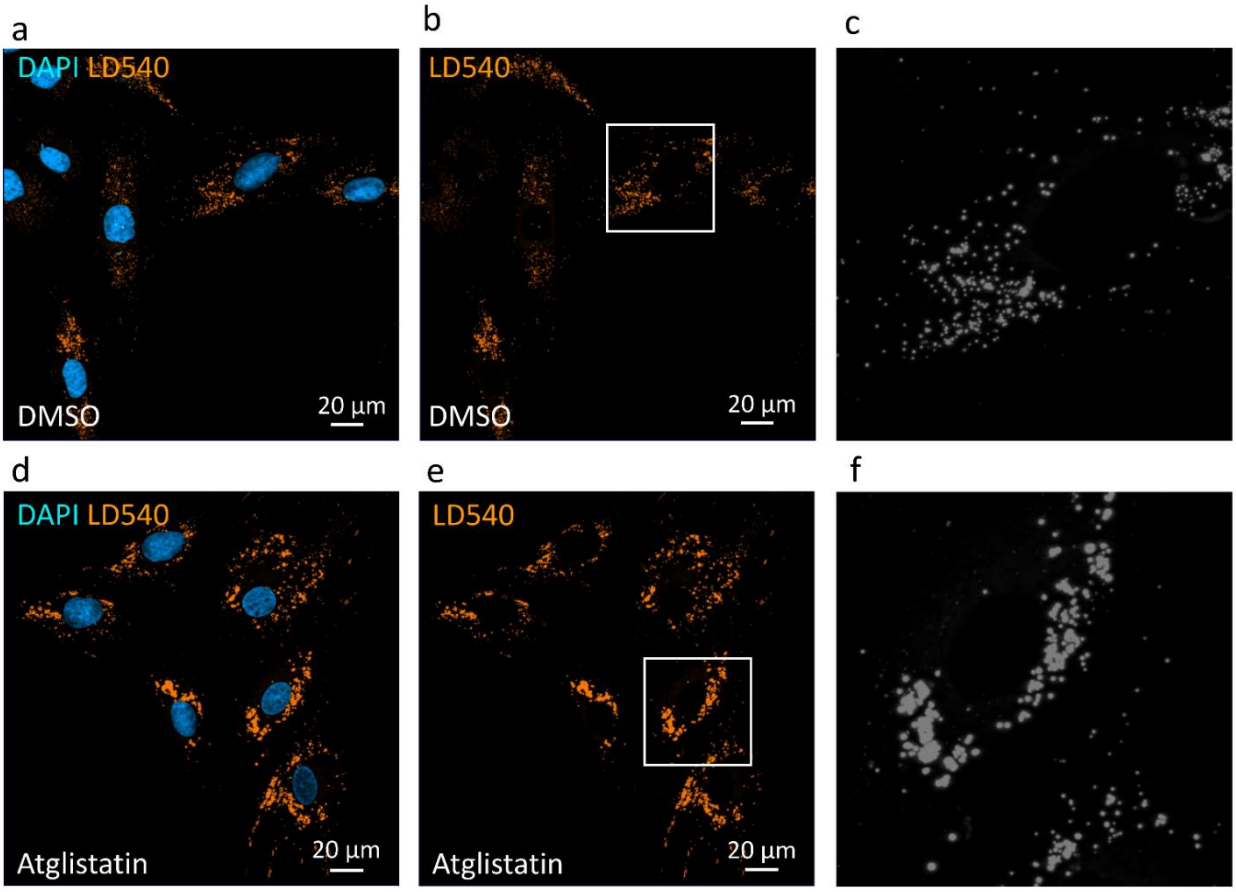

Figure 21: ALGListatin caused cardiac lipid droplets enlargement and their clustering. H9c2 cells were incubated in the presence or absence of 50 µM ATGListatin for 24 hours and fixed with 4 % paraformaldehyde. After the nuclear staining with DAPI (blue) and lipid droplets staining with LD540 lipophilic dye (orange), the samples were visualized by fluorescence microscopy at x40 magnification. In gray **(c,f)** the magnified image of lipid droplets from respective boxed region **(b,e)** is depicted. Lipid droplet images were exported at the same intensity. Optical sectioning was performed with Apotome. The scalebar is 20 µm.

4.3. Erucic acid and cardiac lipid metabolism

4.3.1. The effect of erucic acid on common dietary fatty acids metabolism

Erucic acid affected long-chain fatty acid metabolism and lipid accumulation. To investigate the effect of erucic acid on cardiac lipid accumulation, H9c2 cells were preincubated for 24 hours with increasing concentrations of erucic acid. Alternatively, to compensate for the increase of fatty acid content in the samples, control experiments with combination of palmitic and erucic acids at different concentrations (but the same total concentration) was performed. After preincubation with erucic acid alone or its combination with palmitic acid, cells were washed, and the pulse-chase experiments with some common dietary medium- and long-chain fatty acids were performed. As suggested by mass spectrometric data, erucic acid did not have an effect on medium-chain alkyne-capric acid metabolism, as seen on the figure 22 (a,b). However, erucic acid caused significant accumulation of neutral lipids (cholesterol esters, mono-, di-, and triacylglycerols) derived from long-chain palmitic and linoleic acid (as seen on the figure 22 (a,c,e), 23 and 24 (c,e). Polar lipids (ceramides, glucosylceramides, sphingomyelins, phosphatidylcholines, phosphatidylethanolamines and phosphatidylinositol) did also increase at early chase timepoints, however, after 24 hours of chasing, their amounts returned to the levels similar to non-treated cells (see figures 22 (b,d,f) and 24 (a)). The observed effect on lipid accumulation was strongly dependent on erucic acid concentration. Control experiments, where erucic acid was substituted with palmitic acid, confirmed that the observed systemic changes were specifically caused by erucic acid and not just general increase of fatty acid in the samples (see figure 25). Interestingly, cholesterol esters accumulation followed different trend than other lipid classes, as it could be seen on the figure 25 (a). When fed with combination of palmitic and erucic acid, cardiomyocytes accumulated more cholesterol esters in the presence of palmitic acid at early incubation stages. However, on the long run, more cholesterol esters were accumulated in the presence of erucic acid. Cholesterol ester accumulation seems to follow some switch behavior, and its kinetics and timing tends to highly depend on the chemical structure of the fatty acid fed to cells.

Erucic acid caused increase of arachidonic acid-containing phosphatidylinositol. Pretreatment of cells with erucic acid resulted into accumulation of PI36:4;Y lipid species – phosphatidylinositol, containing alkyne-palmitic acid and arachidonic acid (see figure

24 (a,b) and 25 (d,e)). Accumulation of PI36:4;Y phosphatidylinositol was strongly dependent on erucic acid concentration. This was accompanied by the increase in single- (figure 24 (c,d)) and double-labeled (figure 24 (e,f)) diacylglycerols amounts. To check if this increase in phosphatidylinositol and diacylglycerols could be accompanied by downstream increase of phosphatidylinositol 4,5-bisphosphate (PIP2) – an important member of many signaling pathways – H9c2 cells were treated with erucic acid, and immunostaining to detect PIP2 was performed. While cellular protrusions tend to be more intensively stained for PIP2 in erucic acid-treated cells, in general, not much difference between treated and non-treated cells could be observed (see figure 26).

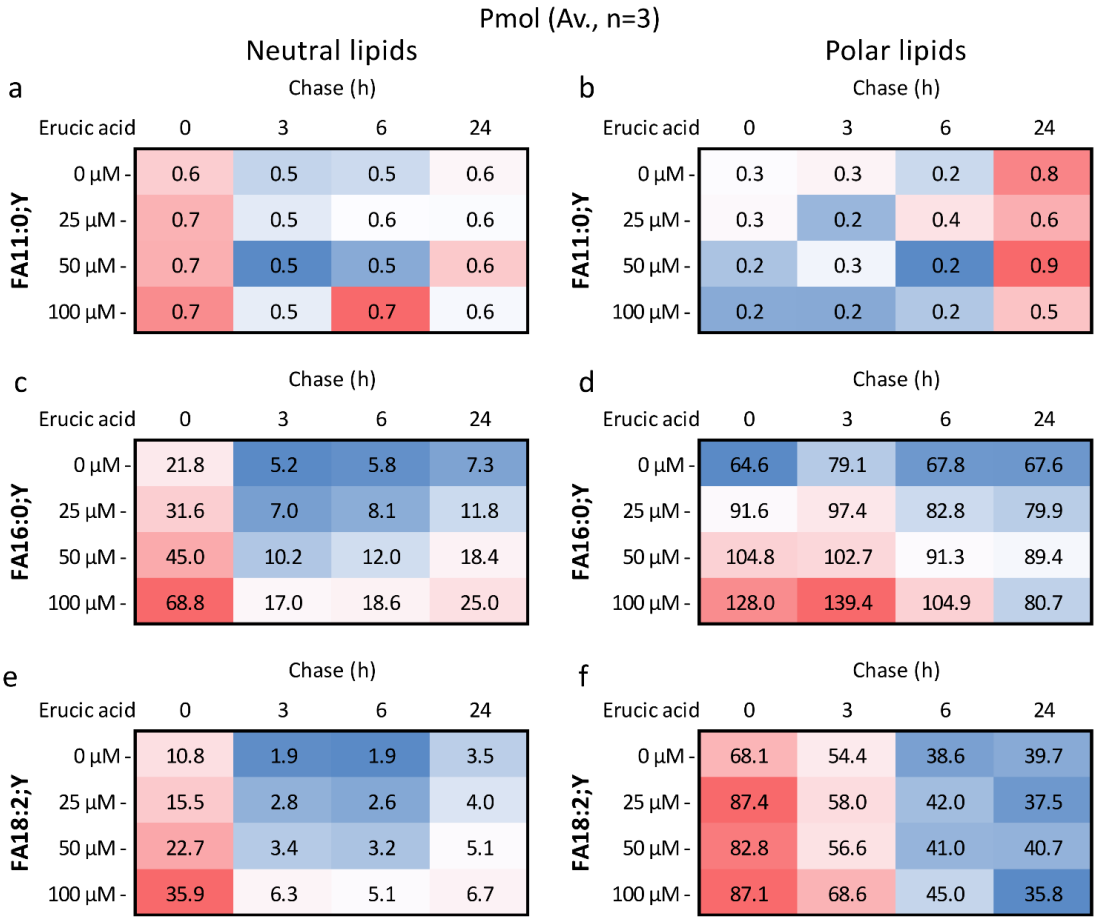

Figure 22: Effect of erucic acid on neutral and polar lipid accumulation in H9c2 cardiomyocytes. H9c2 cells were preincubated with erucic acid at 0, 25, 50 or 100 µM concentration for 24 hours. Thereafter, the media with erucic acid was removed, and the cells were fed with fresh media with the alkyne-fatty acid mix containing alkyne-capric acid (FA11:0;Y), alkyne-palmitic acid (FA16:0;Y($^{13}C_6$)) and alkyne-linoleic acid (FA18:2;Y) for 1 hour. Thereafter, the cells were washed and chased for 0, 3, 6 or 24 hours in the plain media. Extracted lipids were analyzed by mass spectrometry. **(a)** Neutral lipids values for alkyne-capric acid. The value is a sum of all cholesterol esters, mono-, di, and triacylglycerols in picomoles (pmol) recorded for this fatty acid. **(b)** Polar lipids values for alkyne-capric acid. The value is a sum of all ceramides, glucosylceramides, sphingomyelins, phosphatidylcholines, phosphatidylethanolamines and phosphatidylinositol recorded for this fatty acid. **(c)** Neutral lipids (in picomoles) for alkyne-palmitic acid. **(d)** Polar lipids (in picomoles) for alkyne-palmitic acid. **(e)** Neutral lipids (in picomoles) for alkyne-linoleic acid. **(f)** Polar lipids (in picomoles) for alkyne-linoleic acid. All graphs as average, n=3.

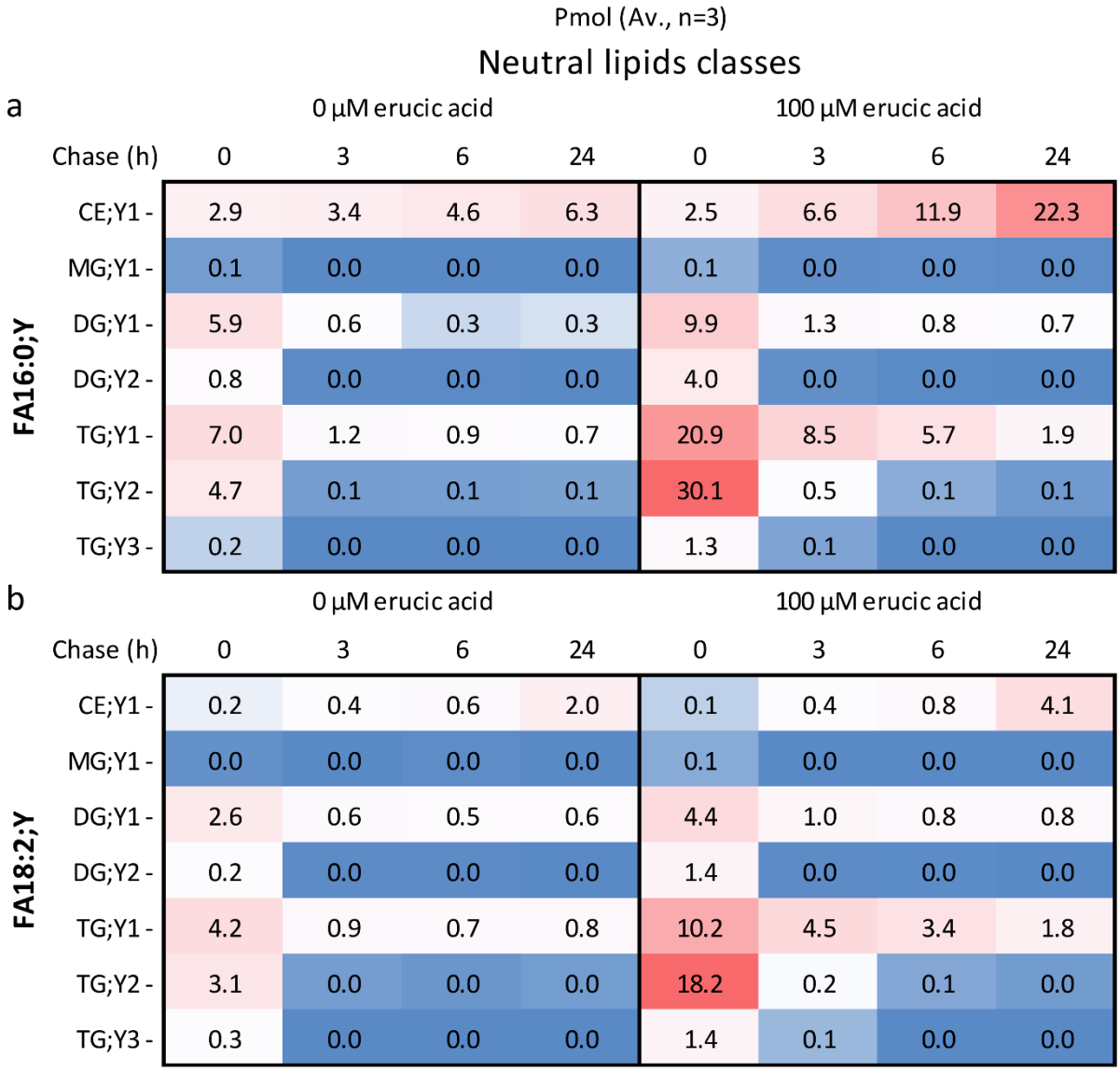

Figure 23: Effect of erucic acid on neutral lipid classes accumulation in H9c2 cardiomyocytes. H9c2 cells were preincubated with erucic acid at 0 or 100 µM concentration for 24 hours. Thereafter, the media with erucic acid was removed and the cells were fed with fresh media with the alkyne-fatty acid mix containing alkyne-palmitic acid (FA16:0;Y($^{13}C_6$)) and alkyne-linoleic acid (FA18:2;Y) for 1 hour. Thereafter, the cells were washed and chased for 0, 3, 6 or 24 hours (h) in the plain media. The extracted lipids were analyzed by mass spectrometry. **(a)** Neutral lipids classes amounts for alkyne-palmitic acid. **(b)** Neutral lipid classes amount for alkyne-linoleic acid. CE;Y1, cholesterol esters; MG;Y1, monoacylglycerols; DG;Y1, single-labeled diacylglycerols; DG;Y2, double-labeled diacylglycerols; TG;Y1; single-labeled triacylglycerols; TG;Y2; double-labeled triacylglycerols; TG;Y3; triple-labeled triacylglycerols. All data in picomoles (pmol), average, n=3.

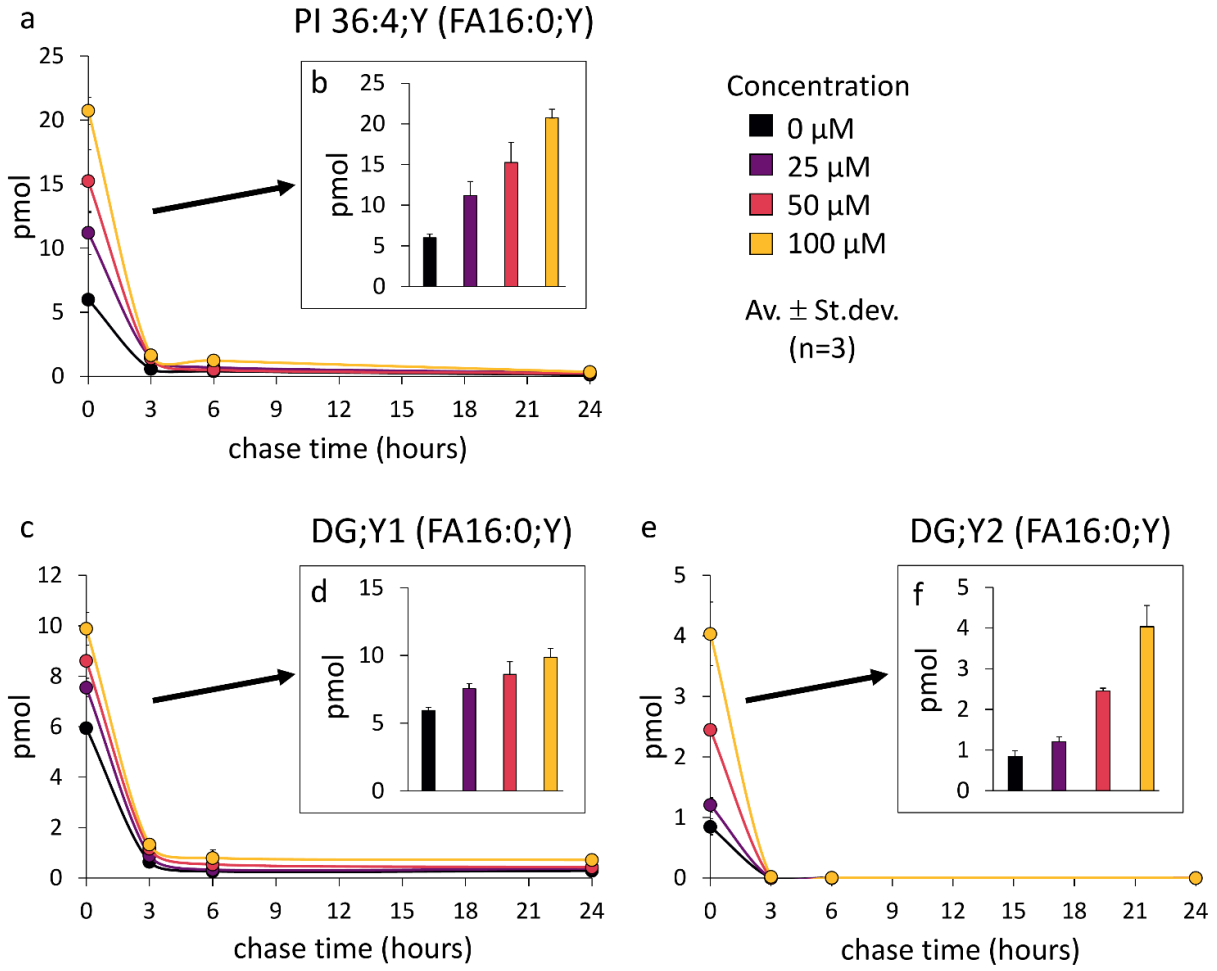

Figure 24: Erucic acid caused concentration-dependent increase of phosphatidylinositol species containing arachidonic and alkyne-palmitic acid in the side-chain, accompanied with single- and double-labelled diacylglycerols increase. H9c2 cells were preincubated with erucic acid at 0, 25, 50 or 100 µM concentration for 24 hours. Thereafter, the media with erucic acid was removed, and the cells were washed and fed with fresh media containing alkyne-palmitic acid (FA16:0;Y($^{13}C_6$)) for 1 hour. Thereafter, the cells were washed again and chased for 0, 3, 6 or 24 hours in the plain media. The extracted lipids were analyzed by mass spectrometry. **(a)** Amounts of phosphatidylinositol containing arachidonic and alkyne-palmitic acid in its side-chain (PI 36:4;Y (FA16:0;Y)) in picomoles (pmol) at different chase timepoints. **(b)** Same data at 0 hours of chasing. **(c)** Amounts of single-labelled diacylglycerols containing alkyne-palmitic acid in their side-chain. **(d)** Same data at 0 hours of chasing. **(e)** Amounts of double-labelled diacylglycerols containing alkyne-palmitic acid in their side-chain. **(f)** Same data at 0 hours of chasing. All graphs as average ± standard deviation, n=3.

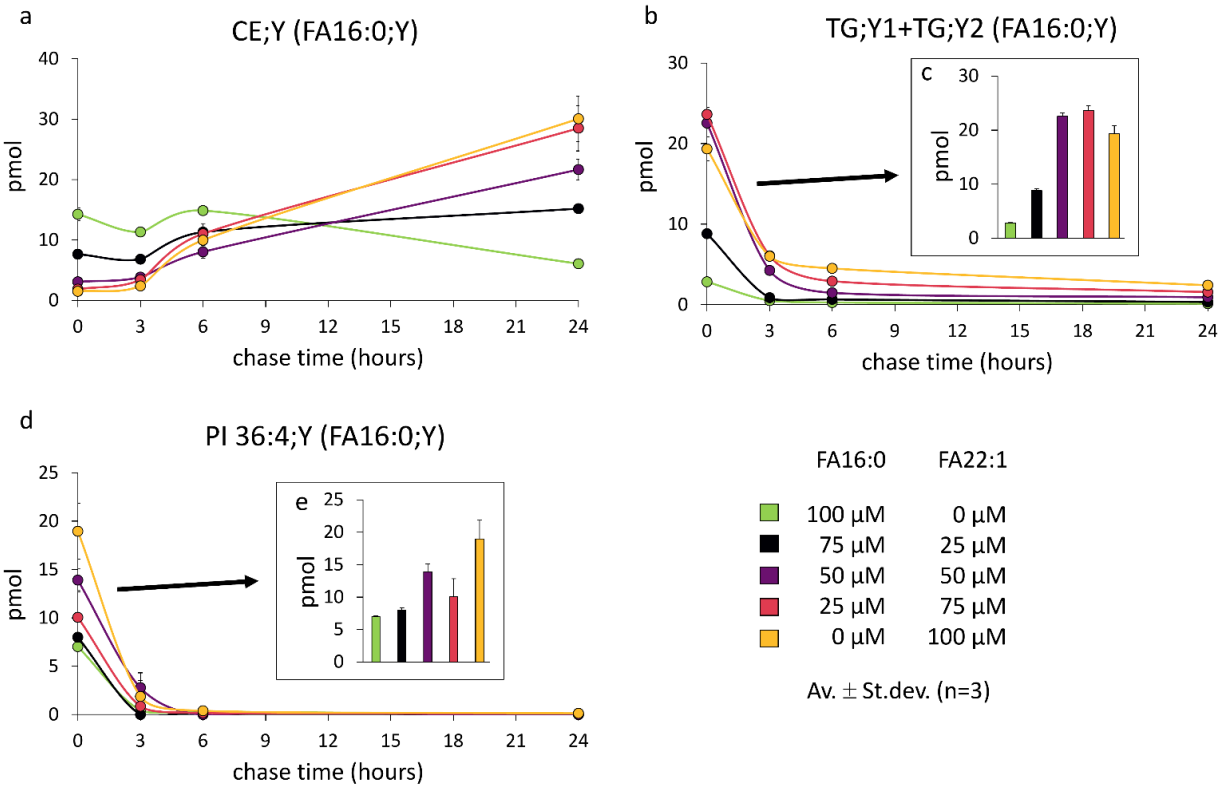

Figure 25: Erucic acid-specific effect on cholesterol esters, triacylglycerols and phosphatidylinositol accumulation in H9c2 cells. To compensate for total fatty acid increase in the preincubation phase, palmitic and erucic acids were fed at different combinations to H9c2 cells, reaching the total fatty acid concentration of 100 µM. Preincubation step continued for 24 hours, followed by a washing step and 1 hour pulse with the media containing 50 µM alkyne-palmitic acid (FA16:0;Y($^{13}C_6$)). Thereafter, cells were washed again and chased for 0, 3, 6 or 24 hours in the plain media. The extracted lipids were analyzed by mass spectrometry. **(a)** amounts of cholesteryl esters (CE;Y) containing alkyne-palmitic tracer. **(b)** Amounts of single- (TG;Y1) and double-labeled (TG;Y2) triglycerides containing alkyne-palmitic acid tracer. **(c)** Same data, only starting chasing point is presented. **(d)** Amounts of phosphatidylinositol containing arachidonic and alkyne-palmitic acid in its side-chain (PI 36:4;Y (FA16:0;Y)) in picomoles (pmol) at different chase timepoints. **(e)** Same data, only starting chasing point is presented. All graphs as average ± standard deviation, n=3.

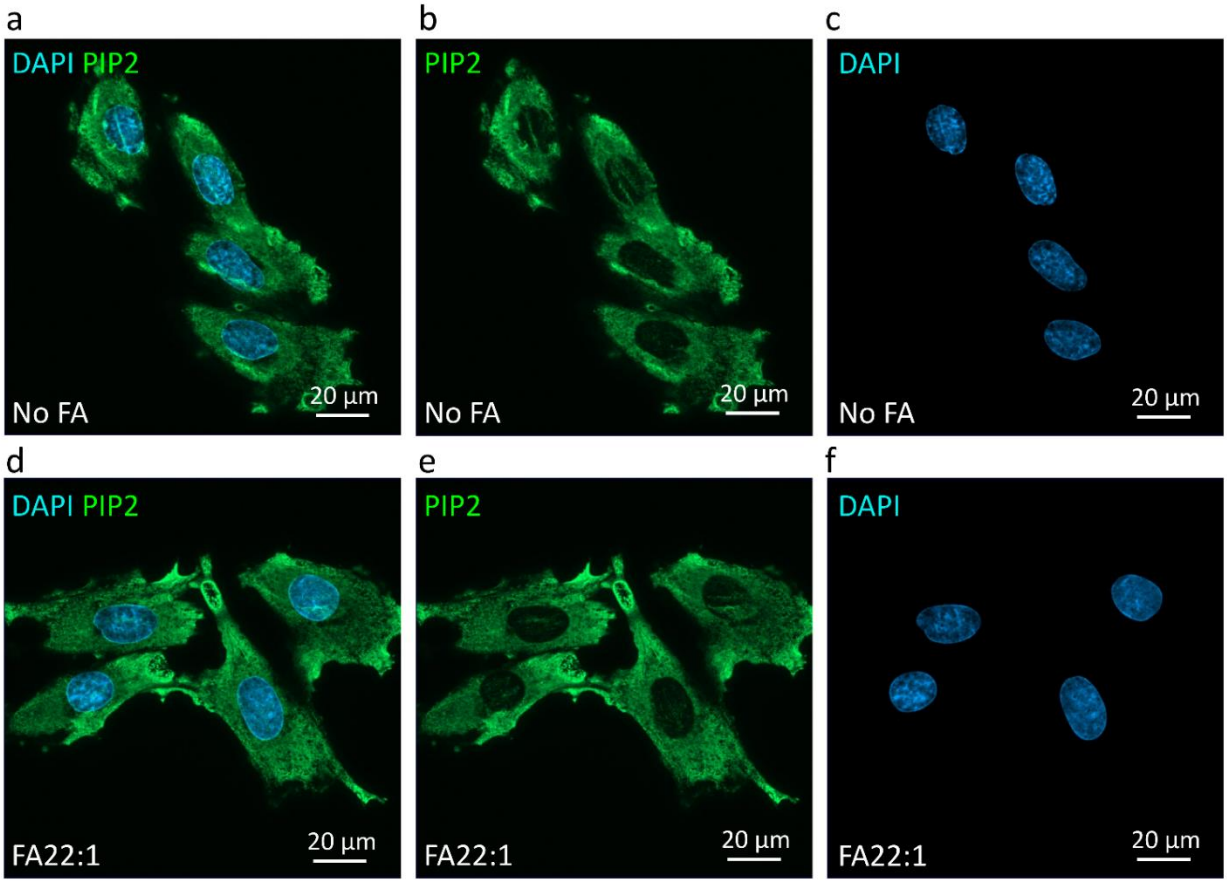

Figure 26: PIP2 staining in erucic acid-treated H9c2 cells. Cells were incubated in the plain media **(a-c)** or media containing 100 µM erucic acid **(d-f)** for 24 hours. After washing step and fixation in 4 % paraformaldehyde in PBS, the cells were incubated with primary antibodies against PIP2. Thereafter, the samples were stained with Alexa Fluor-488 secondary antibodies (green, PIP2) and DAPI (blue, nuclei) and imaged using fluorescence microscope at x63 magnification. Optical sectioning was performed with the Apotome, 9-11 sections at 0.24 µm interval per spot. Images were exported with the same intensity. The scalebar is 20 µm.

Erucic acid affected accumulation of acyl-carnitines, derived from capric and palmitic acid. To investigate the reasons behind systemic changes in lipid metabolism observed under erucic acid influence, additional studies were performed, where the effect of erucic acid on fatty acid oxidation and acyl-carnitines formation was studied. For that mice heart lysates were preincubated with erucic acid and then incubated with alkyne-capric or alkyne-palmitic acid to follow their metabolism via thin-layer chromatography. As seen on the figure 27, erucic acid affected length and amounts of acyl-carnitines formed from alkyne-capric and, to lesser extent, alkyne-palmitic acid. Changes in acyl-carnitines could in turn affect downstream the efficiency of fatty acid transport and oxidation, resulting in the excess of free fatty acids, that would be channeled towards anabolic pathways to prevent their intracellular accumulation.

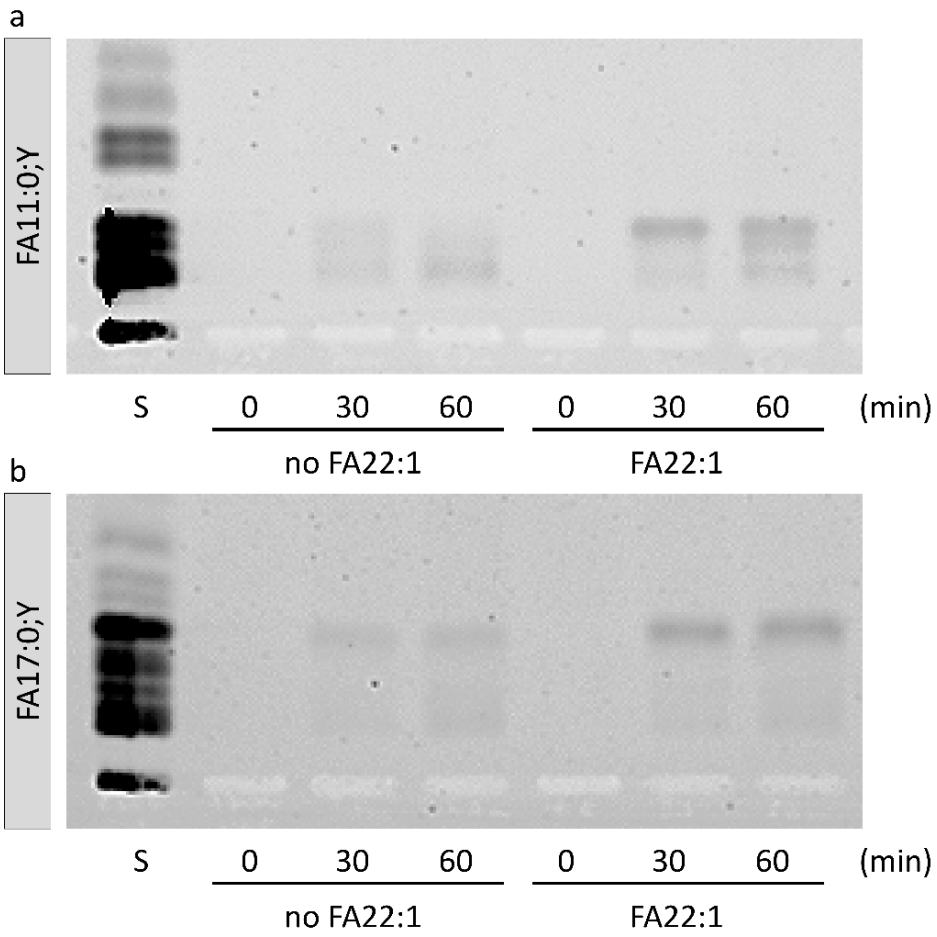

Figure 27: Erucic acid affected length and amounts of acyl-carnitines formed from alkyne-capric and alkyne-palmitic acid. Murine heart homogenates were preincubated with erucic acid FA22:1 for 30 minutes and thereafter incubated for 0, 30 or 60 minutes with alkyne-capric (FA11:0;Y, **(a)**) or alkyne-palmitic (FA17:0;Y, **(b)**) acid. Acyl-carnitines were detected using thin-layer chromatography. S, carnitine standards, here for **(a)** used: CAR5:0;Y, CAR7:0;Y, CAR9:0;Y, CAR11:0;Y; standards for **(b)** used: CAR5:0;Y, CAR7:0;Y, CAR9:0;Y, CAR11:0;Y; CAR13:0;Y and CAR17:0;Y.

4.3.2. Erucic acid effect on cardiac lipidome and lipid droplets formation

Erucic acid caused systemics changes in H9c2 cardiomyocytes lipidome. Erucic acid at different increasing concentrations (from 0 to 100 μM) was fed to H9c2 cardiomyocytes to study the effect of this very long-chain fatty acid on lipid metabolism. Lipidomics analysis does not allow to specifically follow erucic acid alterations in complex cellular system, but could indicate systemic lipid changes, observed in the presence of this fatty acid. These changes were dependent on the concentration of erucic acid applied.

Erucic acid affected total lipid amount and neutral-to-polar lipids ratio. As it could be seen on figure 28 (a), total lipid content increased over long pulse time upon increasing erucic acid concentrations. Erucic acid application caused systemic shift of lipid metabolism towards neutral lipids accumulation, while polar lipids amounts remained on relatively same level (figure 28 (b-d)). Polar lipid amount was estimated as a sum of carnitines, ceramides, dihexosylceramide, hexosylceramide, hexosylsphingosine, lysophosphatidylcholine, lysoalkylphosphatidylcholine, lysophosphatidylethanolamine, ether-linked phosphatidylethanolamine, phosphatidic acid, phosphatidylcholine, ether-linked phosphatidylcholine, phosphatidylethanolamine, phosphatidylglycerol, phosphatidylserine and sphingomyelin. Neutral lipids were calculated as sum of all cholesterol esters, mono-, di, and triacylglycerols recorded. Neutral-to-polar lipid ratio was estimated as a sum of all neutral lipids divided by sum of all polar lipids identified in the sample. At its highest concentration tested (100 μM), erucic acid was responsible for 1.4-fold increase of polar lipids after 24 hours of incubation compared to control, while it caused 16 times increase in neutral lipids. More detailed analysis of lipid classes confirmed, that erucic acid promoted significant accumulation of cholesterol esters, mono-, di-, and, especially, triacylglycerols (1.5, 1.3, 1.8, 16.8-fold increase, respectively, when comparing untreated cells and cells fed with 100 μM erucic acid for 24 hours, see figure 29). Within sphingolipids the increase was caused majorly by sphingomyelin (1.6-fold increase for 100 μM erucic acid after 24 hours of incubation). Within phosphoglycerolipids, phosphatidylcholines changed mostly upon treatment (1.4-fold increase for 100 μM erucic acid after 24 hours of incubation).

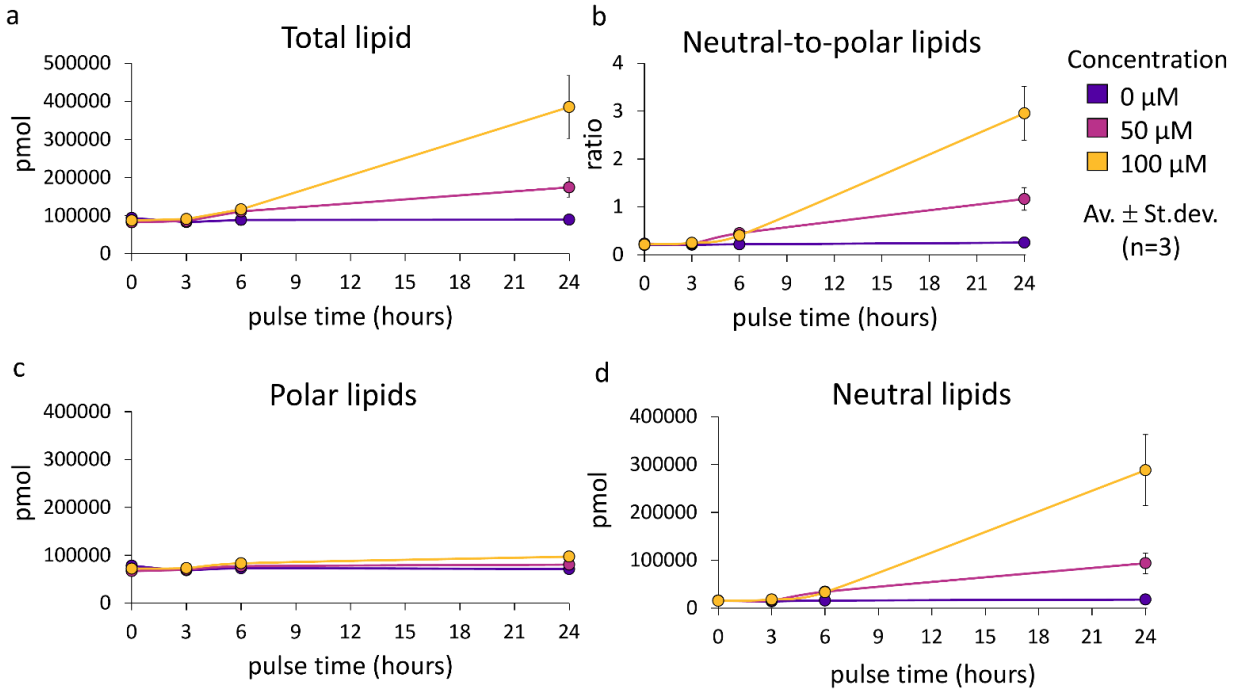

Figure 28: The effect of erucic acid on neutral and polar lipid accumulation in H9c2 cardiomyocytes. H9c2 cells were incubated with erucic acid at 0, 50 or 100 µM concentration for 0, 3, 6 or 24 hours (pulse time in hours since erucic acid is present at all stages). Thereafter, the media with erucic acid was removed, the cells were washed, and were used for the lipid extraction and analysis of the whole lipidome. **(a)** Total lipid amount in picomoles per well (pmol) at different incubation timepoints. **(b)** Neutral-to-polar lipid ratio at different incubation timepoints. **(c)** Polar lipids values in picomoles per well (pmol). The value is calculated as sum of carnitines, ceramides, dihexosylceramide, hexosylceramide, hexosylsphingosine, lysophosphatidylcholine, lysoalkylphosphatidylcholine, lysophosphatidylethanolamine, ether-linked phosphatidylethanolamine, phosphatidic acid, phosphatidylcholine, ether-linked phosphatidylcholine, phosphatidylethanolamine, phosphatidylglycerol, phosphatidylserine and sphingomyelin recorded. **(d)** Neutral lipids values in picomoles per well (pmol). The value is a sum of all cholesterol esters, mono-, di, and triacylglycerols recorded. All data is presented as average ± standard deviation, n=3.

Erucic acid caused long chain species enrichment in the lipidome. The side chain length for the most affected lipid classes was evaluated. As is could be seen on the figure 30, erucic acid increased the average side chain length for triacylglycerides, diacylglycerides, phosphatidylcholines and, to lesser extent, sphingomyelin. Accumulation of erucic acid species within cholesterol esters (CE22:1), lysophosphatidylcholine (LPC22:1) and sphingomyelin (SM22:1) over time could also be confirmed (see figure 31).

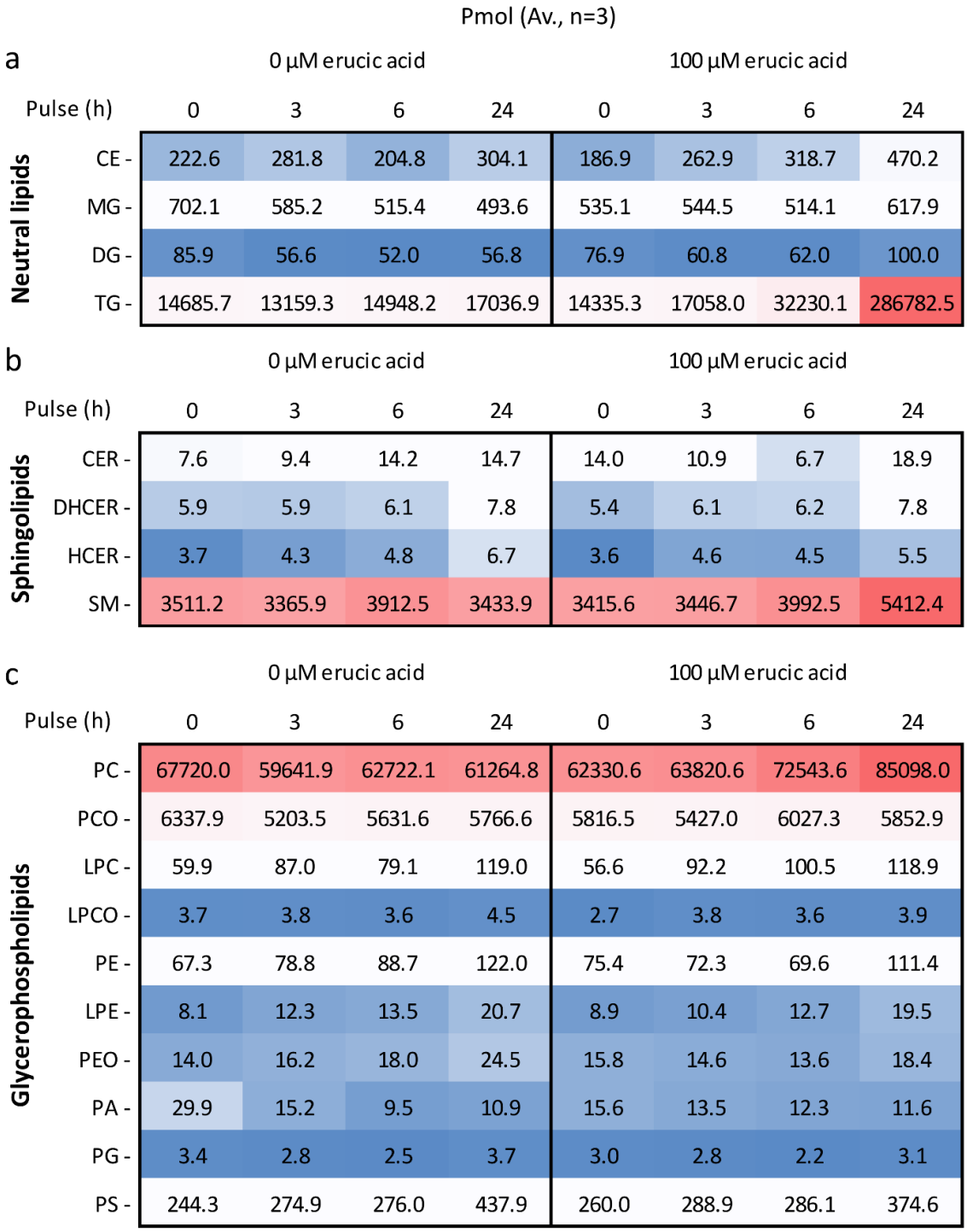

Figure 29: Effect of erucic acid on neutral lipids, sphingolipids and glycerophospholipids. H9c2 cells were incubated with erucic acid at 0, 50 or 100 µM (data only for 0 and 100 µM is shown here) concentration for 0, 3, 6 or 24 hours. Thereafter, the media with erucic acid was removed, the cells were washed and were used for the lipid extraction and analysis of the whole lipidome. **(a)** Neutral lipid classes amounts in picomoles per well (pmol). CE, cholesterol esters; MG, monoacylglycerols; DG, diacylglycerols; TG, triacylglycerols. **(b)** Sphingolipid classes amounts in picomoles per well (pmol). CER, ceramides; DHCER, dihexosylceramide; HCER, hexosylceramide; SM, sphingomyelin. **(c)** Glycerophospholipids classes amounts in picomoles per well (pmol). PC, phosphatidylcholine; PCO, ether-linked phosphatidylcholine; LPC, lysophosphatidylcholine; LPCO, lysoalkylphosphatidylcholine; PE, phosphatidylethanolamine; LPE, lysophosphatidylethanolamine; PEO, ether-linked phosphatidylethanolamine; PA, phosphatidic acid; PG, phosphatidylglycerol; PS, phosphatidylserine. All data is presented as average, n=3.

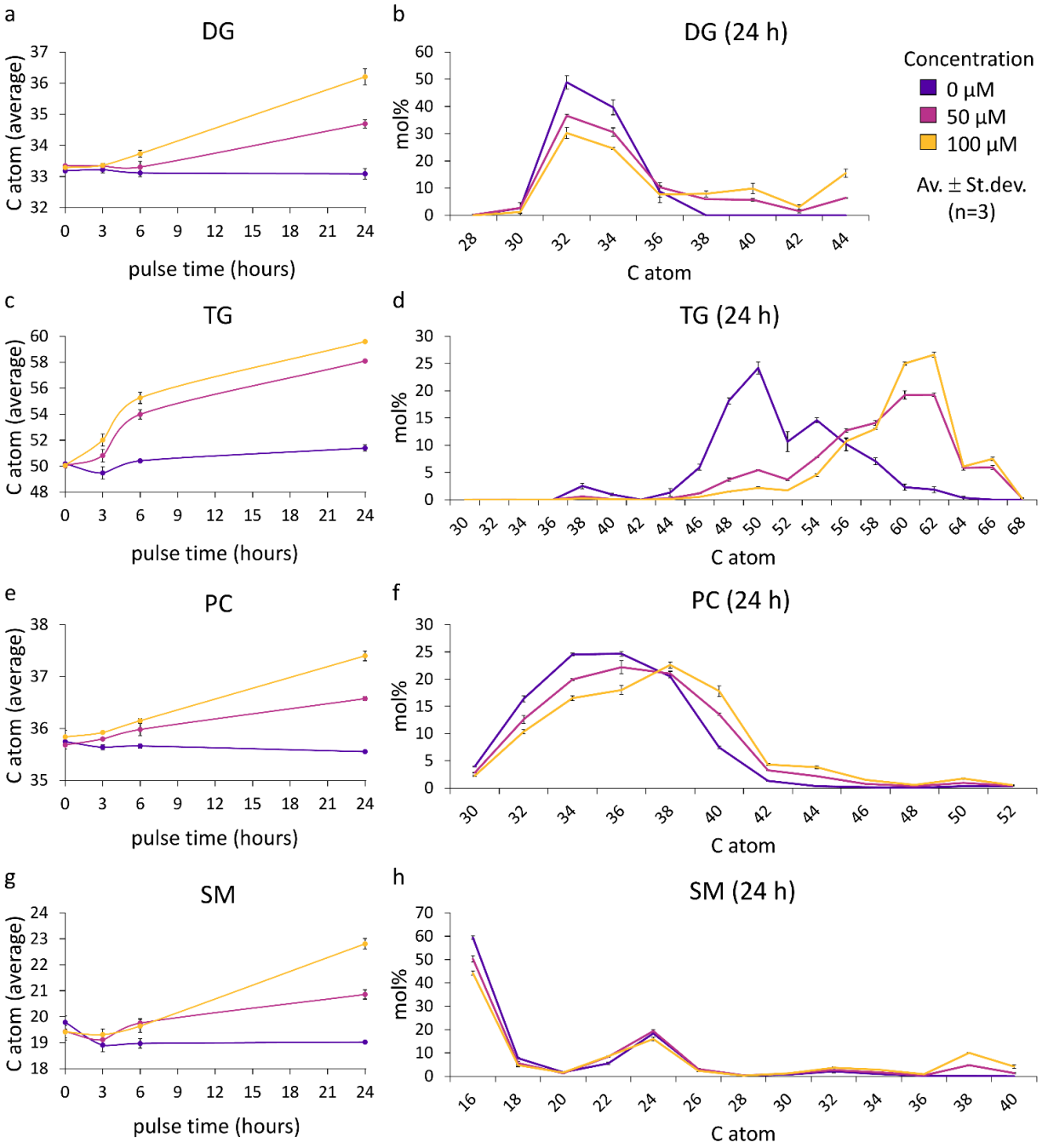

Figure 30: Effect of erucic acid on side-chain length (C atom) of diacylglycerols, triacylglycerols, phosphatidylcholines and sphingomyelin. H9c2 cells were incubated with erucic acid at 0, 50 or 100 µM concentration for 0, 3, 6 or 24 hours (pulse time in hours since erucic acid is present at all stages). Thereafter, the media with erucic acid was removed, the cells were washed and were used for the lipid extraction and analysis of the whole lipidome. **(a)** Diacylglycerols average side chain length at different incubation timepoints. **(b)** Diacylglycerols side chain length in mol% after 24 hours of pulse with erucic acid. **(c)** Triacylglycerols average side chain length at different incubation timepoints. **(d)** Triacylglycerols side chain length in mol% after 24 hours of pulse with erucic acid. **(e)** Phosphatidylcholines average side chain length at different incubation timepoints. **(f)** Phosphatidylcholines side chain length in mol% after 24 hours of pulse with erucic acid. **(g)** Sphingomyelin average side chain length at different incubation timepoints. **(h)** Sphingomyelin side chain length in mol% after 24 hours of pulse with erucic acid. All data is presented as average ± standard deviation, n=3.

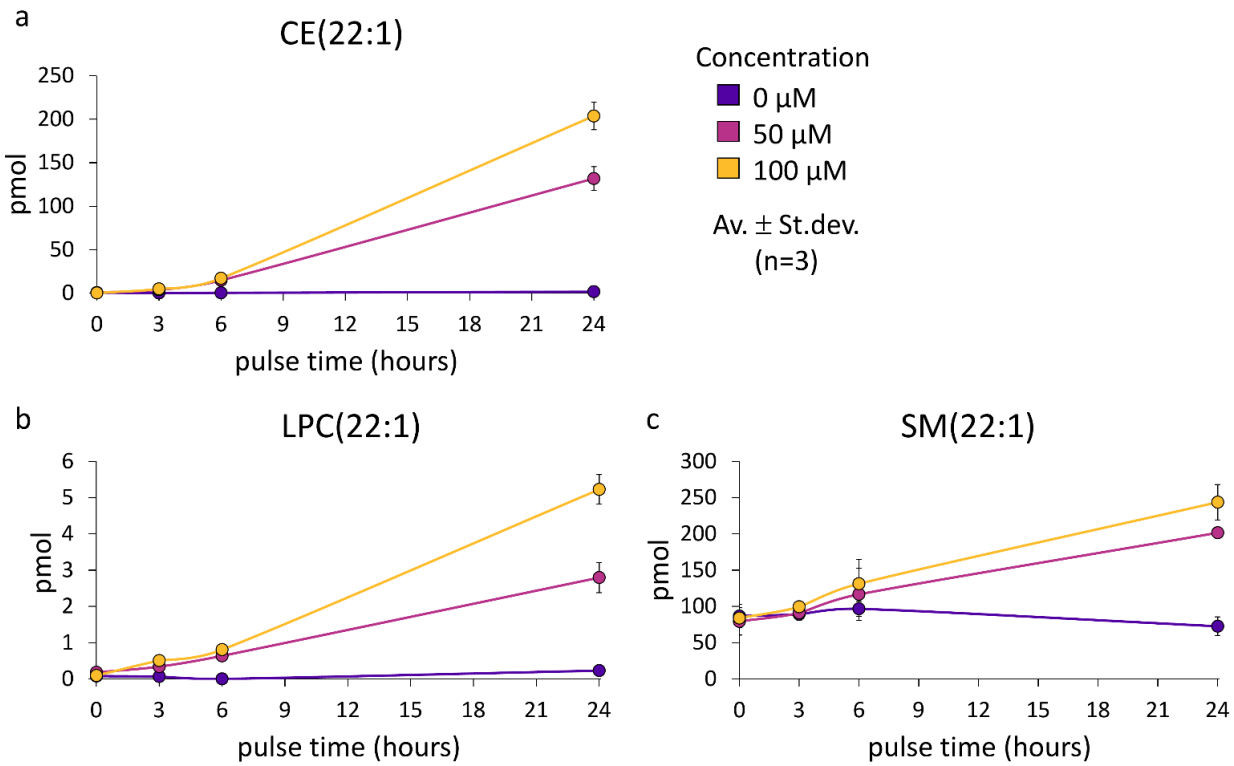

Figure 31: Accumulation of erucic acid species within cholesterol esters, lysophosphatidylcholine and sphingomyelin. H9c2 cells were incubated with erucic acid at 0, 50 or 100 µM concentration for 0, 3, 6 or 24 hours (pulse time in hours since erucic acid is present at all stages). Thereafter, the media with erucic acid was removed, the cells were washed and were used for the lipid extraction and analysis of the whole lipidome. **(a)** Cholesterol ester species containing erucic acid. **(b)** Lysophosphatidylcholine species containing erucic acid. **(c)** Sphingomyelin species containing erucic acid. Amounts in picomoles per well (pmol). All data is presented as average ± standard deviation, n=3.

Erucic acid caused lipid droplets accumulation and enlargement. To test the effect of erucic acid on cardiac lipid droplets formation, H9c2 cells were treated with erucic (FA22:1), palmitic (FA16:0), capric acid (FA10:0) or plain media for 24 hours, fixed and stained with LD540 lipophilic dye for lipid droplets. Alternatively, cells were treated with combination of erucic and palmitic acid. In contrast to other fatty acids tested, erucic acid caused significant increase in amount and size of lipid droplets, as it could be seen on the figures 32 and 33. This data was in alignment to the lipidomics data, additionally confirming, that the observed cardiac lipid accumulation was due to the presence of erucic acid and not just due to increase of fatty acid amount in the system.

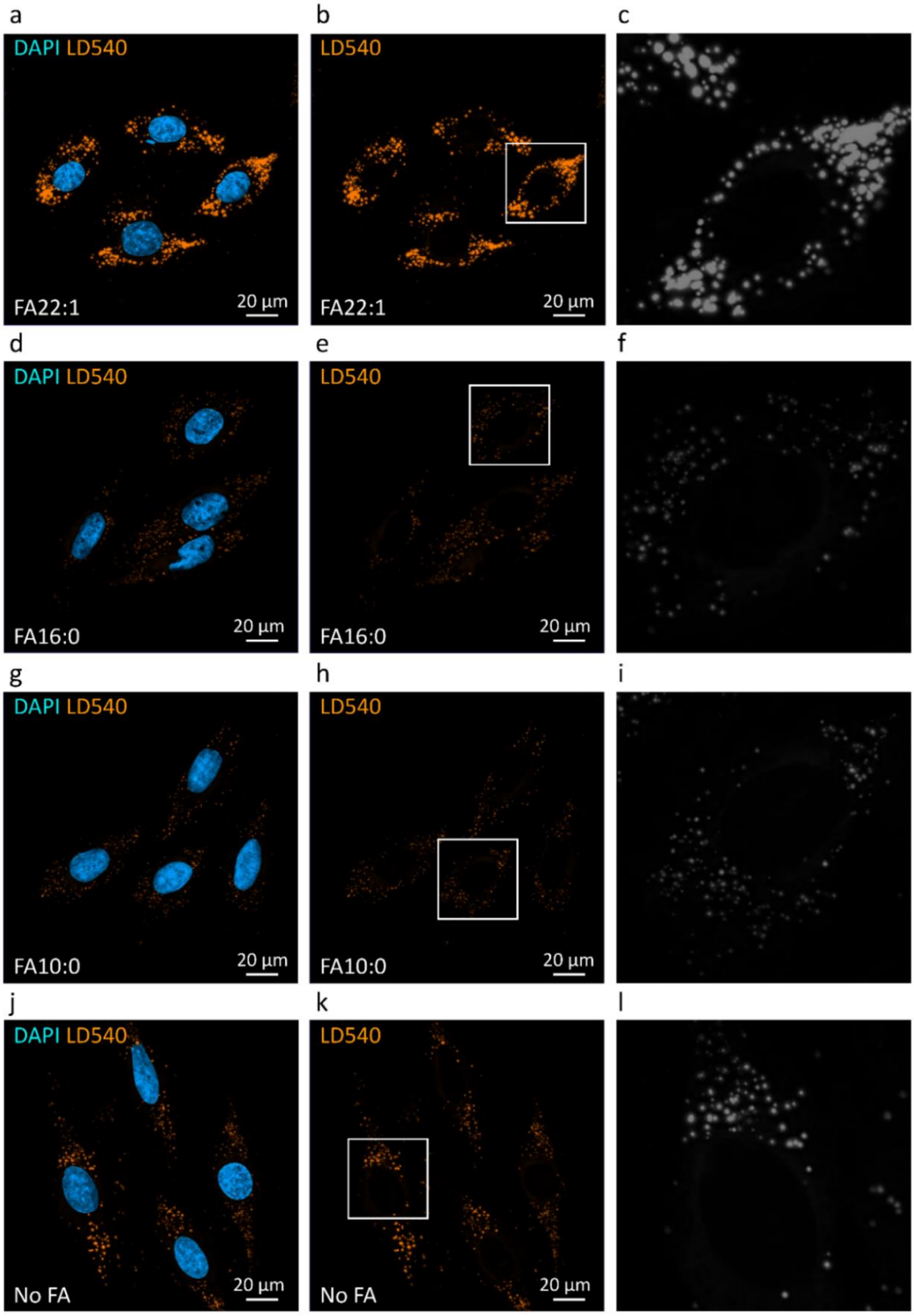

Figure 32: Erucic acid, but not palmitic or capric acid, caused increase in lipid droplets number and size. H9c2 cells were incubated in the presence of 50 µM erucic acid FA22:1 **(a-c)**, or palmitic acid FA16:0 **(d-f)**, or capric acid FA10:0 **(g-i)**, or in the plain media **(j-l)** for 24 hours and fixed with 4 % paraformaldehyde. After the nuclear staining with DAPI (blue) and lipid droplets staining with LD540 lipophilic dye (orange), the samples were visualized by fluorescence microscopy at x63 magnification. In gray **(c,f,l,l)** the magnified image of lipid droplets from respective boxed region **(b,e,h,k)** is depicted. Lipid droplet images were exported at the same intensity. Optical sectioning was performed with the Apotome, 9-11 sections at 0.24 µm interval per spot. The scalebar is 20 µm.

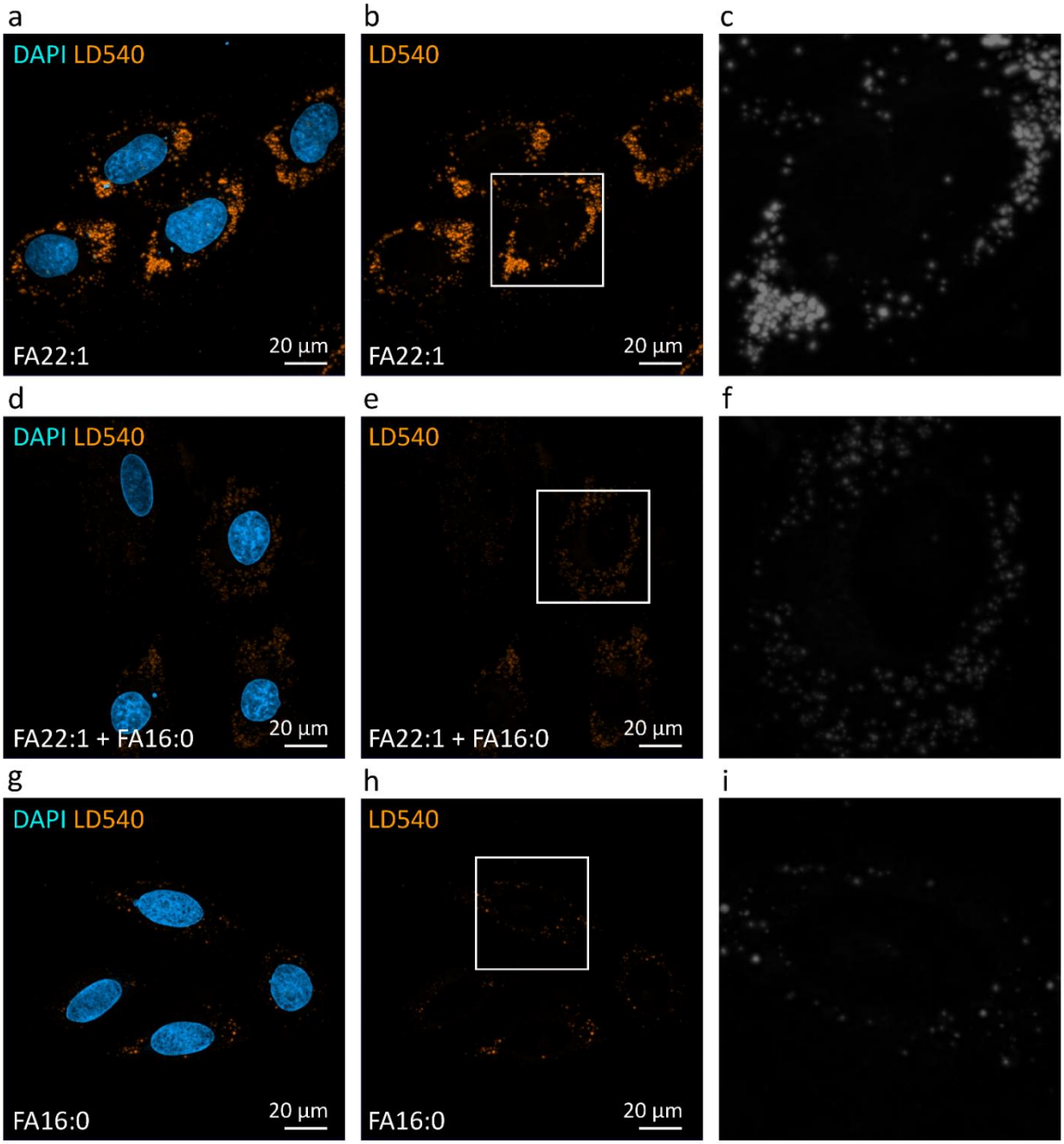

Figure 33: Erucic acid, but not its combination with palmitic acid, or palmitic acid alone, caused significant increase in lipid droplets number and size. H9c2 cells were treated with 100 µM erucic acid alone **(a-c)**, or with combination of 50 µM erucic acid with 50 µM palmitic acid **(d-f)**, or with 100 µM palmitic acid alone **(g-i)** for 24 hours, washed and fixed with 4 % paraformaldehyde. After nuclear staining with DAPI (blue) and lipid droplet staining with LD540 lipophilic dye (orange), the samples were visualized by fluorescence microscopy at x63 magnification. In gray **(c,f,i)** the magnified image of lipid droplets from the respective boxed region **(b,e,h)** is depicted. Lipid droplet images were exported at the same intensity. Optical sectioning was performed with the Apotome, 9-11 sections at 0.24 µm interval per spot. The scalebar is 20 µm.

4.4. The effect of hypoxia and oxidative stress on cardiac lipid metabolism

Chemical hypoxia and oxidative stress resulted into shifts in polar-to-neutral lipid ratio in H9c2 cells. Temporal hypoxia and oxidative stress usually accompany myocardial ischemia-reperfusion injury. Effect of these two factors on cardiac lipid metabolism was simulated on H9c2 cardiomyocytes. Cobalt chloride was used to observe the long-term effects of chemically-induced hypoxia on the lipid metabolism, as this agent stabilizes the hypoxia-inducible factors 1α and 2α under normoxic conditions (Munoz-Sanchez and Chanez-Cardenas, 2018). Hydrogen peroxide was used to expose cells to the oxidative stress, as hydrogen peroxide is the most dominant reactive species in cells due to its much higher stability compared to the other reactive oxygen species (Law et al., 2013). H9c2 cells were exposed to cobalt chloride or hydrogen peroxide, and, thereafter, fed with long-chain alkyne-fatty acid tracers and chased over 0, 3, 6 or 24 hours. Strikingly, the observed lipid patterns were similar for both stress factors and were still detectable even after 24 hours after the stress agent removal. Both chemical hypoxia and oxidative stress resulted into reduction of polar-to-neutral lipid ratio, indicating systemic shifts in handling of long-chain fatty acids under these stress conditions. These changes were persistent even after 24 hours of chasing, dependent on the concentration of cobalt chloride or hydrogen peroxide applied, but independent from the saturation degree of the long-chain fatty acid tracers fed to the cells (see figure 34).

Chemical hypoxia and oxidative stress affect membrane phosphatidylcholine metabolism and remodeling. The total amount of phosphatidylcholines in H9c2 cells tend to be generally decreasing with the increasing concentrations of cobalt chloride or hydrogen peroxide. The effect was especially obvious after long-term incubation, at 24 hours of chasing, as it could be seen on the figure 35. Chemical hypoxia and oxidative stress also tended to influence linoleic-acid-derived phosphatidylcholines remodeling. In non-stressed condition, as seen earlier for slices and cells on the figures 16 (b) and 17 (b), the increase of PC36;Y to PC34;Y ratio is evident over the long chasing times. Here, this ratio was changing much slower under the increasing concentrations of both agents, indicating that cobalt chloride and hydrogen peroxide could have an inhibitory effect on elongation of linoleic-acid-derived phosphatidylcholines (see figure 36).

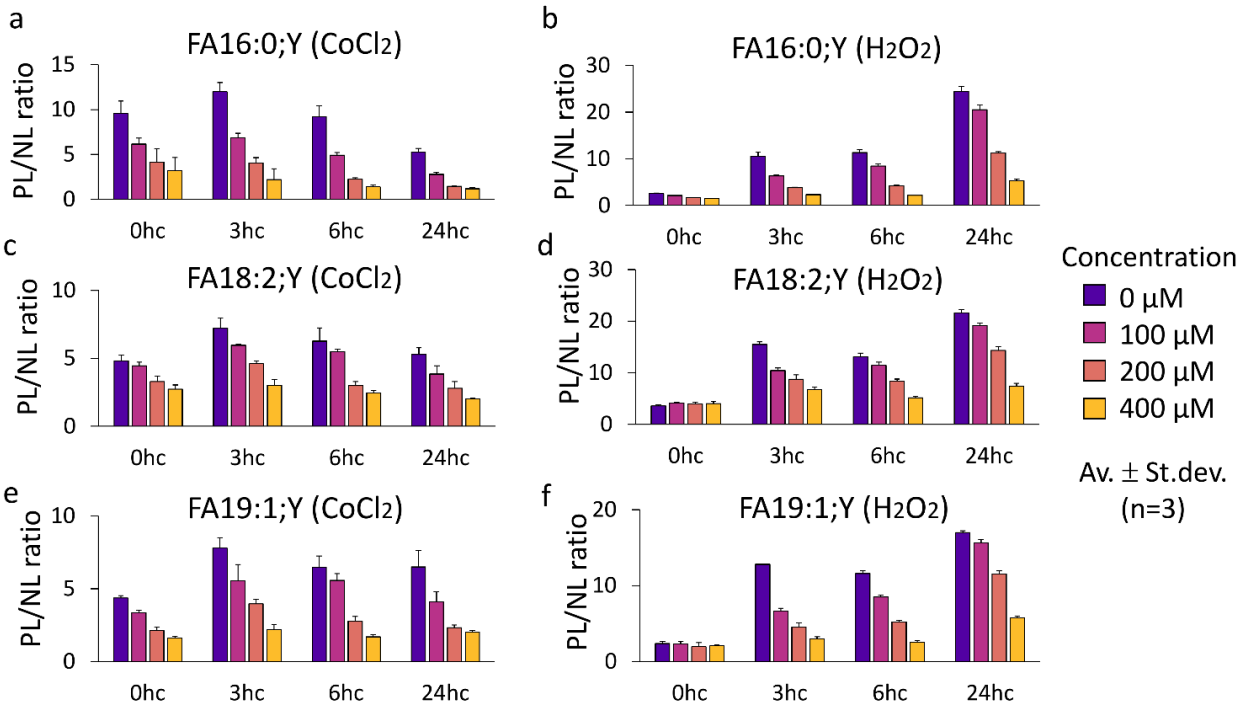

Figure 34: Effect of chemical hypoxia and oxidative stress on cardiac polar-to-neutral lipid ratio in H9c2 cells. Cells were exposed to increasing concentrations of cobalt-chloride for 24 hours to induce chemical hypoxia **(a,c,e)** or were exposed to increasing concentrations of hydrogen peroxide for 3 hours to simulate oxidative stress **(b,d,f).** Thereafter, the cells were fed with a mixture of long-chain alkyne-fatty acids (alkyne-palmitic (FA16:0;Y($^{13}C_6$)), alkyne-linoleic (FA18:2;Y) and alkyne-oleic (FA19:1;Y) acids) for 1 hour and chased for 0, 3, 6 or 24 hours (hc) in the plain media. Lipids were extracted and analyzed via mass spectrometry. Polar (PL) to neutral (NL) lipid ratio for different alkyne-fatty acids was determined as a sum of identified alkyne-polar lipids (phosphatidylcholines, phosphatidylethanolamines, phosphatidylinositol, sphingomyelins, ceramides, glucosylceramides) divided by the sum of identified neutral lipids (mono-, di- and triacylglycerols, cholesterol esters). All data as average ± standard deviation, n=3.

Chemical hypoxia and oxidative stress reduced sphingomyelin content in H9c2 cells. Cobalt chloride and hydrogen peroxide showed an inhibitory effect on sphingomyelin production, as seen on the figure 37. This effect was concentration-dependent and especially prominent after long chasing time.

Trimetazidine allowed to slightly reverse the effect of oxidative stress on sphingomyelin biosynthesis inhibition. Cells were exposed to hydrogen peroxide, pulsed with alkyne-fatty acids, and, thereafter, chased in the media containing trimetazidine. Slightly higher sphingomyelin content was observed in trimetazidine-treated cells. The effect was concentration-dependent and already obvious at low trimetazidine concentrations tested (1 μM), which could indicate potential ability of this medication to reverse the oxidative stress inhibitory effect on sphingomyelin biosynthesis. The observed effect was prominent after long chasing period (24 hours), as seen on the figure 38.

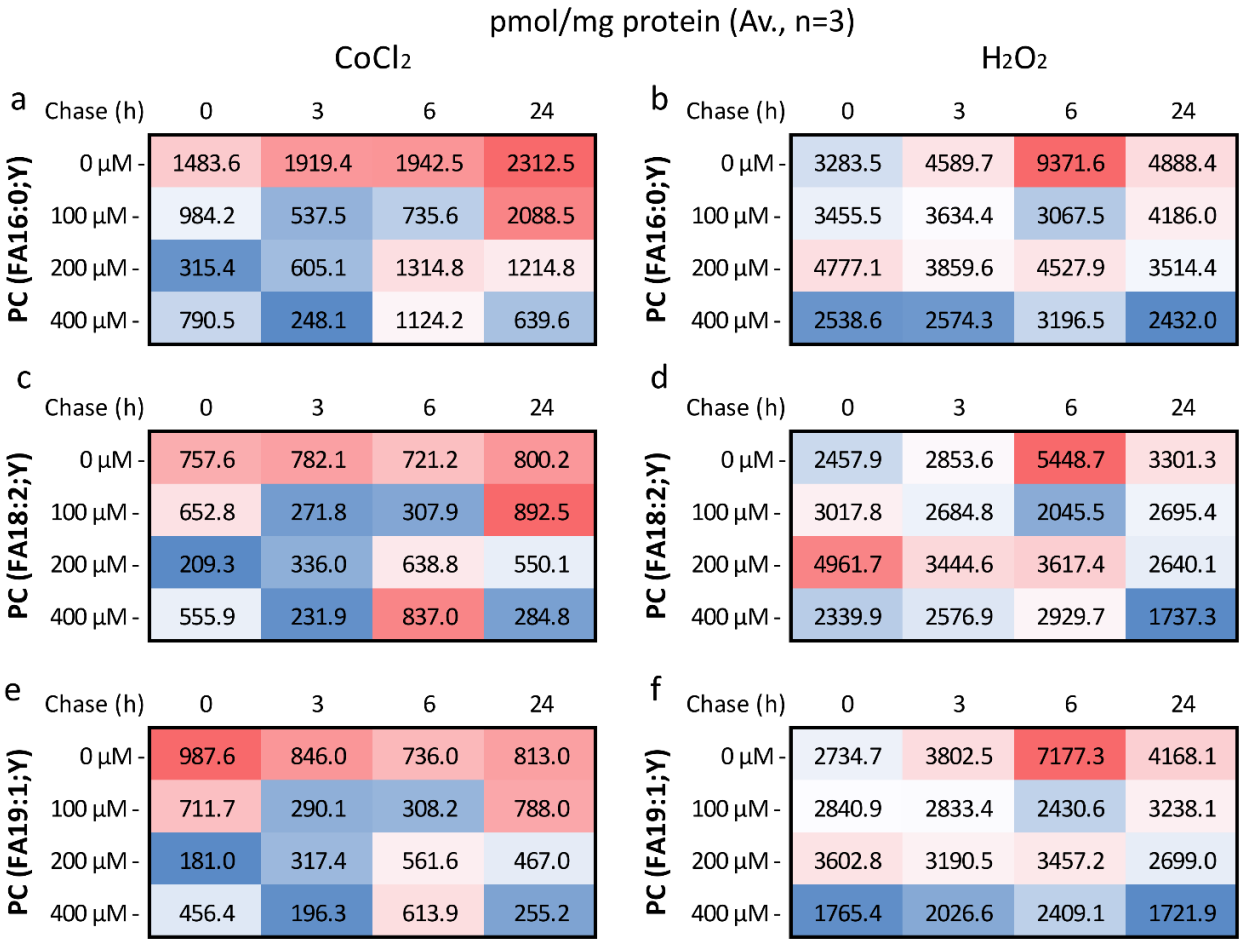

Figure 35: Effect of chemical hypoxia and oxidative stress on cardiac phosphatidylcholines amounts in H9c2 cells. Cells were exposed to increasing concentrations of cobalt-chloride for 24 hours to induce chemical hypoxia **(a,c,e)** or were exposed to increasing concentrations of hydrogen peroxide for 3 hours to simulate oxidative stress **(b,d,f).** Thereafter, the cells were fed with a mixture of alkyne-fatty acids (alkyne-palmitic (FA16:0;Y($^{13}C_6$)), alkyne-linoleic (FA18:2;Y) and alkyne-oleic (FA19:1;Y) acids) for 1 hour and chased for 0, 3, 6 or 24 hours (h) in the plain media. Lipids were extracted and analyzed via mass spectrometry. Alkyne-phosphatidylcholines (PC) amounts are shown in picomoles per milligram protein in the sample. All data as average, n=3.

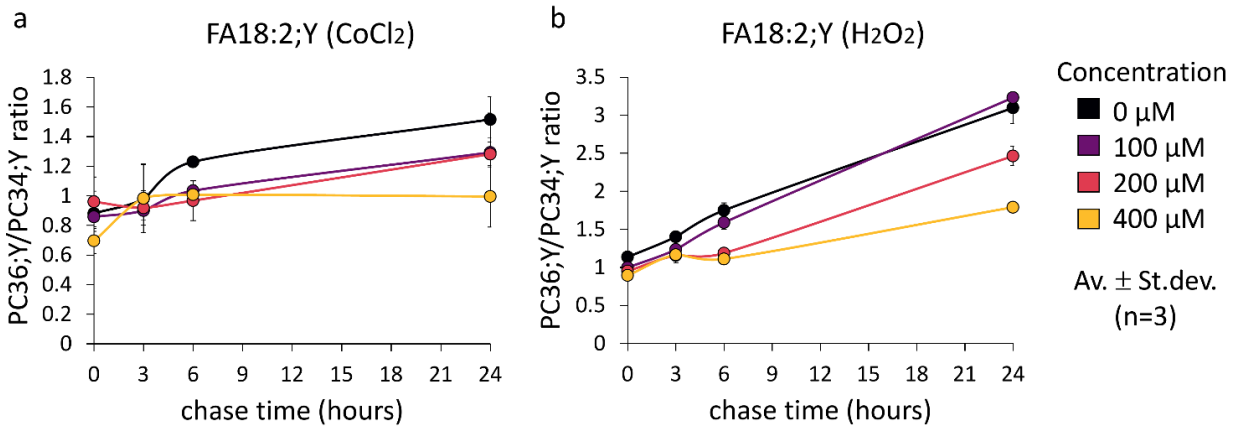

Figure 36: Effect of chemical hypoxia and oxidative stress on linoleic acid phosphatidylcholines remodeling in H9c2 cells. Cells were exposed to increasing concentrations of cobalt-chloride for 24 hours to induce chemical hypoxia **(a)** or were exposed to increasing concentrations of hydrogen peroxide for 3 hours to simulate oxidative stress **(b)**. Thereafter, the cells were fed with alkyne-linoleic acid (FA18:2;Y) for 1 hour and chased for 0, 3, 6 or 24 hours in the plain media. Lipids were extracted and analyzed via mass spectrometry. To determine the effect of cobalt chloride or hydrogen peroxide on the modification of linoleic acid-derived-phosphatidylcholines, the sum of alkyne-phosphatidylcholines with 36 carbon atoms in the side chain was divided by sum of alkyne-phosphatidylcholines with 34 carbons. All data as average ± standard deviation, n=3.

a pmol/mg protein (Av., n=3) $CoCl_2$

SM (FA16:0;Y)	Chase (h) 0	3	6	24
0 µM	20.9	132.2	164.7	384.6
100 µM	0.0	14.6	79.7	295.3
200 µM	0.0	13.3	18.2	91.2
400 µM	31.7	6.5	89.6	87.7

b pmol/mg protein (Av., n=3) H_2O_2

SM (FA16:0;Y)	Chase (h) 0	3	6	24
0 µM	114.6	233.3	868.1	1124.5
100 µM	85.7	269.3	281.1	957.3
200 µM	132.1	160.3	372.2	596.8
400 µM	16.0	117.2	232.0	480.4

Figure 37: Effect of chemical hypoxia and oxidative stress on cardiac sphingomyelin amounts in H9c2 cells. Cells were exposed to increasing concentrations of cobalt-chloride for 24 hours to induce chemical hypoxia **(a)** or were exposed to increasing concentrations of hydrogen peroxide for 3 hours to simulate oxidative stress **(b)**. Thereafter, the cells were fed with isotope version of alkyne-palmitic acid (FA16:0;Y($^{13}C_6$)) for 1 hour and chased for 0, 3, 6 or 24 hours (h) in the plain media. Lipids were extracted and analyzed via mass spectrometry. Sphingomyelins (SM) amounts are shown in picomoles per milligram protein in the sample. average, n=3.

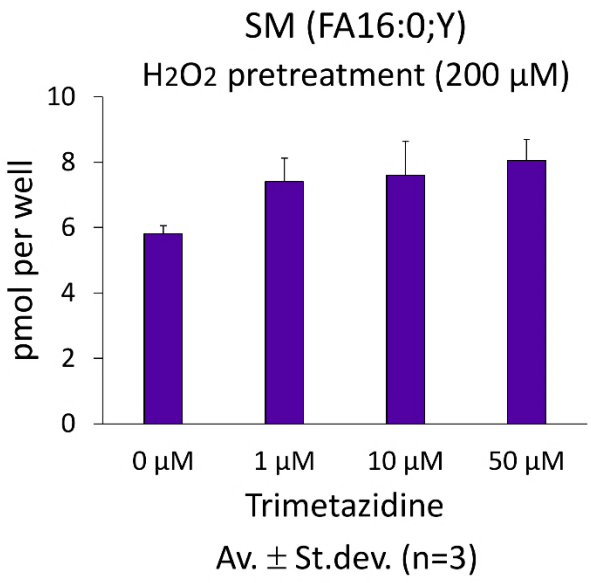

Figure 38: Effect of trimetazidine in hydrogen peroxide-exposed H9c2 cells. Cells were first treated for 3 hours with hydrogen peroxide (200 µM). Thereafter, cells were fed with isotope version of alkyne-palmitic acid (FA16:0;Y($^{13}C_6$)) for 1 hour and chased for 24 hours in the media containing 0, 1, 10 or 50 µM trimetazidine. Data as picomoles per well, average ± standard deviation, n=3

Similarities between lipid responses to hypoxia and oxidative stress could not be explained by apoptosis. Strikingly, cellular responses to cobalt chloride-induced chemical hypoxia and hydrogen peroxide-caused oxidative stress resulted into similar patterns in lipid metabolism: changes in polar-to-neutral lipids ratio, reduction of phosphatidylcholines and sphingomyelin biosynthesis and inhibition of linoleic-acid derived phosphatidylcholines elongation. To find out the possible reason behind these similarities, cells were exposed to cobalt chloride for 24 hours or hydrogen peroxide for 3 hours, and, thereafter, fed with alkyne-linoleic acid (FA18:2;Y). Cells were stained for nuclei and alkyne-lipids to see effect of the stress agents on cell morphology and lipid distribution. As it could be seen on the figure 39, exposure of the cells to cobalt chloride and hydrogen peroxide at 200 µM resulted into nuclei fragmentation, indicating significant damage to the cells or cell death taking place. No significant differences in alkyne-fatty acid uptake or intracellular distribution were seen between conditions tested. To find out the role of apoptosis here, H9c2 cells were exposed to chemical hypoxia or oxidative stress and, thereafter, subjected to the TUNEL assay (see figure 40). While around one quarter of the cells after hydrogen peroxide treatment were positively stained for apoptotic markers, no strong signal was observed in cells exposed to cobalt chloride. Therefore, the similarity of the observed lipid patterns between cobalt chloride and hydrogen peroxide-treated cells could not be explained by apoptosis and might include other cellular pathways.

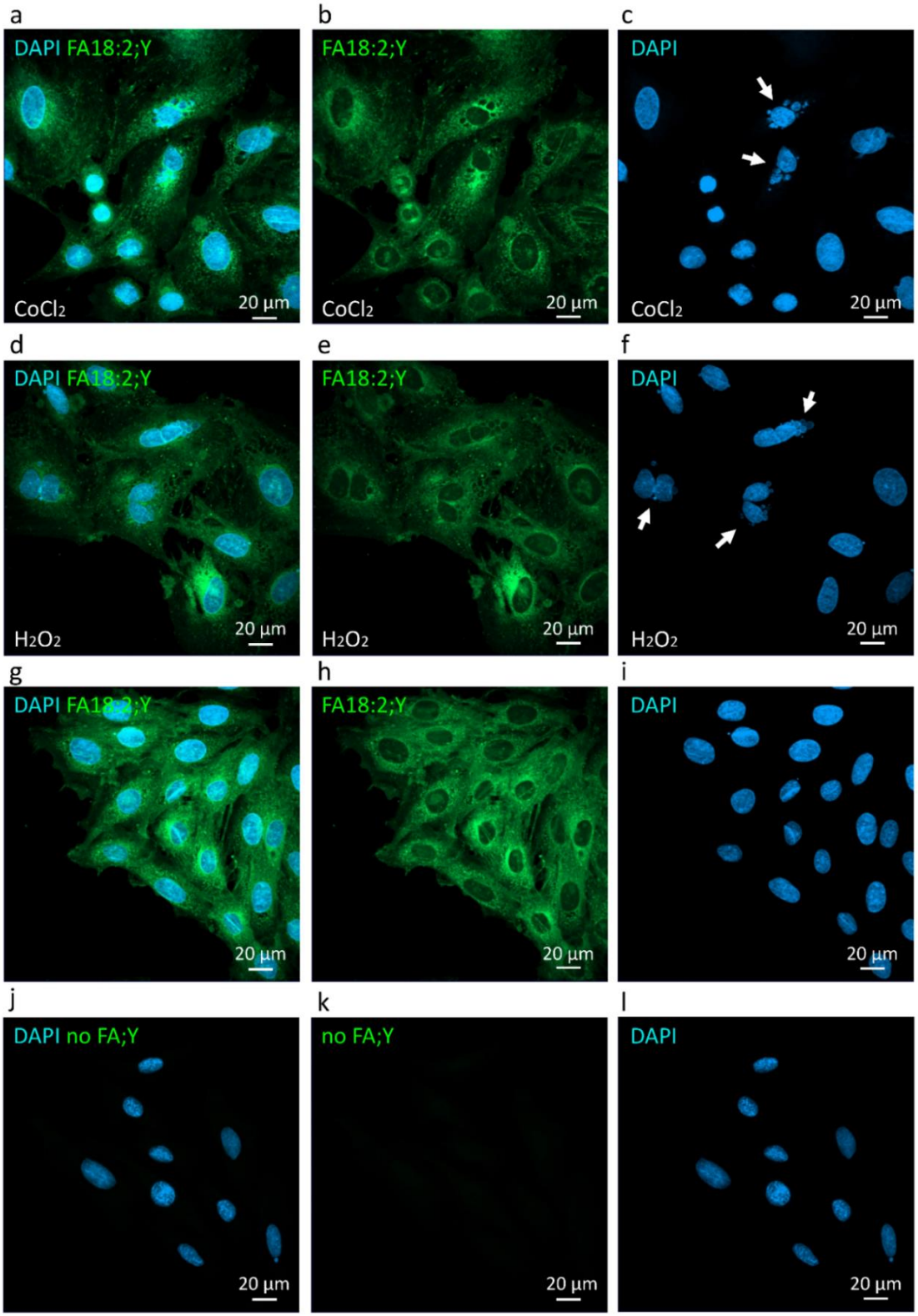

Figure 39: Effect of chemical hypoxia and oxidative stress on alkyne-lipids distribution in H9c2 cells. H9c2 cells were incubated with 200 µM cobalt chloride for 24 hours **(a-c)**, 200 µM hydrogen peroxide for 3 hours **(d-f)** or plain media **(g-l)**. Thereafter the cells **(a-i)** were fed with alkyne-linoleic acid (FA18:2;Y) for 1 hour, or plain media **(j-l)** as a negative control. Cells were washed and fixed with 4 % paraformaldehyde. After the click-reaction with the AF488-picolyl-azide reporter (green) and nuclear staining with DAPI (blue), the uptake and distribution of alkyne-lipids was visualized by fluorescence microscopy at x40 magnification. Optical sectioning was performed with Apotome. The arrows indicate nuclei undergoing fragmentation. The scalebar is 20 µm.

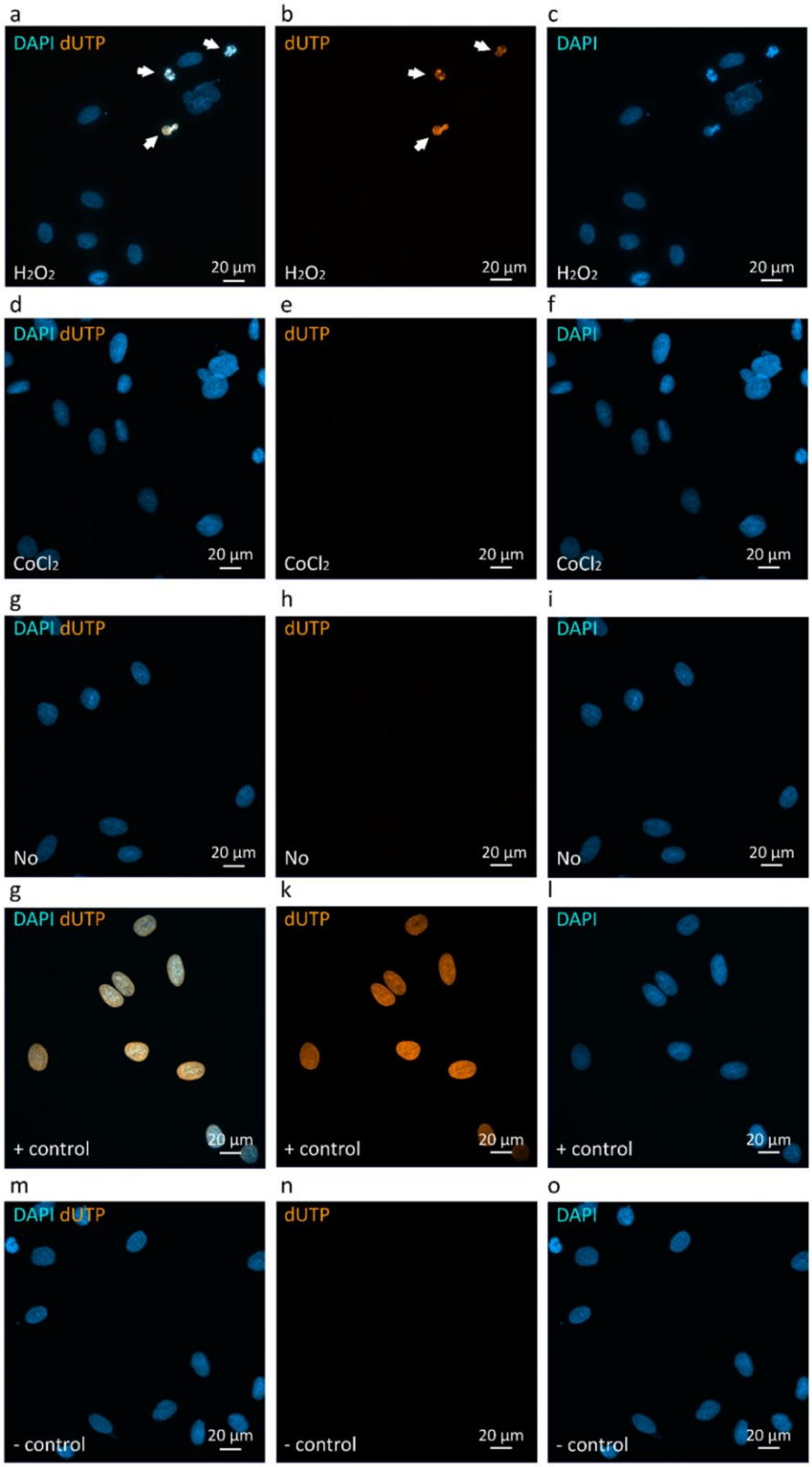

Figure 40: Apoptotic assay of H9c2 cells exposed to oxidative stress and chemical hypoxia. H9c2 cells were incubated with 200 µM hydrogen peroxide for 3 hours **(a-c)**, 200 µM cobalt chloride for 24 hours **(d-f)** or plain media **(g-o)**. Thereafter, cells were subjected to the TUNEL apoptotic assay. Nuclei were stained with DAPI (blue), the exposed 3'-OH ends of the broken DNA were catalyzed with fluorescent dUTP (orange). **(g-l)** Positive control, **(m-o)** Negative control. Optical sectioning was performed with Apotome at x40 magnification. Arrows on **(a,b)** show cells with DAPI and dUTP staining overlap, which indicates cells undergoing apoptosis in the sample. The scalebar is 20 µm.

5. Discussion

5.1. Alkyne-fatty acid metabolism in various cardiac setups

Heart failure still remains a major challenge due to high mortality rate and poor treatment prognosis. Lipid alterations are commonly observed in many cardiac diseases, however, the direct tracing of complex changes in lipid metabolism still remains a challenge due to limited tools available. Majorly, the information on lipid alterations in cardiac disease is derived from patients' cohort studies or "indirectly" through analysis of lipid metabolism-related proteins expression. Although, highly relevant, the patients' data is usually extremely heterogeneous and shows a static snapshot on the lipid metabolism, and does not provide much information on dynamic lipid changes in the complex metabolic networks. Cohort studies often have different participants selection criteria, plus, do not always get full access to the information on medications that patients take, lifestyle details, or genetic predisposes. There is a huge gap between heart pathology research field and available lipid methodology to study complex lipid alterations. Thus, a tool for studying lipid metabolism with a high resolution in the heart is highly needed.

Akyne-fatty acids are convenient, reliable and non-radioactive tracers that allow to follow lipid metabolism in almost any biological system (Thiele et al., 2012). So far, these tracers have been applied only once to heart tissue slices for subsequent analysis via thin-layer chromatography and the identification of the most abundant lipid classes formed (Klizaite, 2017). Alkyne-fatty acids have not been applied to other cardiac setups, and no studies on dynamic lipid alterations down to species resolution with the help of mass spectrometry or alkyne-lipid visualization via fluorescent microscopy were done in the heart so far.

In this work various medium- and long-chain (saturated, mono- and polyunsaturated) fatty acids have been applied to different cardiac setups (heart lysates, H9c2 cardiac cell line, viable heart slices, the Langendorff heart). Alkyne-tracers allowed to detect differences in cardiac anabolism and catabolism of different fatty acids depending on their chain length and number of double bonds. Moreover, in combination with high-resolution mass spectrometric lipid analysis, the mix of several fatty acids could be traced together in one sample, allowing to mimic complex diversity of dietary fatty acids and their cross-effects in the heart.

Significant differences in preferences for long- and medium-chain fatty acids by the heart were observed depending on lipid metabolic pathways involved. While medium-chain fatty acids were the preferred substrate for the energy production by the heart, long-chain fatty acids were more intensively incorporated into cellular lipids. The observed preference of the heart to use medium-chain fatty acids for its catabolism could be explained by the higher availability of medium fatty acids for the mitochondrial β-oxidation: while long-chain fatty acids need to be coupled to carnitine first in order to be able to enter mitochondria for subsequent oxidation and energy production, medium-chain fatty acids can get into mitochondria directly. However, these metabolic properties are proven for the liver and kidney, while for the heart and skeletal muscle contradicting observations in the literature exist. Some studies report, that cardiac medium-chain fatty acid transport is independent from carnitine shuttle, so that these fatty acids can enter mitochondria directly (Labarthe et al., 2008). Others, however, have observed, that in the heart and skeletal muscle – in contrast to liver and kidneys – medium-chain fatty acids still need to be coupled to carnitine first in order to be able to enter mitochondria for catabolism, suggesting dependence of medium-chain fatty acid oxidation on coupling to carnitine being tissue-specific (Pereyra et al., 2023). Due to higher medium-chain fatty acids utilization rate it might be suggested that under energy-deprived conditions and long-chain fatty acid metabolism disorders the heart might benefit from diets, rich on medium-chain fatty acids as an alternative and readily available energy source for the heart. Indeed, dietary interventions with medium-chain fatty acids are a common practice when supporting undernourished patients and patients with metabolic (e.g. long-chain fatty acid oxidation defects) and neurological disorders (Labarthe et al., 2008; Huang et al., 2021; Ismael and Nair, 2021).

As seen in this study, long-chain fatty acids were readily incorporated into cellular lipids with their sufficient part going to the membrane phospholipid synthesis (majorly, phosphatidylcholines – an important structural component of the cellular membrane (Paapstel et al., 2018)). This was in contrast to medium-chain fatty acids, which incorporation into cellular lipids was much lower in general, and they were majorly esterified and stored as triglycerides. Microscopy data additionally confirmed these observations on fatty acid incorporation rate. Following alkyne-lipid fluorescent staining, medium-chain fatty acids tended to be much less incorporated into cardiac lipids in contrast to long-chain fatty acids. This shows differences in fatty acid handling by the myocardium for its anabolic needs depending on fatty acids' side chain length. The data

also confirms, that cardiomyocytes are able to synthesize the medium-chain triglycerides, which was previously showed for the liver cells (Klizaite, 2017).

Some differences in handling of long-chain fatty acids by cardiomyocytes depending on double bond count were observed. In particular, saturated palmitic acid was shown to be more prone to promote biosynthesis of potentially toxic lipid species compared to unsaturated linoleic and oleic acids. Based on the pulse-chase data, saturated palmitic acid feeding resulted into elevated levels of cholesterol esters, ceramides and diacylglycerols compared to other unsaturated long-chain fatty acids tested. Ceramides and diacylglycerols are considered being toxic for the cardiomyocytes, and are believed to be the major drivers of cardiac lipotoxicity and to play the central role in the onset of cardiac diseases (Schulze et al., 2016). Increased amounts of cholesterol esters, ceramides and diacylglycerols formed from alkyne-palmitic acid suggest that palmitic acid might have a negative effect on the heart in contrast to oleic and linoleic acids, and might promote lipotoxicity. This observation was in the alignment with the current scientific view, that the diets rich in saturated palmitic acid (e.g., Western pattern diet) are associated with higher risks of cardiovascular diseases compared to diets rich of mono- and polyunsaturated fatty acids, like Mediterranean diet, Nordic diet and Southern European Atlantic diet (Fattore and Fanelli, 2013; Maki et al., 2021; Lorenzo et al., 2022). The World Health organization in the guideline from 2023 recommended that adults and children strongly reduce saturated fatty acid intake to 10 % of total energy intake, and ensure an adequate intake of unsaturated fatty acids (World Health Organization, 2023).

5.2. Cardiac triglycerides pool

Alkyne-fatty acid tracers allowed to confirm the existence of cardiac triglycerides pool with a very high turnover and its different kinetics for medium- and long-chain fatty acids. This is the first time studying cardiac triglycerides pool employing a variety of fatty acid tracers of different length and saturation degree, since the earlier works used only variations of isotope- or radioactively-labelled palmitate (Olson and Hoeschen, 1967; Saddik and Lopaschuk, 1991; Swanton and Saggerson, 1997; Lewin et al., 2008; Banke et al., 2010).

The adipose triacylglyceride lipase inhibitor (ATGListatin) caused accumulation of long-chain triglycerides and slowed down triglycerides cycling (determined as decrease of double-labelled alkyne-triglycerides species accompanied with simultaneous increase of single-labelled alkyne-triglycerides over time). Since ATGListatin does not cause triglycerides synthesis, but inhibits their hydrolysis and fatty acid release, the observed triglycerides accumulation in ATGListatin-treated cells indicate that the flow of long-chain fatty acids through the system is very high. Additionally, the effect of ATGListatin on lipid droplets was also visually confirmed. The kinetics of cardiac triglycerides pool is suggested to be much higher compared to other organs and its regulation might also be tissue-specific. For example, in the earlier experiments done in adipocytes, triglyceride cycling was happening under physiological condition even without the use of ATGListatin (Wunderling et al., 2023). Cardiac triglycerides pool regulation and kinetics might share similarities with skeletal muscle due to the high mechanical load of striated muscle cells. Indeed, experiments, where entrapment of isotope-labeled fatty acids in subcutaneous adipose tissue and forearm muscle of human participants was assessed, showed that fatty acid trapping in skeletal muscle is fundamentally different from that in adipose tissue (Evans et al., 2002).

ATGListatin application allowed to follow alkyne-palmitic acid tracer modification within triglycerides, which might be heart-specific and differ from palmitic acid fate in other tissues. Cardiac cells tend to majorly modify alkyne-palmitic acid (FA16:0;Y) within triglycerides by its elongation to alkyne-stearic acid FA18:0;Y. Shortening (FA14:0;Y formation) or desaturation (FA16:1;Y and FA18:1;Y formation) were happening much less. Palmitic acid triglycerides modification by cardiac cells was different from that observed earlier in adipocytes, which majorly modified alkyne-palmitic acid by its desaturation to FA16:1;Y (Wunderling et al., 2023). This difference between cardiac and

adipose cells suggested tissue-specific handling of palmitic acid-containing triglycerides. Preferential elongation of palmitic acid to stearic acid instead of its desaturation might have adverse effects on the heart health due to accumulation of long-chain saturated lipid species, which correlate with increased cardiovascular risk. Of note, stearic acid itself was found to be associated with inflammatory and endothelial dysfunction biomarkers in patients at cardiovascular risk (Gonçalinho et al., 2023).

Cardiac triglycerides pool might be of great importance for normal heart functioning. Usually, cardiac cells do not accumulate much triglycerides. Even though triglycerides themselves are not considered to be toxic, the increase in triglyceride content and lipid droplet count has been observed in many pathophysiological conditions and often accompany heart failure progression (Oenarto, 2020). Since the heart has a limited capacity to store fatty acids within triacylglycerides at a time, it does rely heavily on the exogenous fatty acid supply coming from the circulatory system. Due to various reasons (e.g. diet, starvation, physical activity) the fatty acid content in blood can vary dramatically during the day. The cardiac triglycerides pool plays an important role as a gating mechanism, finely guarding fatty acid intracellular concentration depending on fatty acid availability and heart's needs. Due to hearts extremely high energy demands on one side, and it's low capacity to store fatty acids and unpredictable fatty acid supply from blood on the other side, this buffering system needs to be highly flexible (Lopaschuk et al., 2010; Kienesberger et al., 2013 (A); Heier and Haemmerle, 2016). Triglycerides pool within lipid droplets could represent an accessible reserve of fatty acids that allows the heart to meet varying energy demands and to compensate for the fluctuating availability of circulating fatty acids (Da Dalt et al., 2023). Triglycerides pool might offer a protection in case of β-oxidation impairments or mitochondrial fatty acids overload, which, if unmanaged, could promote accumulation of some bioactive lipid species that could negatively affect cellular functioning and signaling pathways (Heier and Haemmerle, 2016; Schulze et al., 2016).

5.3. Effect of erucic acid on cardiac lipid metabolism

Erucic acid (FA22:1) is a monounsaturated fatty acid, synthesized in the seeds of many plans of the Brassicaceae family. The compound was suspected to cause myocardial lipidosis in the heart, therefore, its content in foods in strictly regulated in many countries (Galanty et al., 2023).

In this work the effect of erucic acid on lipid metabolism was studied. Erucic acid pretreatment affected metabolism of common dietary long-chain fatty acids (neutral lipid accumulation, arachidonic acid-containing phosphatidylinositol amount, acyl-carnitines formation) and systematically influenced cardiac lipidome (total lipid amount, neutral-to-polar lipids ratio, long-chain species enrichment). These global changes, observed under erucic acid treatment, could be an indicator of cardiac cells overload with free fatty acids that were not efficiently utilized for the energy production and, thus, have to get esterified and incorporated into cellular lipids, since high intracellular concentrations of free fatty acids are toxic for the cell. As is was shown earlier in experiments with ATGListatin, fatty acid turnover and flow in the heart is very high, thus, any minor imbalances between fatty acid supply and oxidation could promote intracellular lipid accumulation.

Observations from this study are in alignment with earlier experiments done on rats, where animals were fed with rapeseed oil high in erucic acid content. Significant triglycerides accumulation was observed in the hearts from these animals, and the observed effect was more prominent in the heart than in any other organs studied. Thus, erucic acid metabolism is thought to be tissue-specific and affect the heart in the first place (Christophersen and Bremer, 1972). This was confirmed by other research group in experiments, where rat liver and heart were perfused with FA22:1($^{14}C_{14}$) erucic acid tracer. That study showed that liver and heart metabolized erucic acid differently. Only 25 % of the tracer was recovered as erucic acid in the liver, while remaining portion was modified to stearic and oleic acid. At the same time, 75 % of the tracer remained unmodified in the heart (Murphy et al., 2008). This might explain why erucic acid treatment affects the heart more severely than any other organ.

It was suggested that erucic acid might influence mitochondrial β-oxidation of long-chain fatty acids (Christophersen and Bremer, 1972; Murphy et al., 2008). Erucic acid, like other very long-chain fatty acids, is primarily oxidized in peroxisomes. It was

hypothesized that peroxisomal fatty acid oxidation could result into elevated levels of malonyl-CoA, that could inhibit carnitine palmitoyltransferase 1 (cpt1). Cpt1 is responsible for coupling long-chain fatty acids to carnitine, enabling their transport into mitochondria for further oxidation and energy production (Chen et al., 2020). Thus, inhibition of cpt1 by elevated levels of malonyl-CoA, that accompanies increased peroxisomal oxidation of erucic acid, could suppress mitochondrial β-oxidation of long-chain fatty acids by restricting their transport into mitochondria, which eventually would result into their overall accumulation in the cell and explain lipid patterns observed in this thesis. In additional experiments, done on heart lysates, erucic acid tends to affect the length and amounts of acyl-carnitines formed, indicating its potential effect on acyl-carnitines formation and cpt1 activity. Hypothetically, other very long-chain fatty acids might have a similar effect on long-chain fatty acid metabolism as erucic acid does. However, testing other very long-chain fatty acids was beyond this study.

Erucic acid effect on lipid accumulation was also confirmed visually in this thesis. Cardiomyocytes, treated with erucic acid, accumulated significant amounts of lipid droplets, compared to cells, that were incubated with other long- or medium-chain fatty acids. The observed increase in lipid droplets number and size in the presence of erucic acid could potentially result into biological consequences. Excessive deposition of lipid droplets could be mechanically obstructing and spatially blocking contraction of cardiomyocytes, since cardiac cells are already densely packed with contracting elements and mitochondria, leaving relatively little volume of sarcoplasm in between compared to other cell types (D'Souza et al., 2016). Additionally, changes in myocardial lipid droplet metabolism may influence cardiac signaling and function through its connection with phospholipid and cholesterol metabolism, and have a downstream effect on membrane integrity, as well as cardiac electric properties (Kienesberger et al., 2013, B). Impairments in cardiomyocytes contraction and signaling could, in their turn, eventually lead to heart failure. Balancing contractility and metabolic control is crucial for cardiomyocytes and any impairments might directly contribute to the disease development.

In this study erucic acid also caused concentration-dependent increase of arachidonic acid-phosphatidylinositol. Phosphatidylinositol contributes only 2-10 % of total phospholipids; however, this lipid class plays a crucial role in regulation of several fundamental processes such as membrane dynamics and signal transduction. (D'Souza

and Epand, 2014). Accumulation of arachidonic acid-containing phosphatidylinositol has been observed in some pathological conditions, like at the outer edge of colorectal cancer. This discovery highlighted potential importance of arachidonic acid-containing phosphatidylinositol in cancer cell migration and colorectal cancer progression. This lipid species is also preferentially converted to phosphatidylinositol polyphosphates (PIPs) which are known to play a key role in many cellular processes including cell migration, invasion and proliferation (Hiraide et al., 2016). Erucic acid-induced accumulation of arachidonic acid-phosphatidylinositol and diacylglycerides, observed in this study, potentially, could indicate downstream increase of phosphatidylinositol 4,5-bisphosphate (PIP2). PIP2 is a signaling intermediate, which regulates many ion channels and membrane proteins. It has a regulatory effect on calcium mobilization. Therefore, erucic acid might not only affect lipid accumulation, but also potentially influence signaling and calcium handling in cardiomyocytes. Calcium fluxes are critical for contraction in cardiac, skeletal and smooth muscle. Dysregulation of calcium handling is central in many heart disease pathologies. Calcium imbalance is the main cause of contractile dysfunction and arrhythmias in the heart failure (Fearnley et al., 2011; Ghigo et al., 2017).

Lipidomics analysis has its limitations, as it cannot directly follow erucic acid alterations and distinguish lipids derived from this fatty acid from other cellular lipids. Analysis of other alkyne-fatty acids in the presence of erucic acid provides indirect information on erucic acid influence on cellular lipid networks. Development of lipid tracers, like alkyne-erucic acid, would allow to directly follow metabolism of this fatty acid in cardiomyocytes.

5.4. Effect of chemical hypoxia and oxidative stress on cardiac lipid metabolism

Hypoxia and oxidative stress are commonly observed in myocardial ischemia-reperfusion injury during ischemic (I) and reperfusion (II) phases, severely damaging the heart and eventually leading to the heart failure. During ischemic phase (I) the artery gets blocked due to plaque (or gas bubbles in case of arterial gas embolism and decompression sickness in scuba diving) resulting into decreased blood flow, and, hence, decreased substrate availability and hypoxia. Short-term ischemia could also occur due to temporal circulation interruption during heart transplantation. During the following reperfusion state (II) the blood flow to the heart is restored, resulting into sudden oxygen levels increase. Counterintuitively, the following sudden restoration of the blood flow might cause pathological effects, leading to even greater myocardial injury than that could be caused by the original ischemic insult alone. Myocardial ischemia-reperfusion injury arises in situations like heart transplantation, myocardial infarction, acute onset of heart disease and trauma. The mechanism of myocardial ischemia-reperfusion injury is highly complex, and involves oxidative stress, calcium ion imbalance, mitochondrial damage, energy metabolism disorders, cell apoptosis and inflammatory response (He et al., 2022).

To study the effect of hypoxia and oxidative stress on cardiac lipid metabolism, cardiomyocytes were exposed to cobalt chloride-induced chemical hypoxia and hydrogen peroxide-simulated oxidative stress. Cobalt chloride was used to induce chemical hypoxia in cardiomyocytes. It is a widely used chemical highly suitable to mimic hypoxia under normoxic conditions without the need of specific incubator with controlled oxygen levels. Cobalt chloride stabilizes hypoxia inducible factors 1α and 2α under normal oxygen levels with the effect staying for several hours after cobalt chloride removal. This allows more easy and controlled handling of the samples compared to the incubator with oxygen levels control (Munoz-Sanchez and Chanez-Cardenas, 2018). Hydrogen peroxide was used to set cardiomyocytes under oxidative stress. Hydrogen peroxide is a commonly used agent to observe cardiomyocytes metabolism under oxidative stress, since hydrogen peroxide is a dominant reactive oxygen species present in cells due to its much higher stability in comparison to other reactive oxygen species (Law et al., 2013). Both chemical agents were applied in this project to study the effect of hypoxia and oxidative stress on long-chain fatty acid cardiac anabolism.

Strikingly, both chemical hypoxia and oxidative stress resulted into similar responses, which primarily involved inhibition of membrane lipid biosynthesis. The similarity in lipid metabolism response was despite the different nature of these stress agents. Exposure to cobalt chloride and hydrogen peroxide resulted into polar-to-neutral lipid ratio reduction, as well as decrease in sphingomyelin and phosphatidylcholines content. Linoleic acid-derived phosphatidylcholines elongation was also inhibited by both stress factors. Under non-stressed conditions, H9c2 cardiomyocytes and viable heart slices tend to elongate linoleic acid-derived phosphatidylcholines from PC34;Y to PC36;Y. Hypoxia and oxidative stress tend to inhibit this process in a concentration-dependent manner. These data indicated systemic changes in long-chain fatty acid handling and changes in membrane lipid composition in response to chemical hypoxia and oxidative stress.

It was attempted to find out, how could exposure to such different stress agents result into similar patterns in lipid metabolism. The TUNEL assay was performed and the rate of cells undergoing apoptosis was measured to check if apoptosis could be the reason. While small number of cells exposed to oxidative stress were positively stained for apoptotic markers, no positive staining was observed in cells exposed to chemical hypoxia. According to the literature, typically, much higher concentrations are used in cardiomyocytes for apoptosis induction by cobalt chloride and hydrogen peroxide than those used in this study. Therefore, apoptosis cannot be the reason behind the observed similarities in lipid metabolism. Stabilization of hypoxia inducible factors might be a common denominator; however, activation of this pathway was not studied in detail in this project.

Cobalt chloride and hydrogen peroxide-induced lipid alterations could be part of generalized cardiac response to stress factors, termed “cardiac remodeling”. Cardiac remodeling is a fundament to the heart failure progression, initially being adaptive to stress factors (hypoxia, oxidative stress, genetic factors, increased workload in athletes) but at later steps failing to outbalance hearts’ metabolic needs and leading to energy depletion and irreversible changes. Some authors say that reversing cardiac remodeling might represent a novel attractive approach for treating cardiovascular diseases and preventing heart failure (Lionetty et al., 2011).

Since some authors express hope that reversing cardiac remodeling might be a good strategy to treat cardiovascular diseases, it was interesting to study if the effect of oxidative stress on lipid metabolism could be reversed by use of medications. Among the compounds tested here, trimetazidine was the one that allowed to reverse hydrogen peroxide-induced inhibition of sphingomyelin biosynthesis.

Membranes lipid content and properties are crucial for heart health. In cardiomyocytes the cellular membrane connects tightly to the cytoskeleton, therefore any alterations in membrane lipid metabolism could result into direct adverse effects in cardiomyocytes, potentially affecting the health of the whole organ. As it was shown in the earlier studies, the lowering of phospholipids levels has led to membrane instability and electrophysiological changes, which could result into life-threatening arrhythmias (Wu et al., 2017; Pistritu et al., 2023). Modification of phospholipid composition in the heart muscle might result into changes in membrane fluidity and permeability, which in its turn could affect membrane-bound enzymes and receptors, and, this way, influence various signaling pathways and membrane functioning (Benediktsdottir and Gudbjarnason, 1988). Thus, changes in membrane lipid composition (like reduction in phosphatidylcholines and sphingomyelins amounts and affected phosphatidylcholines remodeling, observed in this study) might potentially result into alterations in membrane properties of cardiomyocytes, intervene with their contraction-relaxation cycles, impair signal conductivity necessary for uninterrupted synchronized work, and, eventually, affect the health of the whole heart and be life-threatening for patients (Samarel, 2014).

Indeed, membrane lipid alterations and changes in phospholipid remodeling have been reported in several cardiac disease models and patients' samples. Alterations in neutral and phospholipid metabolism could contribute to the development of the irreversible injury in ischemic myocardium (Lionetty et al., 2011). Decreased phospholipids and increased lysophospholipids were reported in ischemic myocardium, with the effect even more pronounced in myocardial ischemia-reperfusion model compared to chronic ischemia in *ex vivo* rat model and pig heart (Pistritu et al., 2023). Similar effect was reported for rats with induced pressure overload by abdominal constriction, where decrease in total phospholipid, phosphatidylcholine, phosphatidylethanolamine, phosphatidylglycerol and phosphatidylinositol content in both ventricles was observed (Mrnka et al., 1996).

5.5 Limitations and outlook

This is a pioneering study employing different alkyne-fatty acid tracers in various cardiac setups using highly-sensitive mass spectrometric lipid tracing and fluorescent microscopic imaging. Applicability of alkyne-fatty acids in different cardiac setups was tested and compared. This study allowed to see the differences in various fatty acids handling by the heart under normal and stressed conditions (erucic acid overload, inhibition of adipose triglyceride lipase, chemical hypoxia and oxidative stress). This project confirmed the existence of cardiac triglycerides pool and showed the effect of the erucic acid on cardiac lipid accumulation.

While alkyne-fatty acids allowed to account for unique biological characteristics of fatty acids having different chemical structures, this study has several limitations. Alkyne-fatty acid tracing did not allow to simultaneously follow anabolic and catabolic pathways. Microscopy allowed only to visualize synthesized lipids but not to visually follow their oxidation. Also, some minor differences in cellular and slices setups in terms of triglycerides synthesis and phosphatidylcholines remodeling were seen, which could be due to unavoidable short hypoxia during viable slices preparation. Effect of hypoxia in a chamber with controlled oxygen levels in addition to cobalt chloride-induced chemical hypoxia experiments was not studied here.

It would be interesting in the future to develop methodology to follow cardiac alkyne-cardiolipins metabolism and alterations due to their central role in the heart physiology. Also, synthesis of alkyne-erucic acid would allow to directly follow its transformations in the heart. Additionally, it would be of high interest to develop heart-specific lipid tracers, that could be fed to the living animal and would be exclusively metabolized by the heart without the influence from other metabolically active organs. Comparing cardiac and skeletal muscle triglycerides pool kinetics could provide an interesting insight into lipid biology of striated muscle cells. Identifying pathways behind chemical hypoxia and oxidative stress-induced lipid changes would explain the similarity of the observed lipid patterns for such different stress agents.

References

Abdellatif, A. M. M. (1972). Cardiopathogenic effects of dietary rapeseed oil. *Nutrition Reviews*, 30(1), 2-6.

Adusumilli, R., and P. Mallick (2017). Data conversion with ProteoWizard msConvert. *Springer Proteomics: methods and protocols*, 339-368.

Andersson, L., Cinato, M., Mardani, I., Milijanovic, A., Arif, M., Koh, A., Lindbom, M., Laudette, M., Bollano, E., Omerovic, El., Klevstig, M., Henricsson, M., Fogelstrand, P., Swärd, K., Ekstrand, M., Levin, M., Wikström, J., Doran, S., Hyötyläinen, T., Sinisalu, L., Oresic, M., Tivesten, A., Adiels, M., Bergo, M. O., Proia, R., Mardinoglu, A., Jeppsson, A., Boren, J., and M. C. Levin (2021). Glucosylceramide synthase deficiency in the heart compromises β1-adrenergic receptor trafficking. *European Heart Journal*, 42, 4481-4492.

Aubourg, P., Adamsbaum, C., Lavallard-Rousseau, M. C., Rocchiccioli, F., Cartier, N., Jambaque, I., Jakobezak, C., Lemaitre, A., Boureau, F., Wolf, C., and P. F. Bougneres (1993). A two-year trial of oleic and erucic acids ("Lorenzo's oil") as treatment for adrenomyeloneuropathy. *New England Journal of Medicine*, 329(11), 745-752.

Banke, N. H., Wende, A. R., Leone, T. C., O'Donnell, J. M., Abel, E. D., Kelly, D. P., and E. D. Lewandowski (2010). Preferential oxidation of triacylglyceride-derived fatty acids in heart is augmented by the nuclear receptor PPARα. *Circulation research,* 107(2), 233-241.

Benediktsdottir, V. E., and S. Gudbjarnason (1988). Reversible alterations in fatty acid composition of heart muscle membrane phospholipids induced by epinephrine in rats fed different fats. *Journal of Lipid Research,* 29(6), 765-772.

Bourre, J. M., Daudu, O., and N. Baumann (1976). Nervonic acid biosynthesis by erucyl-CoA elongation in normal and quaking mouse brain microsomes. Elongation of other unsaturated fatty acyl-CoAs (mono and polyunsaturated). *Biochimica et Biophysica Acta (BBA)-Lipids and Lipid Metabolism*, 424(1), 1-7.

Carré, P., and A. Pouzet (2014). Rapeseed market, worldwide and in Europe. *Ocl*, 21(1), D102.

Chen, X., Shang, L., Deng, S., Li, P., Chen, K., Gao, T., Zhang, X., Chen, Z., and J. Zeng (2020). Peroxisomal oxidation of erucic acid suppresses mitochondrial fatty acid oxidation by stimulating malonyl-CoA formation in the rat liver. *Journal of Biological Chemistry*, 295(30), 10168-10179.

Chien, K. R., Bellary, A., Nicar, M., Mukherjee, A., and L. M. Buja (1983). Induction of a reversible cardiac lipidosis by a dietary long-chain fatty acid (erucic acid). Relationship to lipid accumulation in border zones of myocardial infarcts. *The American Journal of Pathology,* 112(1), 68.

Chow, C. K. (2008). Fatty acids in foods and their health implications. *CRC press,* 1-14.

Christophersen, B. O., and J. Bremer (1972). Erucic acid—an inhibitor of fatty acid oxidation in the heart. *Biochimica et Biophysica Acta (BBA)-Lipids and Lipid Metabolism*, 280(4), 506-514.

Cordis, G. A., Yoshida, T., and D. K. Das (1998). HPTLC analysis of sphingomylein, ceramide and sphingosine in ischemic/reperfused rat heart. *Journal of pharmaceutical and biomedical analysis,* 16(7), 1189-1193.

Da Dalt, L., Cabodevilla, A. G., Goldberg, I. J., and G. D. Norata (2023). Cardiac lipid metabolism, mitochondrial function, and heart failure. *Cardiovascular research*, 119(10), 1905-1914.

Das, D. K., Engelman, R. M., Rousou, J. A., Breyer, R. H., Otani, H., and S. Lemeshow (1986). Role of membrane phospholipids in myocardial injury induced by ischemia and reperfusion. *American Journal of Physiology-Heart and Circulatory Physiology*, 251(1), 71-79.

Dorni, C., Sharma, P., Saikia, G., and T. Longvah (2018). Fatty acid profile of edible oils and fats consumed in India. *Food chemistry*, 238, 9-15.

D'Souza, K., and R. M. Epand (2014). Enrichment of phosphatidylinositols with specific acyl chains. *Biochimica et Biophysica Acta (BBA)-Biomembranes*, 1838(6), 1501-1508.

D'Souza, K., Nzirorera, C., and P. C. Kienesberger (2016). Lipid metabolism and signaling in cardiac lipotoxicity. *Biochimica et Biophysica Acta (BBA)-Molecular and Cell Biology of Lipids*, 1861(10), 1513-1524.

Evans, K., Burdge, G. C., Wootton, S. A., Clark, M. L., and K. N. Frayn (2002). Regulation of dietary fatty acid entrapment in subcutaneous adipose tissue and skeletal muscle. *Diabetes*, 51(9), 2684-2690.

Fahy, E., Subramaniam, S., Brown, H. A., Glass, C. K., Merrill, A. H. J., Murphy, R. C., Raetz, C. R. H., Russell, D. W., Seyama, Y., Shaw, W., Shimizu, T., Spener, F., van Meer, G., VanNieuwenhze, M. S., White, S. H., Witztum, J. L., and E. A. Dennis (2005). A comprehensive classification system for lipids. *Eur. J. Lipid Sci. Technol*., 107, 337-364.

Fattore, E., and R. Fanelli (2013). Palm oil and palmitic acid: a review on cardiovascular effects and carcinogenicity. *International journal of food sciences and nutrition*, 64(5), 648-659.

Fearnley, C. J., Roderick, H. L., and M. D. Bootman (2011). Calcium signaling in cardiac myocytes. *Cold Spring Harbor perspectives in biology*, 3(11), a004242.

Fedak, P. W., Verma, S., Weisel, R. D., and R. K. Li (2005). Cardiac remodeling and failure: from molecules to man (Part I). *Cardiovascular Pathology*, 14(1), 1-11.

Fischer, J., Lefèvre, C., Morava, E., Mussini, J. M., Laforêt, P., Negre-Salvayre, A., Lathrop, M., and R. Salvayre (2007). The gene encoding adipose triglyceride lipase (PNPLA2) is mutated in neutral lipid storage disease with myopathy. *Nature genetics*, 39(1), 28-30.

Gaebler, A., Penno, A., Kuerschner, L., and C. Thiele (2016). A highly sensitive protocol for microscopy of alkyne lipids and fluorescently tagged or immunostained proteins. *Journal of lipid research*, 57(10), 1934-1947.

Galanty, A., Grudzińska, M., Paździora, W., and P. Paśko (2023). Erucic acid—Both sides of the story: A concise review on its beneficial and toxic properties. *Molecules*, 28(4), 1924.

Ghigo, A., Laffargue, M., Li, M., and E. Hirsch (2017). PI3K and calcium signaling in cardiovascular disease. *Circulation research*, 121(3), 282-292.

Gonçalinho, G. H. F., Sampaio, G. R., Soares-Freitas, R. A. M., and N. R. T. Damasceno (2023). Stearic Acid, but not palmitic acid, is associated with inflammatory and endothelial dysfunction biomarkers in individuals at cardiovascular risk. *Arquivos Brasileiros de Cardiologia*, 120, e20220598.

Haemmerle, G., Lass, A., Zimmermann, R., Gorkiewicz, G., Meyer, C., Rozman, J., Heldmaier, G., Maier, R., Theussl, C., Eder, S., Kratky, D., Wagner, E., Klingenspor, M., Hoefler, G., and R. Zechner (2006). Defective lipolysis and altered energy metabolism in mice lacking adipose triglyceride lipase. *Science*, 312(5774), 734-737.

He, J., Liu, D., Zhao, L., Zhou, D., Rong, J., Zhang, L., and Z. Xia (2022). Myocardial ischemia/reperfusion injury: Mechanisms of injury and implications for management. *Experimental and therapeutic medicine*, 23(6), 430.

Heier, C., and G. Haemmerle (2016). Fat in the heart: The enzymatic machinery regulating cardiac triacylglycerol metabolism. *Biochimica et Biophysica Acta (BBA)-Molecular and Cell Biology of Lipids*, 1861(10), 1500-1512.

Herzog, R., Schuhmann, K., Schwudke, D., Sampaio, J. L., Bornstein, S. R., Schroeder, M., and A. Shevchenko (2012). LipidXplorer: a software for consensual cross-platform lipidomics. *PloS one*, 7(1), e29851.

Herzog, R., Schwudke, D., Schuhmann, K., Sampaio, J. L., Bornstein, S. R., Schroeder, M., and A. Shevchenko (2011). A novel informatics concept for high-throughput shotgun lipidomics based on the molecular fragmentation query language. *Genome biology*, 12, 1-25.

Hescheler, J., Meyer, R., Plant, S., Krautwurst, D., Rosenthal, W., and G. Schultz (1991). Morphological, biochemical, and electrophysiological characterization of a clonal cell (H9c2) line from rat heart. *Circulation research*, 69(6), 1476-1486.

Hiraide, T., Ikegami, K., Sakaguchi, T., Morita, Y., Hayasaka, T., Masaki, N., Waki, M., Sugiyama, E., Shinriki, S., Takeda, M., Shibasaki, Y., Miyazaki, S., Kikuchi, H., Okuyama, H., Inoue, M., Setou, M., and H. Konno (2016). Accumulation of arachidonic acid-containing phosphatidylinositol at the outer edge of colorectal cancer. *Scientific Reports*, 6(1), 29935.

Hofmann, K., Rodriguez-Rodriguez, R., Gaebler, A., Casals, N., Scheller, A., and L. Kuerschner (2017). Astrocytes and oligodendrocytes in grey and white matter regions of the brain metabolize fatty acids. *Scientific reports*, 7(1), 10779.

Huang, J. P., Cheng, M. L., Wang, C. H., Shiao, M. S., Chen, J. K., and L. M. Hung (2016). High-fructose and high-fat feeding correspondingly lead to the development of lysoPC-associated apoptotic cardiomyopathy and adrenergic signaling-related cardiac hypertrophy. *International journal of cardiology*, 215, 65-76.

Huang, L., Gao, L., and C. Chen (2021). Role of Medium-Chain Fatty acids in Healthy Metabolism: A Clinical Perspective. *Trends in Endocrinology & Metabolism*. 32 (6), 351-364.

Ismael, S., and R. R. Nair (2021). Reactivation of fatty acid oxidation by medium chain fatty acid prevents myocyte hypertrophy in H9c2 cell line. *Molecular and Cellular Biochemistry,* 476(1), 483-491.

Ježová, J., Nováková, O., Kolář, F., Tvrzická, E., Neckář, J., and F. Novák (2002). Chronic hypoxia alters fatty acid composition of phospholipids in right and left ventricular myocardium. *Molecular and cellular biochemistry*, 232, 49-56.

Joukar, S. (2021). A comparative review on heart ion channels, action potentials and electrocardiogram in rodents and human: extrapolation of experimental insights to clinic. *Laboratory Animal Research*, 37(1), 25.

Kickler, T. S., Zinkham, W. H., Moser, A., Shankroff, J., Borel, J., and H. Moser (1996). Effect of erucic acid on platelets in patients with adrenoleukodystrophy. *Biochemical and molecular medicine*, 57(2), 125-133.

Kienesberger, P. C., Pulinilkunnil, T., Nagendran, J., and J. R. Dyck (2013). Myocardial triacylglycerol metabolism. *Journal of molecular and cellular cardiology*, 55, 101-110. **(A)**

Kienesberger, P. C., Pulinilkunnil, T., Nagendran, J., Young, M. E., Bogner-Strauss, J. G., Hackl, H and J. R. Dyck (2013). Early structural and metabolic cardiac remodelling in response to inducible adipose triglyceride lipase ablation. *Cardiovascular research*, 99(3), 442-451. **(B)**

Kimes, B. W., and B. L. Brandt (1976). Properties of a clonal muscle cell line from rat heart. *Experimental cell research*, 98(2), 367-381.

Klizaite, K. (2017). Medium-chain fatty acid metabolism in hepatocytes and adipocytes. *Doctoral dissertation, Universitäts-und Landesbibliothek Bonn*, 1-123.

Knutsen, H. K., Alexander, J., Barregård, L., Bignami, M., Brüschweiler, B., Ceccatelli, S., Dinovi, M., Edler, L., Grasl-Kraupp, B., Hogstrand, C., Hoogenboom, L., Nebbia, C. S., Oswald, I., Petersen, A., Rose, M., Roudot, A.-C., Schwerdtle, T., Vollmer, G., Wallace, H., Cottrill, B., Dogliotti, E., Laakso, J., Metzler, M., Velasco, L., Baert, K., Ruis, J. A. G., Varga, E., Dorr, B., Sousa, R., and C. Vleminckx (2016). Erucic acid in feed and food. *EFSA Journal*, 14(11), e04593.

Kobayashi, K., Sakata, Y., Miyauchi, H., Ikeda, Y., Nagasawa, Y., Nakajima, K., Shimada, K., Kozawa, J., Hao, H., Amano, T., Yoshida, H., Inaba, T., Hashimoto, C., and K. Hirano (2020). The diagnostic criteria 2020 for triglyceride deposit cardiomyovasculopathy. *Annals of Nuclear Cardiology*, 6(1), 99-104.

Koehler, W., and P. Sokolowski (2005). Clinical phenotypes, diagnosis and treatment of adulthood X-linked adrenoleukodystrophy. *Understanding and treating adrenoleukodystrophy: Present state and future perspectives*, 28-60.

Kovilakath, A., and L. A. Cowart (2020). Sphingolipid mediators of myocardial pathology. *Journal of Lipid and Atherosclerosis*, 9(1), 23-49.

Kuerschner, L., Leyendecker, P., Klizaite, K., Fiedler, M., Saam, J., and C. Thiele (2022). Development of oxaalkyne and alkyne fatty acids as novel tracers to study fatty acid beta-oxidation pathways and intermediates. *Journal of Lipid Research*, 63(4).

Kuerschner, L., and C. Thiele (2014). Multiple bonds for the lipid interest. *Biochimica et Biophysica Acta (BBA)-Molecular and Cell Biology of Lipids*, 1841(8), 1031-1037.

Kuerschner, L., and C. Thiele (2022). Tracing lipid metabolism by alkyne lipids and mass spectrometry: the state of the art. *Frontiers in Molecular Biosciences*, 9, 880559.

Labarthe, F., Gélinas, R., and C. Des Rosiers (2008). Medium-chain fatty acids as metabolic therapy in cardiac disease. *Cardiovascular drugs and therapy*, 22, 97-106.

Laryea, M. D., Jiang, Y. F., Xu, G. L., and I. Lombeck (1992). Fatty acid composition of blood lipids in Chinese children consuming high erucic acid rapeseed oil. *Annals of nutrition and metabolism*, 36(5-6), 273-278.

Law, C.-H., Li, J.-M., Chou, H.-C., Chen, Y.-H., and H.-L. Chan (2013). Hyaluronic acid-dependent protection in H9c2 cardiomyocytes: A cell model of heart ischemia-reperfusion injury and treatment. *Toxicology*, 303, 54-71.

Lewin, T. M., de Jong, H., Schwerbrock, N. J., Hammond, L. E., Watkins, S. M., Combs, T. P., and R. A. Coleman (2008). Mice deficient in mitochondrial glycerol-3-phosphate acyltransferase-1 have diminished myocardial triacylglycerol accumulation during lipogenic diet and altered phospholipid fatty acid composition. *Biochimica et Biophysica Acta (BBA)-Molecular and Cell Biology of Lipids*, 1781(6-7), 352-358.

Li, M., Hirano, K. I., Ikeda, Y., Higashi, M., Hashimoto, C., Zhang, B., Kozawa, J., Sugimura, K., Miyauchi, H., Suzuki, A., Hara, Y., Takagi, A., Ikeda, Y., Kobayashi, K., Futsukaichi, Y., Zaima, N., Yamaguchi, S., Shrestha, R., Nakamura, H., Kawaguchi, K., Sai, E., Hui, S.-P., Nakano, Y., Sawamura, A., Inaba, T., Sakata, Y., Yasui, Y., Nagasawa, Y., Kinugawa, S., Shimada, K., Yamada, S., Hao, H., Nakatani, D., Ide, T., Amano, T., Naito, H., Nagasaka, H., and K. Kobayashi (2019). Triglyceride deposit cardiomyovasculopathy: a rare cardiovascular disorder. *Orphanet journal of rare diseases*, 14, 1-9.

LIPID MAPS (2025). Abbreviations of functional groups / side chains and carbohydrate structures according to IUPAC hierarchy. *Available at (accessed 29.09.2025): https://www.lipidmaps.org/lipid_nomenclature/rules/abbreviations*

Lopaschuk, G. D., Ussher, J. R., Folmes, C. D., Jaswal, J. S., and W. C. Stanley (2010). Myocardial fatty acid metabolism in health and disease. *Physiological reviews*, 90(1), 207-258.

Lorenzo, P. M., Izquierdo, A. G., Rodriguez-Carnero, G., Fernández-Pombo, A., Iglesias, A., Carreira, M. C., Tejera, C., Bellido, D., Martinez-Olmos, M. A., Leis, R., Casanueva, F. F., and A. B. Crujeiras (2022). Epigenetic effects of healthy foods and lifestyle habits from the Southern European Atlantic Diet pattern: a narrative review. *Advances in nutrition*, 13(5), 1725-1747.

Liao, R., Podesser, B. K., and C. C. Lim (2012). The continuing evolution of the Langendorff and ejecting murine heart: new advances in cardiac phenotyping. *American Journal of Physiology-Heart and Circulatory Physiology*, 303(2), H156-H167.

Liu, Y., Ma, D., Li, Q., Liu, L., Gao, W., Xie, Y., and C. Wu (2024). High Levels of Erucic Acid Cause Lipid Deposition, Decreased Antioxidant and Immune Abilities via Inhibiting Lipid Catabolism and Increasing Lipogenesis in Black Carp (*Mylopharyngodon piceus*). *Animals*, 14(14), 2102.

Ma, D., Li, Q., Xie, Y., Kong, Y., Ding, Z., Ye, J., Wu, C., and Y. Liu (2024). Dietary Erucic Acid Induces Fat Accumulation, Hepatic Oxidative Damage, and Abnormal Lipid Metabolism in Nile Tilapia (*Oreochromis niloticus*). *Aquaculture Nutrition*, 1, 6670740.

Maki, K. C., Dicklin, M. R., and C. F. Kirkpatrick (2021). Saturated fats and cardiovascular health: Current evidence and controversies. *Journal of clinical lipidology*, 15(6), 765-772.

Milani-Nejad, N., and P. M. Janssen (2014). Small and large animal models in cardiac contraction research: advantages and disadvantages. *Pharmacology & therapeutics*, 141(3), 235-249.

Mitsnefes, M. M., Fitzpatrick, J., Sozio, S. M., Jaar, B. G., Estrella, M. M., Monroy-Trujillo, J. M., Zhang, W., Setchell, K., and R. S. Parekh (2018). Plasma glucosylceramides and cardiovascular risk in incident hemodialysis patients. *Journal of clinical lipidology*, 12(6), 1513-1522.

Moser, H. W., Raymond, G. V., Lu, S. E., Muenz, L. R., Moser, A. B., Xu, J., Jones, R. O., Loes, D. J., Melhem, E. R., Dubey, P., Bezman, L., Brereton, N. H., and A. Odone (2005). Follow-up of 89 asymptomatic patients with adrenoleukodystrophy treated with Lorenzo's oil. *Archives of neurology*, 62(7), 1073-1080.

Moser, H. W., Moser, A. B., Hollandsworth, K., Brereton, N. H., and G. V. Raymond (2007). "Lorenzo's oil" therapy for X-linked adrenoleukodystrophy: rationale and current assessment of efficacy. *Journal of molecular neuroscience*, 33, 105-113.

Motayagheni, N. (2017). Modified Langendorff technique for mouse heart cannulation: improved heart quality and decreased risk of ischemia. *MethodsX*, 4, 508-512.

Mrnka, L., Novakova, O., Pelouch, V., and F. Novak (1996). Phospholipid composition in the rat heart exposed to pressure overload from birth. *Physiological research*, 45, 83-86.

Munoz-Sanchez, J. and M. E. Chanez-Cardenas (2018). The use of cobalt chloride as a chemical hypoxia model. *J Appl Toxicol.*, 39, 556-570.

Murphy C. C., Murphy, E. J., and M. Y. Golovko (2008). Erucic acid is differentially taken up and metabolized in rat liver and heart. *Lipids*, 43, 391-400.

Neubauer, S. (2007). The failing heart—an engine out of fuel. *New England Journal of Medicine*, 356(11), 1140-1151.

Odone, A., and M. Odone (1989). Lorenzo's oil: a new treatment for adrenoleukodystrophy. *J Pediatr Neurosci*, 5(1), 55-61.

Oenarto, V. (2020). Interorgan Crosstalk between the Heart and Adipose Tissue during Heart Failure Establishment. *Doctoral dissertation, Heinrich-Heine-Universität Düsseldorf*, 1-103.

Olson, R. E., and R. J. Hoeschen (1967). Utilization of endogenous lipid by the isolated perfused rat heart. *Biochemical Journal*, 103(3), 796.

Paapstel, K., Kals, J., Eha, J., Tootsi, K., Ottas, A., Piir, A., Jakobson, M., Lieberg, J., and M. Zilmer (2018). Inverse relations of serum phosphatidylcholines and lysophosphatidylcholines with vascular damage and heart rate in patients with atherosclerosis. *Nutrition, Metabolism and Cardiovascular Diseases*, 28(1), 44-52.

Palm, C. L., Nijholt, K. T., Bakker, B. M., and B. D. Westenbrink (2022). Short-Chain Fatty Acids in the Metabolism of Heart Failure – Rethinking the Fat Stigma. *Frontiers in Cardiovascular Medicine*. 9, 915102, 1-7.

Papamandjaris, A. A., MacDougall, D. E., and P. J. H. Jones (1998). Medium chain fatty acid metabolism and energy expenditure: obesity treatment implications. *Life Sciences*. 62, 1203-1215.

Park, J. Y., Lee, S. H., Shin, M. J., and G. S. Hwang (2015). Alteration in metabolic signature and lipid metabolism in patients with angina pectoris and myocardial infarction. *PloS one*, 10(8), e0135228.

Pereyra, A. S., McLaughlin, K. L., Buddo, K. A., and J. M. Ellis (2023). Medium-chain fatty acid oxidation is independent of l-carnitine in liver and kidney but not in heart and skeletal muscle. *American Journal of Physiology-Gastrointestinal and Liver Physiology*, 325 (4), 287-294.

Pistritu, D. V., Vasiliniuc, A. C., Vasiliu, A., Visinescu, E. F., Visoiu, I. E., Vizdei, S., Anghel, P. M., Tanca, A., Bucur, O., and E. A. Liehn (2023). Phospholipids, the Masters in the Shadows during Healing after Acute Myocardial Infarction. *International Journal of Molecular Sciences*, 24(9), 8360.

Pulinilkunnil, T., Kienesberger, P. C., Nagendran, J., Sharma, N., Young, M. E., and J. R. B. Dyck (2014). Cardiac-specific adipose triglyceride lipase overexpression protects from cardiac steatosis and dilated cardiomyopathy following diet-induced obesity. *International journal of obesity*, 38(2), 205-215.

Saddik, M., and G. Lopaschuk (1991). Myocardial triglyceride turnover and contribution to energy substrate utilization in isolated working rat hearts. *Journal of Biological Chemistry*, 266(13), 8162-8170.

Samarel, A. M. (2014). Focal adhesion signaling in heart failure. *Pflügers Archiv-European Journal of Physiology*, 466, 1101-1111.

Sassa, T., Wakashima, T., Ohno, Y., and A. Kihara (2014). Lorenzo's oil inhibits ELOVL1 and lowers the level of sphingomyelin with a saturated very long-chain fatty acid. *Journal of lipid research*, 55(3), 524-530.

Schulze, P. C., Drosatos, K., and I. J. Goldberg (2016). Lipid use and misuse by the heart. *Circulation research*, 118(11), 1736-1751.

Sharma, S., Adrogue, J. V., Golfman, L., Uray, I., Lemm, J., Youker, K., Noon, G. P., Frazier, O. H., and H. Taegtmeyer (2004). Intramyocardial lipid accumulation in the failing human heart resembles the lipotoxic rat heart. *FASEB J*., 18, 1692-1700.

Sipido, K. R., and E. Marban (1991). L-type calcium channels, potassium channels, and novel nonspecific cation channels in a clonal muscle cell line derived from embryonic rat ventricle. *Circulation research*, 69(6), 1487-1499.

Spandl, J., White, D. J., Peychl, J., and C. Thiele (2009). Live cell multicolor imaging of lipid droplets with a new dye, LD540. *Traffic*, 10(11), 1579-1584.

Stam, H., Geelhoed-Mieras, T., and W. C. Hülsmann (1980). Erucic acid-induced alteration of cardiac triglyceride hydrolysis. *Lipids*, 15 (4), 242-250.

Sternberg, F., Sternberg, C., Dunkel, A., Beikbaghban, T., Gregor, A., Szarzynski, A., Somoza, V., Walter, I., Duszka, K., Kofler B., and E. Pohl (2023). Ketogenic diets composed of long-chain and medium-chain fatty acids induce cardiac fibrosis in mice. *Molecular Metabolism*, 72, 101711.

Swanton, M. E., and E. D. Saggerson (1997). Effects of adrenaline on triacylglycerol synthesis and turnover in ventricular myocytes from adult rats. *Biochemical Journal*, 328(3), 913-922

Takano, H., Hasegawa, H., Nagai, T., and I. Komuro (2003). Implication of cardiac remodeling in heart failure: mechanisms and therapeutic strategies. *Internal Medicine*, 42(6), 465-469.

Thiele, C., Papan, C., Hoelper, D., Kusserow, K., Gaebler, A., Schoene, M., Piotrowitz, K., Lohmann, D., Spandl, J., Stevanovic, A., Shevchenko, A., and L. Kuerschner (2012). Tracing fatty acid metabolism by click chemistry. *ACS chemical biology*, 7(12), 2004-2011.

Thiele, C., Wunderling, K., and P. Leyendecker (2019). Multiplexed and single cell tracing of lipid metabolism. *Nature Methods*, 16(11), 1123-1130.

Tse, G., Tse, V., Yeo, J. M., and B. Sun (2016). Atrial Anti-Arrhythmic Effects of Heptanol in Langendorff-Perfused Mouse Hearts. *PLOS ONE*, 11(2), e0148858.

Udelson, J. E., and M. A. Konstam (2011). Ventricular remodeling: fundamental to the progression (and regression) of heart failure. *Journal of the American College of Cardiology*, 57(13), 1477-1479.

Wang, P., Xiong, X., Zhang, X., Wu, G., and F. Liu (2022). A review of erucic acid production in Brassicaceae oilseeds: Progress and prospects for the genetic engineering of high and low-erucic acid rapeseeds (*Brassica napus*). *Frontiers in Plant Science*, 13, 899076.

Watkins, S. J., Borthwick, G. M. and H. M. Arthur (2011). The H9C2 cell line and primary neonatal cardiomyocyte cells show similar hypertrophic responses in vitro. *In Vitro Cell.Dev.Biol.-Animal* 47, 125-131.

Watson, S. A., Scigliano, M., Bardi, I., Ascione, R., Terraciano, C. M. and F. Perbellini (2017). Preparation of viable adult ventricular myocardial slices from large and small animals. *Nature Protocols*, 12 (12), 2623-2639.

Wittenbecher, C., Eichelmann, F., Toledo, E., Guasch-Ferré, M., Ruiz-Canela, M., Li, J., Arós, F., Lee C.-H., Liang, L., Salas-Salvadó, J., Clish C. B., Schulze, M. B., Martínez-González, M. A., and F. B. Hu (2021). Lipid Profiles and Heart Failure Risk Results from Two Prospective Studies. *Circulation Research,* 128, 309-320.

World Health Organization. (2023). Saturated fatty acid and trans-fatty acid intake for adults and children: WHO guideline. *World Health Organization*.

Wu, J., Wu, Q., Wang, D., Kong, J., Dai, W., Wang, X., and X. Yu (2017). Common lipid features of lethal ventricular tarchyarrhythmias (LVTAs) induced by myocardial infarction and myocardial ion channel diseases. *Scientific reports*, 7(1), 4220.

Wunderling, K., Zurkovic, J., Zink, F., Kuerschner, L., and C. Thiele (2023). Triglyceride cycling enables modification of stored fatty acids. *Nature Metabolism*, 5(4), 699-709.

Zietzer, A., Düsing, P., Reese, L., Nickenig, G., and F. Jansen (2022). Ceramide Metabolism in Cardiovascular Disease: A Network With High Therapeutic Potential. *Arterioscler Thromb Vasc Biol*, 42, 1220-1228.

Zimmermann, R., Lass, A., Haemmerle, G., and R. Zechner (2009). Fate of fat: the role of adipose triglyceride lipase in lipolysis. *Biochimica et Biophysica Acta (BBA)-Molecular and Cell Biology of Lipids*, 1791(6), 494-500.

Supplementary data

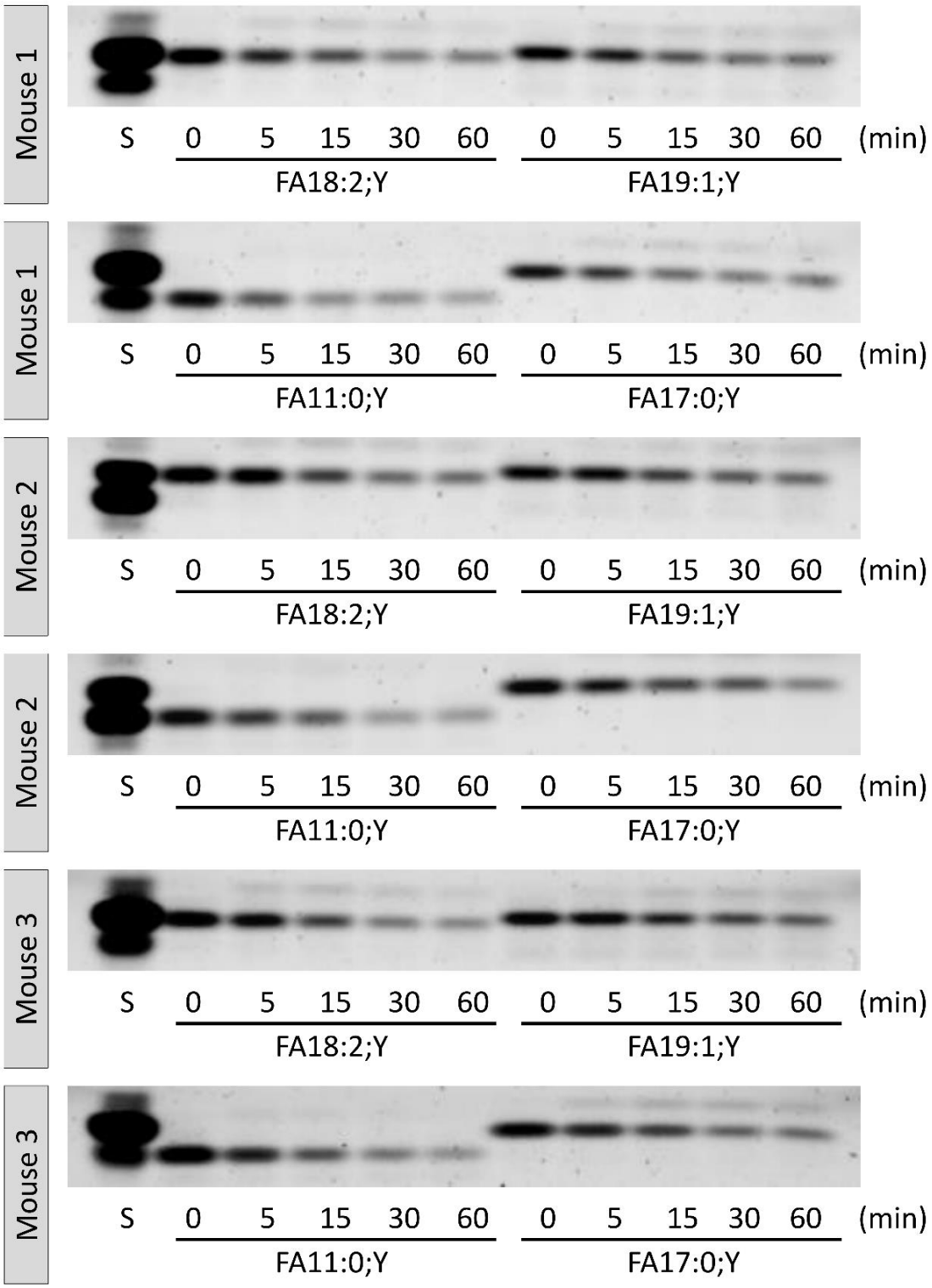

Supplementary figure 1: Inverted thin layer chromatography images used for integrated optical density calculation on the figure 7 (a). Alkyne-fatty acid tracers (alkyne-capric acid FA11:0;Y, alkyne-palmitic acid FA17:0;Y, alkyne-linoleic acid FA18:2;Y or alkyne-oleic acid FA19:1;Y) were incubated with heat lysates from 3 different mice. The assay was performed for 0, 5, 15, 30 and 60 minutes (min). After the click-reaction with fluorescent azide-reporter, samples were run on thin layer chromatography plate. As standard (S), two corresponding alkyne-fatty acids were used.

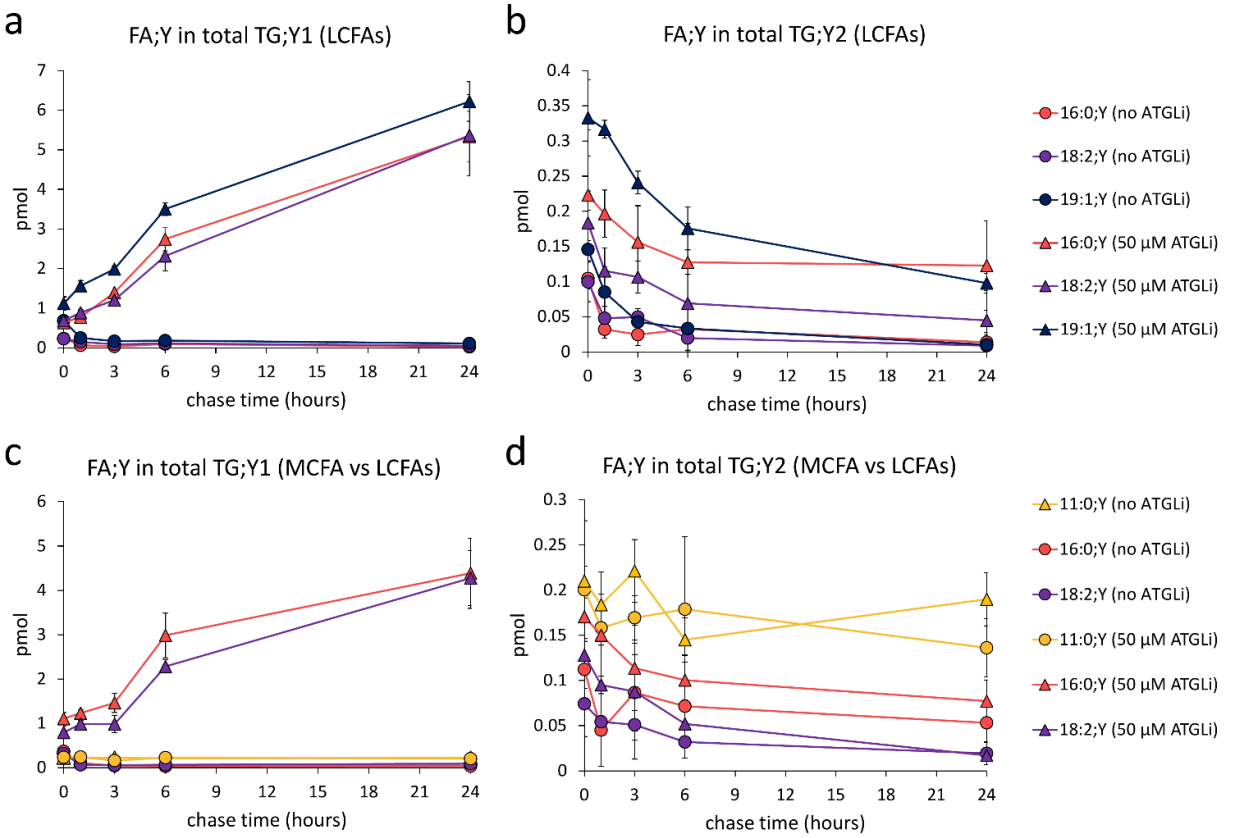

Supplementary figure 2: Effect of ATGListatin (ATGLi) on triglycerides accumulation in H9c2 cardiomyocytes. H9c2 cells were fed with alkyne-fatty acid **mix 1 (a,b)** (alkyne-palmitic acid (FA16:0;Y($^{13}C_6$)),alkyne-linoleic acid (FA18:2;Y) and alkyne-oleic acid (FA19:1;Y)) or **mix 2 (c,d)** (alkyne-capric acid (FA11:0;Y), alkyne-palmitic acid (FA16:0;Y($^{13}C_6$)) and alkyne-linoleic acid (FA18:2;Y)) for 1 hour. Thereafter, the cells were washed and chased for 0, 3, 6 or 24 hours in the media with 50 µM ATGListatin (dissolved in DMSO, triangle markers) or DMSO as carrier control (round markers). The extracted lipids were analyzed by mass spectrometry. **(a)** Single-labelled triglycerides (TG;Y1) carrying one of the long-chain alkyne fatty acids (LCFAs). **(b)** Double-labeled triacylglycerides (TG;Y2) carrying 2 long-chain fatty acids (LCFAs). **(c)** Single-labelled triglycerides (TG;Y1) carrying either one medium-chain fatty acid (MCFA) or one of the long-chain alkyne fatty acids (LCFAs). **(d)** Double-labeled triacylglycerides (TG;Y2) carrying 2 fatty acids, medium- (MCFA) and/or long-chain fatty acids (LCFAs). All graphs show triacylglycerides amounts in picomoles (pmol), average ± standard deviation, n=3.

Acknowledgments

I couldn’t have reached this goal without the help of many people in my life. I’d like to take this opportunity to thank them for their support.

First, my sincere thanks to Prof. Dr. Christoph Thiele. I would like to thank for giving me a great opportunity to work in your research group and for offering me this interesting subject. Thank you for the expertise, advice and all the necessary support for the success of my work.

I want to especially thank all the members of my thesis committee. I am very grateful to Prof. Dr. Christoph Wilhelm for being my second supervisor and reviewing my thesis. My sincere thanks go as well to Prof. Dr. Sven Burgdorf and Prof. Dr. Sebastian Zimmer for completing my thesis committee.

This project was generously supported by the “Deutsche Forschungsgemeinschaft” (461705208 to C.T.).

My most sincere thanks to all current and former lab members for their support and help during this long journey: Mohamed Yagmour, Theja Sajeevan, Konstantin Beckschaefer, Helena Shkuro, PD Dr. Lars Kuerschner, Dr. Anne Gaebler, Dr. Christopher Weber, Heike Sievert, Heike Hupfer, Mickel Mikhael, Dr. Klaus Wunderling, Dr. Jelena Zurkovic, Paula Moore-Dilleke, Fabian Zink, Isabell Jamitzky. Thank you for all the nice moments we shared in the lab and during coffee breaks. I want to express my gratitude and thanks to the entire LIMES Institute and BFB community for such a nice working atmosphere.

I’d like to acknowledge the emotional support provided by my family and friends. We made it to the top of the mountain! I look forward to celebrating with all of you.

Last but not least, I would like to thank my close ones. My warmest thanks go to my parents for always supporting me in every step of my life. Thank you for believing in me. I’d like to thank my partner, Raoul. Your votes of confidence kept me going when my spirits dipped. I couldn’t have done this without you. Thank you!